



University of
Stavanger

Faculty of Science and Technology

MASTER'S THESIS

Study program/ Specialization: MSc in Petroleum Engineering Specialization- Reservoir Engineering	Spring semester, 2015 Open / Restricted access
Writer: Maiya Medetbekova (Writer's signature)
Faculty supervisor: Professor Merete V. Madland	
Thesis title: EVOLUTION OF POROSITY AND PERMEABILITY IN CHALKS AS AN EFFECT OF VARIATIONS IN NON-CARBONATE MINERALS AND TESTING TEMPERATURE	
Credits (ECTS): 30	
Key words: Chalk, Rock Mechanics, Creep, Hydrostatic test, Compaction, Dissolution, Precipitation, Porosity Evolution, Permeability Evolution	Pages: 100 Stavanger, 15.06.2015 Date/year

ABSTRACT

Pressure decline during oil recovery from chalk reservoirs exhibit increase in effective stress and this in turn leads to reservoir compaction causing seabed subsidence. Although, there is positive impact of compaction on the oil recovery, the necessity of pressure maintenance brought the introduction of water injection to chalk fields in the southern part of North Sea (eg. Ekofisk and Valhall). Sea water injection has successfully resulted in an increase in petroleum output. However, as sea water displaces oil and increases pore pressure, the reservoir continues to compact. The phenomenon is referred to as the water weakening effect on chalks. Since little was understood about the impact of aqueous chemistry on the mechanical behaviour of chalk reservoirs, there have been several many studies to better understand this phenomenon.

In the present study, the main goal is to get an improved understanding of how variations in original porosity, non-carbonate content, in addition to temperature effects on final porosity, dynamic compaction and permeability evolution when injecting chemically reactive brine.

Chalk cores from two different sources, one pure chalk (Mons, ~99.5 wt% calcite), and one containing a higher non-carbonate content (Kansas, ~97.5 wt% calcite) were tested in hydraulically operated tri-axial cells. Chalk cores were isotropically loaded beyond yield and thereafter left to deform at a constant stress (creep) for 60 days. Test temperatures were 60°C, 92°C and 130°C, while MgCl₂ brine was used as injection fluid.

Results from the conducted compaction experiments show that the porosity evolution is in coupling with the change in bulk volume, induced by the applied stress, as well as with change in solid volume due to rock-fluid interactions involving dissolution/precipitation processes induced by temperature. Moreover, it has been observed that implication of dissolution/precipitation has also effect on flow properties and to a great extent depends on temperature and non-carbonate minerals initially present in the chalk. Chemical analysis of the effluent show that at high temperatures (92°C and 130°C), considerable loss of magnesium and excess production of calcium is observed, thereby promoting volumetric change of solid phase. Scanning electron microscope images of newly formed magnesium-bearing minerals support the effluent analysis.

TABLE OF CONTENTS

ABSTRACT	i
TABLE OF CONTENTS	ii
LIST OF FIGURES	v
LIST OF TABLES	viii
ACKNOWLEDGEMENTS	x
CHAPTER 1 INTRODUCTION	1
1.1 Background.....	1
1.2 Statement of the problem.....	4
1.3 Objective	5
1.4 Structure of the thesis.....	5
CHAPTER 2 LITERATURE REVIEW	7
2.1 Chalk as petroleum reservoir	7
2.1.1 Geological aspects of chalk	7
2.1.2 Outcrop chalk.....	10
2.2 Rock-mechanical properties	11
2.2.1 Elasticity.....	11
2.2.2 Stress-strain relationship.....	12
2.2.3 Hydrostatic compression test and interpretation of elastic moduli.....	13
2.2.4 Time dependent behaviour	14
2.2.5 Effective stress principle	15
2.2.6 Porosity estimation	16
2.2.7 Permeability estimation	18
2.3 Proposed mechanisms affecting rock-fluid interaction	19
2.3.1 Chemical mechanisms of water weakening.....	20
CHAPTER 3 METHODS AND EXPERIMENTAL PROCEDURES	23
3.1 Preparation of core material and flooding fluids.....	23
3.1.1 Outcrop chalk.....	23
3.1.2 Saturating and flooding fluids	26

3.2 Test equipment	26
3.2.1 The triaxial cell	26
3.2.2 Additional belongings of the test apparatus	27
3.3 Testing procedure	30
3.3.1 Mounting the cell	30
3.3.2 Starting the test	32
3.3.3 Increasing pore pressure	33
3.3.4 Increasing temperature	33
3.3.5 Pushing down the piston	34
3.3.6 Hydrostatic compression test	34
3.3.7 Creep phase	35
3.3.8 Sampling fractioned effluent	35
3.3.9 Dismantling the test	36
3.4 Chemical analysis of fractioned effluent	36
3.5 Measurement of chalk mineral density	37
3.6 Scanning Electron Microscopy (SEM)	38
3.7 Post processing of data	38
3.7.1 Triaxial test	38
3.7.2 Chemical test	38
Chapter 4 EXPERIMENTAL RESULTS AND COMMENTS	40
4.1 Mechanical tests- Mons cores	40
4.1.1 Hydrostatic loading phase	40
4.1.2 Creep phase	42
4.1.3 Relationship between permeability and strain	44
4.2 Mechanical tests - Kansas cores	46
4.2.1 Hydrostatic loading phase	46
4.2.2 Creep phase	47
4.2.3 Relationship between permeability and strain	49
4.3 Chemical analysis of fractioned effluent	50
4.3.1 IC analysis – Mons cores	50

4.3.2 IC analysis - Kansas cores.....	53
4.4 pH analysis – Mons and Kansas cores	56
4.5 Analysing the core after test	59
4.5.1 Bulk volume measurement.....	59
4.5.2 Solid volume measurement by pycnometer	61
4.5.3 Textural analysis.....	62
4.5.4 PHREEQC simulation	65
4.6 Estimation of porosity evolution.....	67
4.6.1 Mons core tested at 60°C.....	67
4.6.2 Mons core tested at 130°C	69
4.6.3 Kansas core tested at 92°C.....	70
Chapter 5 DISCUSSIONS.....	71
5.1 The link between mechanical behaviour, porosity and temperature.....	71
5.2 The link between creep behaviour and dissolution/precipitation.....	72
5.3 The link between flow properties and chemical alterations.....	75
5.4 Effect of chemical alterations on solid volume change.....	78
5.5 Effect of mineralogy and temperature on porosity evolution	79
Chapter 6 CONCLUSIONS.....	81
6.1 Concluding remarks	82
6.2 Future work.....	84
REFERENCES.....	85

LIST OF FIGURES

Figure 1.1 Picture depicts a consequence of compaction in the Ekofisk field.....	2
Figure 1.2 Subsidence from depletion and from water effect in Ekofisk field.	3
Figure 2.1 a) Skeletal structure of coccospheres and coccoliths.	8
Figure 2.1 b) SEM picture of Mons chalk consisting of a mixture of coccoliths and loose plate calcite crystals.....	9
Figure 2.2 Stress-strain paths for linear and non-linear elastic materials.	12
Figure 2.3 Bulk modulus is determined from the calculation of linear slope in the elastic region.....	14
Figure 2.4 Typical Creep developments.....	15
Figure 3.1 a) Saturating the plug in the vacuum chamber with distilled water	25
Figure 3.1 b) the conical flask is placed on a magnetic stirrer.....	25
Figure 3.1 c) Filtrate-apparatus from Millipore used to filtrate the brine. A 0.65 μm filter used consistently for all the brine prepared.	25
Figure 3.2 Principle sketch of the interior of a triaxial cell.....	29
Figure 3.3 Illustration of the exterior of a triaxial cell.....	29
Figure 3.4 Step-wise mounting process of the core in the triaxial cell.	31
Figure 3.5 Illustration of the experimental setup.....	32
Figure 4.1 Axial stress versus axial strain for Mons cores tested at three different temperatures.	41
Figure 4.2 Axial creep strain versus creep time for Mons cores tested at three different temperatures.	43
Figure 4.3 Permeability and axial strain relationship for Mons cores tested under hydrostatic loading at three different temperatures.	45
Figure 4.4 Permeability and creep time relationship for Mons cores tested under creep phase at three different temperatures.....	45
Figure 4.5 Axial stress versus axial strain for Kansas cores tested at three different temperatures.	47

Figure 4.6 Axial creep strain versus creep time for Kansas cores tested at three different temperatures.	48
Figure 4.7 Permeability and axial strain relationship for Kansas cores tested under hydrostatic loading at three different temperatures.	49
Figure 4.8 Permeability and creep time relationship for Kansas cores tested under creep phase at three different temperatures.....	50
Figure 4.9 Mg ²⁺ , Ca ²⁺ and Cl ⁻ concentrations in sampled effluents from core tested at 60°C flooded with 0.219 M MgCl ₂	52
Figure 4.10 Mg ²⁺ , Ca ²⁺ and Cl ⁻ concentrations in sampled effluents from core tested at 92°C flooded with 0.219 M MgCl ₂	52
Figure 4.11 Mg ²⁺ , Ca ²⁺ and Cl ⁻ concentrations in sampled effluents from core tested at 130°C flooded with 0.219 M MgCl ₂	53
Figure 4.12 Mg ²⁺ , Ca ²⁺ and Cl ⁻ concentrations in sampled effluents from Kansas core tested at 60°C flooded with 0.219 M MgCl ₂	55
Figure 4.13 Mg ²⁺ , Ca ²⁺ and Cl ⁻ concentrations in sampled effluents from Kansas core tested at 92°C flooded with 0.219 M MgCl ₂	55
Figure 4.14 Mg ²⁺ , Ca ²⁺ and Cl ⁻ concentrations in sampled effluents from Kansas core tested at 130°C flooded with 0.219 M MgCl ₂	56
Figure 4.15 Evolution of pH with time for Mons cores tested at three different temperatures.	58
Figure 4.16 Evolution of pH with time cores tested at three different temperatures.....	58
Figure 4.17 Evolution of pH with temperature. Simulated using PHREEQC considering mineralogical content of chalk and injected tested brine composition.....	59
Figure 4.18 EDS analysis showing distribution of Mg ²⁺ , Si ²⁺ , Al ³⁺ elements from the inlet towards outlet part of the Mons core tested at 60°C	63
Figure 4.19 EDS analysis showing distribution of Mg ²⁺ , Si ²⁺ , Al ³⁺ elements from the inlet towards outlet part of the Kansas core tested at 92°C.	64
Figure 4.20 EDS analysis showing distribution of Mg ²⁺ , Si ²⁺ , Al ³⁺ elements from the inlet towards outlet part of the Mons core tested at 130°C.....	64
Figure 4.21 SEM micrograph shows common occurrence of magnesite crystals with rhombic habit (arrows) in the Mons core tested at 130 °C.	65

Figure 5.1 Axial stress versus axial strain for the Mons and Kansas cores flooded with MgCl₂ testing brine at three different temperatures..... 72

Figure 5.2 Creep development and fractioned effluent concentrations for Mons and Kansas cores tested at 130°C..... 74

Figure 5.3 Permeability evolution during creep phase for the Mons cores tested at three different temperatures. 77

Figure 5.4 Permeability evolution during creep phase for the Kansas cores tested. 77

LIST OF TABLES

Table 2.1 Characteristics of outcrop Mons and Kansas chalks (Megawati, 2015).....	11
Table 3.1 Physical data for Mons cores	25
Table 3.2 Physical data for Kansas core	25
Table 3.3 Ionic composition of test brine	26
Table 4.1 Defined hydrostatic yield strength and calculated bulk modulus values for Mons cores tested at 3 different temperatures.	42
Table 4.2 Accumulated axial creep deformation from creep phase for Mons cores.....	43
Table 4.3 Defined hydrostatic yield strength and calculated bulk modulus values for Kansas cores tested at 3 different temperatures.	46
Table 4.4 Axial creep strain versus creep time for Kansas cores tested at three different temperatures.	48
Table 4.5 Produced Ca^{2+} and retained Mg^{2+} concentrations in sampled effluents from Mons cores tested at three different testing temperatures.	53
Table 4.6 Produced Ca^{2+} and retained Mg^{2+} concentrations in sampled effluents from Kansas cores tested at three different testing temperatures.....	56
Table 4.11 Input values for the simulation	66
Table 4.12 Output values from simulation for Mons core tested at 60°C.	66
Table 4.13 Output values from simulation for Mons core tested at 130°C.	67
Table 4.14 Output values from simulation for Kansas core tested at 92°C.....	67
Table 4.15 Collected data before and after experiment for Mons core tested at 60°C.	68
Table 4.16 Collected data before and after experiment for Mons core tested at 130°C.....	69
Table 4.17 Collected data before and after experiment for Kansas core tested at 92°C.....	70
Table 4.7 Diameter measurements from inlet to outlet for Mons core tested at 60°C and calculated bulk volume using truncated wedge equation.....	60
Table 4.8 Diameter measurements from inlet to outlet for Kansas core tested at 92°C and calculated bulk volume using truncated wedge equation.....	61
Table 4.9 Diameter measurements from inlet to outlet for Mons core tested at 130°C and calculated bulk volume using truncated wedge equation.....	61

Table 4.10 Measurements of the average solid densities for Mons cores tested at 60°C and 130°C, and also Kansas core tested at 92°C..... 62

Table 5.1 Mass losses for Mons and Kansas cores at three different temperatures from both IC analysis and dry weight measurements after testing..... 79

ACKNOWLEDGEMENTS

Several persons have made dedicated and kind contributions to this thesis project. I would sincerely like to express my gratitude to all these persons.

I would like to express special thanks to my supervisor, Dr. Merete Vadla Madland, for her constant support, guidance and encouragement. It was a great honour to have worked under her supervision and knowledge she gave me will always be a part of me.

I also would like to thank Dr. Reidar Inge Korsnes, for his invaluable continuous contribution. Without his support I wouldn't have made it so far in my thesis. I am grateful to Wenxia Wang for helping carrying out laboratory experiments and for giving insightful suggestions. I like to thank also Dr. Anders Nerموen for sharing his expertise on the topic. Also thanks go to Kaia Olsen for sharing all the fun time we had in the laboratory.

I am grateful to friends, Dhruvit and John, for their incredible amounts of friendly help they have granted me academically and personally through the years.

Finally, I am grateful for my family for their endless love, support and trust.

CHAPTER 1

INTRODUCTION

This chapter starts with an introduction to producing chalk reservoirs of the North Sea and highlights some challenges associated with hydrocarbon production from chalk reservoirs and its corresponding consequences. In the latter half, we will look into the statement of problem followed by the objective of this thesis.

1.1 Background

Hydrocarbon bearing chalk fields within the North Sea basin are of significant economic importance since a province accounts for about 2% of world proven oil reserves and 8% of production, as well as acts as a pricing fulcrum (Watkins, 2002). Moreover, majority of the recoverable oil in the North Sea is represented by clastic reservoirs; however since 1985 chalk reservoir oil fields have exhibited significant growth in the recoverable oil (Gautier and Klett, 2005). It is considered that the complexity of chalk reservoirs and their better response on the implementation of Enhanced Oil Recovery (EOR) techniques, completion and also stimulation techniques might contribute to this growth (Megson and Tygesen, 2005).

Even though the potential rewards are great, chalk reservoirs in the North Sea present a picture of extremes. Early stage of oil production from chalk fields in the North Sea caused pressure depletion, notably Ekofisk and Valhall fields, the reservoirs have experienced compaction, and the resulting subsidence at the mudline created platform safety issues (Fig.1.1) (Doornhof et al., 2006). Although reservoir compaction has resulted in 40% and 50% of the drive mechanism in the Ekofisk and Valhall fields respectively, on the other hand the sea floor subsidence necessitated investments for field production facilities (Austad et al., 2008, Barkved et al., 2003).

After the primary production stage by pure pressure depletion, injection of seawater introduced as a secondary improved oil recovery (IOR) method to maintain the pore pressure above bubble point of the oil and production enhancement mechanism (Barkved et al., 2003, 2005; Hermansen et al., 1997). Seawater appeared to be exceptional injection fluid in the Ekofisk field, where up to 50% oil recovery has been achieved. Laboratory studies show that potential determining ions such as Mg^{2+} , Ca^{2+} and SO_4^{2-} present in the seawater was able to improve the wetting state of the chalk (Austad et al., 2005). Despite this, as waterflooding continued under voidage balancing, the subsidence rate developed with constant rate, reaching a maximum rate of 42 cm/year (Fig. 1.2) (Doornhof et al., 2006). Hence, water has a profound weakening effect on the chalk framework which regarded as water weakening phenomenon.



Figure 1.1 Picture depicts a consequence of compaction in the Ekofisk field.

Due to subsidence, the resulting loss of airgap and potential impacts on platform safety became a major concern. The 6 m increase in platform height was performed in 1987; later a new complex of platforms was installed (Doornhof et al., 2006).

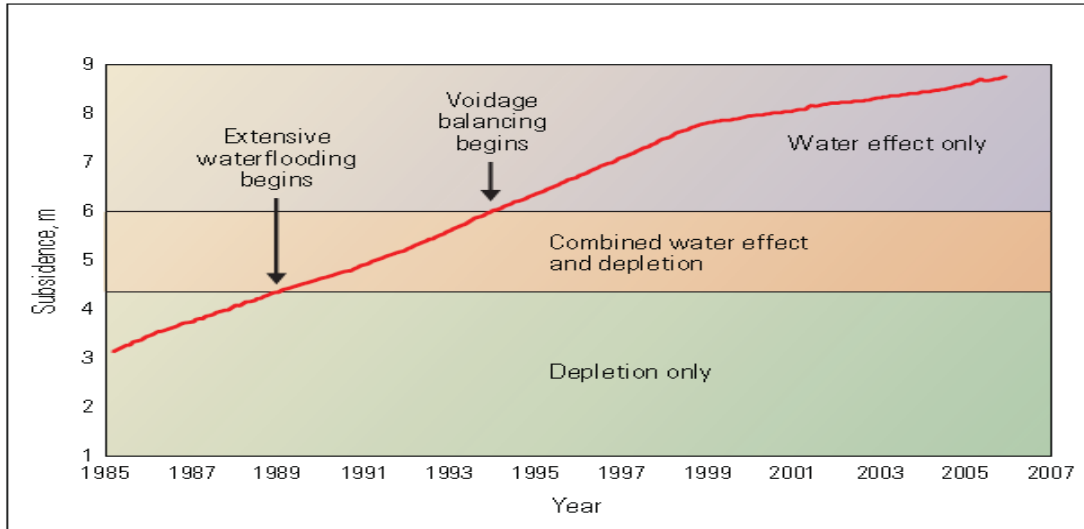


Figure 1.2 Subsidence from depletion and from water effect in Ekofisk field.

Until 1989, all subsidence at the hotel complex was due to pressure depletion. After the injection rate balanced the voidage rate in 1984, the subsidence was all due to water-induced compaction (Doornhof et al., 2006).

The mechanism for this water weakening of chalk is not fully understood, and several physico-chemical models have been suggested: change in capillary forces (Delage et al., 1996), pressure solution (Hellmann et al., 2002a,b), added pressure on the grains caused by attraction of water molecules to the chalk surface (Risnes et al., 2005), and chemical dissolution (Heggheim et al., 2005; Korsnes et al., 2006a,b, 2008; Madland et al., 2008, 2011; Hiorth et al., 2010, 2013).

Taking experimental studies of (Heggheim et al., 2005; Korsnes et al., 2006a,b; Madland et al., 2011; Nermoen et al., 2015a,b; Megawati et al., 2012, 2015; Megawati, 2015; Wang et al., 2015) and mathematical modelling of (Hiorth et al., 2010, 2013) as representative examples of water-induced compaction in chalks, they have shown that the aqueous chemistry of the pore fluid in addition to presence of non-carbonate minerals such as silica and clay minerals control the chalk mechanical behavior. Madland et al. (2011) demonstrated that injecting reactive $MgCl_2$ brine leads to supersaturation of new magnesium bearing minerals which triggers further dissolution of calcite; while injecting

NaCl brine with equal ionic strength, it was documented that minor change occurs in the aqueous chemistry.

1.2 Statement of the problem

The void fraction and flow properties are important for accurate estimation of the resource potential of the reservoirs, since the porosity determines the amount of hydrocarbon trapped inside the pores, while permeability determines the rate of production. In addition, numerous experimental studies show the link between the porosity and mechanical behavior of chalks as well as connection between the porosity and permeability (Nermoen et al., 2015a; Wang et al., 2015).

Because calcite is a reactive common mineral, its precipitation and dissolution are of great importance in the creation and destruction of secondary porosity in the subsurface. Although the importance of carbonate mineral dissolution during sediment diagenesis has been known since late 1800s, experimental determination of dissolution rates as a function of solution composition did not receive considerable attention until 1960s. Since that time a large number of investigations examined the effect of 'foreign' ions, temperature, CO₂, partial pressure and other variables on calcite dissolution rate where ionic strength of solutions did not generally exceed that of seawater (Gledhill and Morse, 2004).

The reservoir temperature at Ekofisk is 130°C and Valhall is 92°C, while the temperature of injected water is normally colder than reservoir temperature. When the formation water, which has a higher salinity and low sulfate content, is displaced by seawater, chemical processes involving dissolution-precipitation contributes to the changes in rock properties. Certainly, changing the temperature can induce strain in the material, as cold water is injected into the formation, the concern here is to what extend the rock properties are temperature dependent in contact with high ionic strength solutions and whether the non-carbonate phase has an effect on that.

When non-equilibrium nature of the rock-fluid interaction taking place inside the core, dissolution-precipitation induces mineralogical changes, thus affecting the rock and fluid

flow properties. Thus, when estimating porosity evolution, mineralogical changes must be taken into account; than solely considering porosity reduction caused by mechanical compaction. Moreover, the effect of chemical reactions on the permeability development has to be understood since the permeability is reflected in the porosity evolution.

1.3 Objective

The primary focus of this thesis is to link dissolution-precipitation to the mechanical and physical properties of chalk, and to investigate how variations in original porosity, non-carbonate minerals initially present in chalk, in addition to temperature effect on end porosity, dynamic compaction and permeability evolution.

Obviously, seawater interaction with chalk surface is complex, due to different chemical processes involving different ions present. Therefore, it is required to simplify the system and study the effect of each ion individually. Within this study, the role of Mg^{2+} ion is studied and discussed in detail from experimental point of view, although it is not an optimal EOR fluid. The ionic strength of the solution designed as same as that of seawater, to get better understanding of rock-fluid interaction when seawater injected into the reservoir. However, the purpose of this study is not to simulate water injection into North Sea chalk reservoirs at real in-situ stress and pressure conditions, rather perform a repeatable type of mechanical tests to further study and get an improved understanding of mechanisms behind the water-weakening phenomenon.

1.4 Structure of the thesis

This thesis covers literature review on the North Sea chalk reservoir characteristics and basics of rock-mechanics in Chapter 2 presenting established theories and concepts. Moreover brief review of previously proposed mechanisms for chalk-fluid interaction is also covered.

Chapter 3 highlights the experimental methodology of conducted chemo-mechanical experiments and procedures. Moreover, chemical analysis of fractioned effluent and subsequent core analysis after testing is also portrayed.

In the course of analyzing the test results, Chapter 4 presents the results from chemo-mechanical compaction experiments, chemical and core analysis. Moreover results of porosity evolution will be studied in terms of mechanical and chemical methods of estimating porosity, in addition evolved permeability through time is presented.

A general discussion on the results obtained is given in Chapter 5.

Towards the end in Chapter 6, summary and concluding remarks are mentioned followed by recommendations for future work described in Chapter 7.

CHAPTER 2

LITERATURE REVIEW

In the beginning of this chapter, a brief introduction to the geological aspects of chalk and characteristics of North Sea chalk reservoirs is given which is followed by theoretical basics of the rock mechanics to describe the response of sample during the performed mechanical test and approaches to estimate the evolution of porosity and permeability. Towards the end, we will look into brief review of previously proposed mechanisms for the fluid and temperature effects observed in chalk.

2.1 Chalk as petroleum reservoir

2.1.1 Geological aspects of chalk

Chalk is fine-grained biogenic carbonate sediments that originate as skeletons of algae known as coccospheres, with a size of about 30 μm across. The building blocks of these spheres are small calcite plates which are on the order of 0.5 - 2 μm across and the plates form assemblages of rings and rosettes with diameter of 3-15 μm , widely known as coccoliths (Fig. 2.1) (Andersen, 1995). There are other components present in chalk such as coarser calcareous skeletal grains, detrital quartz, chert, phosphate pellets and clay, that are important in some units, but are subordinate constitutions (Scholle, 1977, 1978). Thus, chalk can be very pure consisting of primarily calcite coccoliths (higher than 98%) or impure with a greater percentages of constitutions as silica, clay or calcite overgrowths between the coccoliths. The pure chalk is generally mechanically weak; on the other hand the impure chalk has greater mechanical strength from the cementation provided by silica or calcite overgrowth (Andersen, 1995, pp.2).

Mineralogically, chalks were secreted and deposited as stable low-magnesium calcite. Low magnesium calcite is less soluble in sea water than opposed, and therefore they have great

chemical stability over geologic time. Any deep ocean sediments (pelagic sediments) buried at 2000 - 3000 meter have less than 15% porosities, in contrast North Sea chalk hydrocarbon fields possess abnormally high porosities ranging from 30% up to 50% buried at the same interval. The possible mechanisms that invoked to explain the porosity preservation in this area: firstly, mechanical compaction linked to the overpressured reservoirs where the porosity is preserved as the overburden is supported by the fluids, thus the chalks are not exposed to grain-to-grain stresses at high burial depth; secondly, chemical compaction related to early oil emplacement, that retarded carbonate reactions (Scholle, 1977).

Although their porosity is high, permeability of the chalk matrix is relatively low (less than a few μD) due to small pore-throat diameters (less than 1 μD). Therefore, hydrocarbon-filled interparticle pores in chalks are productive together with only other pore types, preferably fracture pores that increase the permeability (Bjørlykke, 2010, p.150).

According to Hardmann (1982) chalk reservoir quality is dictated by variety factors, however four factors have primary significance: the purity of the chalk; the rate of the deposition that have effect on early frame-work cement; the tectonic setting of the basin and the size distribution of the coccoliths during chalk deposition.

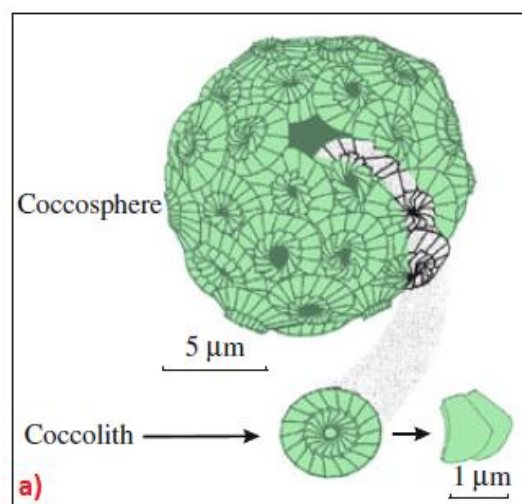


Figure 2.1 a) Skeletal structure of coccospheres and coccoliths.

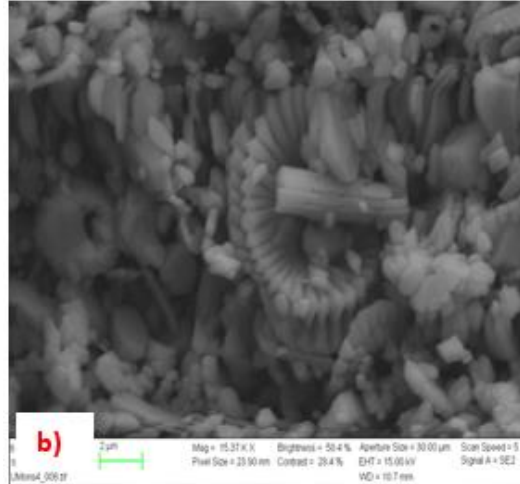


Figure 2.1 b) SEM picture of Mons chalk consisting of a mixture of coccoliths and loose plate calcite crystals.

In this example the spheroidal coccosphere is made up with many calcareous plates (coccoliths) that consist of small plate calcite crystals stacked in an imbricate pattern. From Bjørlykke, 2010.

To sum up, the geologic history conditions of chalks of the North Sea Central Graben resulted in development of high porosity, overpressured, highly saturated in live oil and fractured permeability reservoirs making the quality of reservoirs economically profitable. The Ekofisk and Valhall fields are located within the Central Graben of North Sea. Both of the field are influenced by the Tor formation which is of Maastrichtian age which is typically clean and may contain less than 5% non-carbonate minerals (Andersen, 1995). In chalk of the Valhall field high pore pressure and presence of hydrocarbons worked against recrystallization and cementation, where despite the burial depth of 3 km the porosity is preserved (35-50%). As a result, the intergranular connections are poorly developed, making the reservoir chalk mechanically weak. In contrast, in chalk of the Ekofisk field recrystallization and cementation better developed compared to Valhall, thus calcite redistribution has strengthened grain contacts providing geo-mechanically stronger chalk with lower porosity (40%) (Hueler et al., 2006).

2.1.2 Outcrop chalk

Due to scarcity of reservoir material, usually outcrop chalk of corresponding age and with similar porosity used as reservoir chalk substitutes in geo-mechanical and flooding experiments. However, the fact that outcrop and reservoir chinks have experienced different diagenetic history and the reservoir core properties altered when it is taken to the surface have raised concerns on the correlation between the outcrop and reservoir chinks. Studies on offshore and onshore chalk in the North Sea area by Huler and Fabricius (2009) suggests that chalk from Liège (Belgium), also Stevns Klint and Aalborg (Denmark) can be used as suitable geo-mechanical analogues to Valhall field due to modest calcite redistribution and poorly connected particles. Specific surface area of these chinks is comparable to that of reservoir chalk, and may constitute acceptable substitutes in flooding tests. Moreover, they emphasize that this substitution further implies comparable porosity-permeability relationship of outcrop and reservoir chalk.

The test chinks in this study are from two different localities: Mons chalk from a quarry in Belgium, Kansas chalk from quarry in Niobrara, US. The physical properties vary among the outcrop chinks (table 2.1), with Mons being characterized as pure chalk matrix with a porosity of generally 40-43% and a permeability 2-4 mD (Richard and Sizum, 2011), whereas Kansas chalk with higher content of non-carbonate mineral generally has 30-40% porosity and a slightly higher permeability 2-5 of mD (Tang and Firoozabadi, 2001). As reported by Wang et al. (2013), Upper Cretaceous chinks from Stevns Klint and Mons are very pure and like Aalborg samples contain only few amount of clastic. On the other hand, the same age Kansas chalk has highest amount of clastic similar to Liège. Thus, in overall these outcrop chinks represents suitable proxy for reservoir chalk from the Valhall and Ekofisk fields.

Chalk type	Mons	Kansas
Age	Late Campanian	Upper Cretaceous
Carbonate content, %	~99.5	~97.5
Porosity, %	42-44	37-40
Permeability, mD	2-4	2-5
Non-carbonate minerals	quartz, possibly talc	quartz, possibly talc

Table 2.1 Characteristics of outcrop Mons and Kansas chalks (Megawati, 2015).

2.2 Rock-mechanical properties

One of the significant problems that engineers and geosciences are facing when working with North Sea chalk is the mechanical behaviour of the material. Since it is of great importance to be familiarized with the rock mechanical properties of the chalk, a brief introduction to rock mechanics is given in this chapter which is mainly based on the Petroleum Related Rock Mechanics by Fjær et al. (2008) while porosity estimations is based on studies of Wang et al. (2015).

2.2.1 Elasticity

The theory of elasticity relies on the two concepts: stress and strain. Stress (σ) defined as the average force (F) acting through the cross-section area (A) and in SI unit denoted as Pa ($\text{Pa}=\text{N}/\text{m}^2$):

$$\sigma = \frac{F}{A} \quad (2.1)$$

Strain is defined as a deformation in axial or/and radial directions caused by the external forces. It is a dimensionless quantity and in the present work it is given in percentage. Since the triaxial cells were only equipped with LDVT to measure the axial strain, and no extensometers were used to measure the lateral deformations, the axial deformation will be calculated based on the changes in length in the axial direction, where L is the initial length of the outcrop, while L' is the length after the stress is applied:

$$\varepsilon = \frac{L-L'}{L} \quad (2.2)$$

2.2.2 Stress-strain relationship

The ability of the material to return to the same state after the force is released describes the primary feature of elastic material. While most of rocks behave nonlinearly when large stresses are applied, but for sufficiently small stresses their behaviour may be described by linear relationship. A material's elastic region is only a part of its behaviour as rocks, particularly chalks, can be stressed beyond the elastic limit. The failure mode for rocks can be divided into three types: tensile failure, shear failure, and yielding (pore collapse). In tensile failure when tensile stress exceeds the tensile strength, the material pulls apart. In the second shear failure mode, differences between the principal stresses are significantly larger than shear strength of the material such that material fails. In this case fractures localized in a plane can form in the material. The last type of failure mode is caused by the excess average stress on the material. In this type of failure, breakdown in the structure can be observed throughout the material. Within the chalk community, pore collapse stress is known as the one that initiates failure, and more widespread term for this is yield strength (Fig.2.1). The region beyond the yield point is called the plastic region, where even if the stress is relaxed, the material will never go back to its original shape.

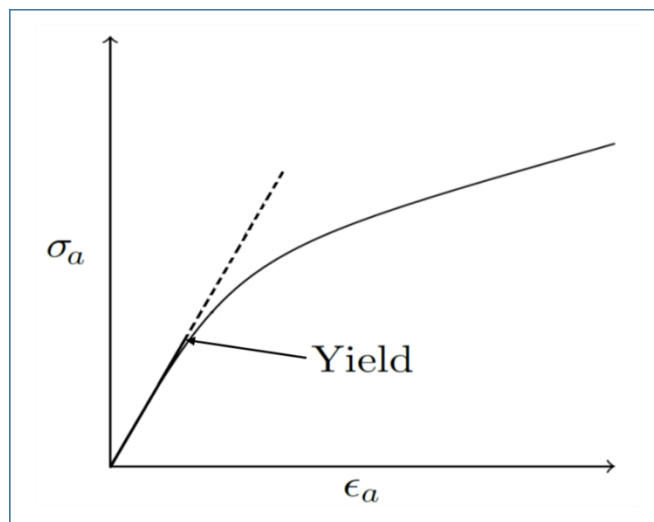


Figure 2.2 Stress-strain paths for linear and non-linear elastic materials.

2.2.3 Hydrostatic compression test and interpretation of elastic moduli

All the mechanical tests in the present work were performed under hydrostatic (isotropic) loading, where applied stress is the same in all three directions. The conducted hydrostatic test used to determine yield and bulk modulus of the rocks.

The yield point is determined from the linear regression method which is applied to the elastic region in the stress-strain curve and where the line deviated from the linear trend (Fig. 2.2). However, other methods exist and can be used to determine yield point; for example, drawing tangential line to the elastic and plastic regions, then intersection of the lines will be yield point.

Bulk modulus (K) is elastic modulus that characterizes the sample's resistance against hydrostatic compression. Under assumption in hydrostatic test, stress state in every direction is same:

$$\sigma_h = \sigma_x = \sigma_y = \sigma_z \quad (2.3)$$

Now, K can be found as a ratio of hydrostatic stress relative to volumetric strain:

$$K = \frac{\sigma_h}{\varepsilon_{vol}} \quad (2.4)$$

For calculating the bulk modulus, linear regression (curve fitting to a straight line) method is used in the graph where σ_h plotted against ε_{vol} (see fig. 2.3).

Assuming isotropic condition on the core samples, volumetric strain will be three times of axial strain ε_a , and above relation becomes

$$K = \frac{\sigma_h}{3 \cdot \varepsilon_a} \quad (2.5)$$

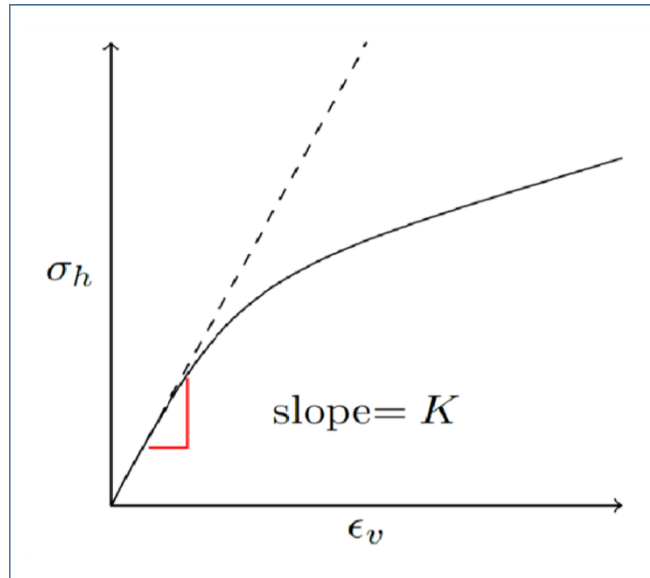


Figure 2.3 Bulk modulus is determined from the calculation of linear slope in the elastic region

When performing linear regression in the stress-strain plot, the output slope value has to be divided by 100 to stay in line with units.

2.2.4 Time dependent behaviour

Creep is a time-dependent deformation that occurs under constant stress and in our experiment is followed after the hydrostatic loading. Three distinct stages of creep during the constant loading can be observed, although depending on the physical properties of the material not all of them might be seen.

The stages of time dependent creep are illustrated in fig. 2.4.

- Primary phase (transient) is an initial period where rate of time dependent deformation decreases with time.
- In the secondary (steady state) creep phase, the strain rate is constant.
- Tertiary (accelerating) phase described by rapid increase in strain leading to failure.

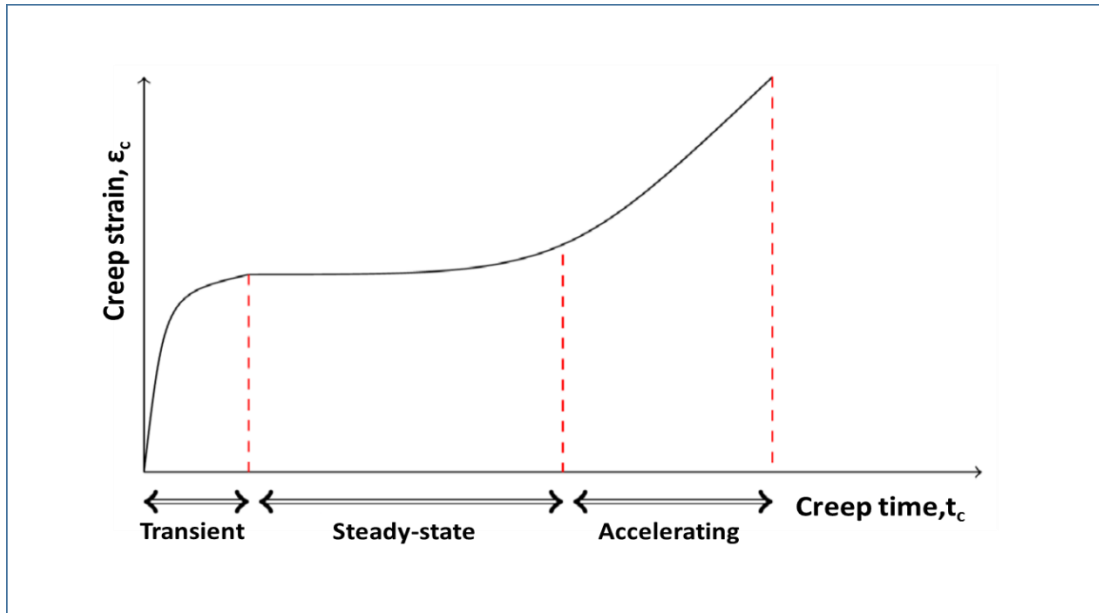


Figure 2.4 Typical Creep developments.

2.2.5 Effective stress principle

When dealing with the rock mechanical response of a porous medium, the effective stress rather important than the applied external stress on the material.

Rocks are porous media and this fact complicates the stress analysis of the state of the materials since the pressure of saturating fluid affects the stress on the solid. There are two aspects of this: firstly, the effect of the pore pressure on the grains that makes up the solid porous material; secondly effect on bulk material, including the fluid (Andersen, 1995).

The effective stress (σ_{ef}) is defined as the difference between the total (σ_h) and pore fluid (P_f) stresses:

$$\sigma_{ef} = \sigma_h - \alpha \cdot P_f \quad (2.6)$$

Here α represents Biot coefficient, which is a measure of change in pore volume relative to the change in bulk volume at constant pore pressure.

Thus, as outlined by Terzaghi, increasing external hydrostatic pressure produces the same volume change as reducing the pore pressure with the same amount.

2.2.6 Porosity estimation

At any given time, the bulk volume (V_b) of a bi-phase material is given by the sum of the volume of the pores (V_p) and solids (V_s):

$$V_b = V_p + V_s \quad (2.7)$$

Porosity is a fraction of pore volume given by the ratio of pore volume to the bulk volume:

$$\Phi = \frac{V_p}{V_b} \quad (2.8)$$

The initial porosity (Φ_0) is estimated from the weight difference between saturated ($M_{sat,0}$) and dry ($M_{dry,0}$) core divided by the density of the distilled water (ρ_{dw}) times the initial bulk volume ($V_{b,0}$):

$$\Phi_0 = \frac{M_{sat,0} - M_{dry,0}}{\rho_{dw} \cdot V_{b,0}} \quad (2.9)$$

After dismantling the test, the diameter was measured at intervals (L_i) along the core to enable accurately estimate the total bulk volume from the sum of truncated wedges $i = 1, 2 \dots 7$ along the core:

$$V_{b,end} = \sum_i^7 \frac{L_i \cdot \pi}{3} \cdot \left(\left(\frac{D_i}{2} \right)^2 + \left(\frac{D_i}{2} \right) \cdot \left(\frac{D_{i+1}}{2} \right) + \left(\frac{D_{i+1}}{2} \right)^2 \right) \quad (2.10)$$

To estimate the total volumetric strain (ϵ_{vol}) change in bulk volume before ($V_{b,0}$) and after $V_{b,end}$ testing was used:

$$\varepsilon_{vol} = -\frac{V_{b,0}-V_{b,end}}{V_{b,0}} \quad (2.11)$$

It is standard procedure in triaxial compression experiment to obtain positive volumetric strain since the volume or length of the core is reduced as an effect of applied stress. For a bi-phase material, any change in the bulk volume (ΔV_b) is given by the change in the pore volume (ΔV_p) plus change in the solid volume (ΔV_s):

$$\Delta V_b = \Delta V_p + \Delta V_s \quad (2.12)$$

Assuming that all the deformation is induced by the pure pore volume reduction due to mechanical compaction, and neglecting chemical reactions taking place inside the core by setting the solid volume is constant ($\Delta V_s = 0$), the bulk volume change becomes equal to pore volume change as:

$$\Delta V_b = \Delta V_p \quad (2.13)$$

If this assumption is valid, the porosity evolution can be estimated combining the equations (2.8, 2.10, 2.11, and 2.12) as:

$$\phi_{end,1} = \frac{V_p + \Delta V_b}{V_b + \Delta V_b} = \frac{\phi_o - \varepsilon_{vol}}{1 - \varepsilon_{vol}} \quad (2.14)$$

The index 1 refers to the first method of calculating porosity evolution and regarded as mechanical porosity.

The second approach of estimating porosity evolution is using the difference between saturated ($M_{sat,end}$) and dry ($M_{dry,end}$) core after the test:

$$\phi_{end,2} = \frac{M_{sat,end} - M_{dry,end}}{V_{b,end}} \quad (2.15)$$

This method is referred to chemical porosity where rock-fluid interaction is taken into account by including in the formula new pore volume and new bulk volume after test.

Another approach of estimating porosity development after testing is by utilizing new density, new dry mass and new bulk volume. Following the core dismantling, to provide accurate estimation of solid volume measurements, the core was divided into seven pieces. Dry mass of each core measured on the scale, while solid volume was measured by the pycnometer. Hence, the average mineral density of each slice was estimated from the relation between dry weight and measured solid volume as:

$$\rho_{s,i} = \frac{M_{dry,i}}{V_{s,i}} \quad (2.16)$$

where $i = 1, 2, \dots, 7$. The average solid mineral density of the flooded core after testing was estimated from the weighted average by volume:

$$\rho_{s,end} = \frac{V_{s,1}\rho_{s,1} + V_{s,2}\rho_{s,2} + \dots + V_{s,7}\rho_{s,7}}{\sum_i V_{s,i}} \quad (2.17)$$

With average mineral density after flooding test, the dry mass and bulk volume after the experiment is used to estimate the porosity evolution:

$$\phi_{end,3} = \frac{V_p}{V_b} = 1 - \frac{M_{sat,end}}{\rho_{s,end}V_{b,end}} \quad (2.18)$$

Equation (2.18) is referred to as third method of estimating porosity.

To sum up, method 1 is mechanical porosity, where only bulk volumetric deformation is accounted, while method 2 and 3 is based on chemical alterations inside the core, where changes in density and mass is taken into account.

2.2.7 Permeability estimation

Core plugs permeability has been determined from the measured pressure drop across the core when the testing brine is flooded through the core. Assuming laminar flow in the

porous media, Darcy law can be used to estimate the dynamic permeability which is dependent of hydraulic pressure difference across the core (ΔP):

$$k = \frac{4\mu_w L q}{\pi d^2 \Delta P} \quad (2.19)$$

where L is the core length, and πd^2 is cross sectional area, and μ_w is viscosity of the brine. Brine viscosity is determined from CREWES Fluid Properties Explorer. The software calculates the viscosity of NaCl brine based on the temperature state of the fluid. Since no other sources were found to calculate directly the viscosity of MgCl₂, NaCl viscosity values were used assuming that both of the brines have the same ionic strength.

2.3 Proposed mechanisms affecting rock-fluid interaction

In petroleum engineering, the concepts of water-weakening and temperature weakening are important mechanisms for achieving increased production of hydrocarbons. It is well documented that the chalk is stronger when oil-saturated than water-saturated and the temperature weakens the fluid saturated chalk. This section briefly discusses comprehensive review of diverse work done by Andreasen (2011) and Gutierrez et al. (2000) of previously proposed mechanisms for the fluid and temperature effects observed in chalk. However, a complete review of all the mechanisms of water weakening is beyond the scope of thesis.

The main mechanisms proposed to explain rock-fluid interaction fall into three groups. The first method is physical mechanism. Often-encountered physical mechanism states that the water-weakening is based on capillary effects, where local water menisci around the grain contacts strengthen the chalk for dry and oil-saturated specimens, while disappear for fully saturated chalk. However, capillary effects may not be the cause for the water weakening in fully saturated chalk that is demonstrated by test series on water-ethylene glycol mixtures, with water completely miscible in glycol (Risnes et al., 2005).

Physico-chemical effect is another approach and physico-chemical stated mechanism refers to the adsorption of water on chalk surface by Rhett (1999), water activity when changing the ion concentration in the pore fluid by Risnes et al. (2003), etc.

Finally, chemical effects are another explanation for the weakening of chalk. Since primary focus on this thesis is to link the chemical effects on the rock-mechanical and flow properties, this method in the following will be reviewed in detail.

2.3.1 Chemical mechanisms of water weakening

In the last decades, extensive research has been devoted for the chemical effect. Although first attempts state back to early 1980s, when Newman suggested that the ionic composition of the brine injected to already aqueous saturated chalk impacts the mechanical strength, chemical aspect of water weakening of chalks have received relatively less attention. The reason is the very low solubility of calcium carbonate in water. Another reason is related to the inverse relation between the solubility product of CaCO_3 and temperature, where it is controversial to explain why water weakening is more profound at higher temperatures (Korsnes et al., 2008; Madland et al., 2011).

Discovery by Heggheim et al. (2005) suggests that non-equilibrium brines might trigger the dissolution process which has an impact on the mechanical strength of chalk. This furthermore encouraged to examine the chemical aspects of water-weakening as per (Madland et al., 2006, 2008, 2011; Korsnes et al., 2006a,b, 2008a; Zangiabadi et al., 2009; Megawati et al. 2011, 2015) numerous flooding experiments with brines of various ionic composition have been carried out. Thus, often-encountered the mechanisms are the substitution and dissolution/precipitation processes.

The chalk fluid interaction is shown to be strongly influenced by variations in testing temperature. The chemical effects of seawater-like brines, Ekofisk formation water and distilled water have been studied extensively to what extent these brine affect the mechanical strength of chalk (Korsnes, 2007; Korsnes et al., 2006a,b, 2008; Madland et al., 2008; Zangiabadi et al., 2009). Rock-mechanical and pure flooding studies at elevated

temperatures for Stevns Klint, Rørdal, Lixhe, or Kansas have usually shown that the chemical composition of the saturating fluid has significant effect on the mechanical strength of the chalk. Moreover, the presence of sulphate ions in the seawater-like brines has pronounced effect on the chalk framework at elevated temperatures. Studies by Korsnes et al. (2006a, b, 2008) suggest that the chemical weakening of chalk in contact with seawater-like brines seems to take place when Mg^{2+} ions in solution substituted Ca^{2+} ions at the intergranular contacts if SO_4^{2-} ions are present. Moreover it was also suggested that this weakening progresses with increased temperature. Furthermore, this suggested substitution mechanism of water-weakening cannot support results of experiments conducted on the Kansas cores at 90°C (Madland et al., 2008; Zangiabadi et al., 2009) where weakening of chalk exposed to seawater-like brine observed without Mg^{2+} ion in the solution (Madland et al., 2011).

Moreover, studies by Madland et al. (2011) further examined this substitution mechanism, by comparing the loss of magnesium from flooding experiment with the maximum available absorption site. The amount of magnesium lost was significantly higher than calculated number of available sites, thus substitution mechanism of Ca^{2+} by Mg^{2+} cannot solely explain the weakening phenomenon.

Furthermore, as per studies by Heggeim et al. (2005) concluded that chemical mechanism involving dissolution-precipitation plays an important role when the chalk is subjected to seawater at 130°C. In light of this study, Madland et al. (2011) introduced a new hypothesis of water-weakening phenomenon: precipitation of magnesium as new phase of mineral. In their studies, assuming that a chemical equilibrium can establish between the rock matrix and fluid, equilibrium calculations pointed out that huntite is the most oversaturated mineral. From modelling studies, it was observed that even though at pH value close to a natural in order to equilibrate with the fluid, the chalk has to dissolve.

This findings further motivated in depth investigate the dissolution/precipitation effect on the chalk rock-mechanical behaviour and several valuable experimental investigations and modelling carried out by (Megawati et al., 2011, 2015; Hiorth et al., 2013; Nermoen et al., 2015a,b). These studies clearly point out that disturbance of the chemical equilibrium

impacts the macroscopic behavior of chalk. For example, Mg-rich brine is shown to impact the equilibrium chemistry towards precipitation of secondary minerals and dissolution of calcite. Whereas, in combination with sulfate ions, calcium favors supersaturation of anhydrate. Moreover, it was observed that at higher concentration, addition of calcium into Mg-rich brine prevents further dissolution of calcite (Megawati, 2015). In addition, evidence of mineral precipitation has been seen from SEM images after analyzing the flooded cores (Madland et al., 2011), as well as supported by geo-chemical analysis (Zimmermann et al., 2015).

CHAPTER 3

METHODS AND EXPERIMENTAL PROCEDURES

This chapter highlights the experimental methodology of conducted chemo-mechanical experiments. The chapter starts with the core and fluid preparation procedures, and then presents detailed description of the experimental setup. The sections following this cover methodology of the rock-mechanical tests and analysis of the plug after testing. In addition, description of chemical and textural analysis is also included.

All mechanical tests were performed in a hydraulically operated triaxial cells. The cells are designed such that high pressure and high temperature rock mechanical tests can be performed. The testing temperatures were: 60°C, 92°C and 130°C. Reservoir temperature of Valhall field is 92°C whereas that of Ekofisk field 130°C. Both tests provide necessary data to evaluate the mechanical strength of the chalk cores. The injected reactive $MgCl_2$ brine enables to evaluate the porosity and permeability evolution when chemical reactions take place inside the core. Tests were performed under drained condition, which has two advantages: the core permeability is easily determined from the measured pressure drop across the core; in addition, quantification of chemical composition of fractioned effluent is also possible.

3.1 Preparation of core material and flooding fluids

3.1.1 Outcrop chalk

Large sample blocks from two different sources (outcrop chalk Mons from Mons basin, Belgium and Kansas from Niobrara, Kansas quarry, US) were used in the present study.

For homogeneity, all samples for the experiment were taken from the same block of chalk, and then drilled out using a drilling machine in the same direction with an oversized bit and circulating water for cooling. When doing research it is important to have comparable testing material and this has been studied by Korsnes, 2008. His experiment results

showed that mechanical properties of the chalk such as bulk modulus, yield strength, axial and radial creep displayed anisotropic behaviour depending on the vertically or horizontally drilled direction, but it had minor effect on the permeability measurements that is likely to be controlled by the total volumetric strain.

The drilling direction was marked on each drilled sample to ensure that all mechanical tests performed with similar orientation. Afterwards, cores were put in a heating chamber and left to dry overnight at 120°C. Then the oversized samples were shaped in a lathe machine to get diameter of 38.1 mm and cut to length approximately of twice the diameter size by a diamond saw. In order to have a reference sample to compare the flooded cores after the testing with un-flooded one, a small pieces from the top and bottom of the core were cut off, so this end samples will be used later to study the chemical effects of test brine during SEM analysis.

Before testing, the dry mass of the core was measured after being dried in a heating chamber for more than 24 hours at 120°C. Then, to estimate the initial porosity, the samples were put in a vacuum chamber to saturate with distilled water and the pressure was lowered to 4-5 Pa inside the chamber (Fig. 3.1 a). This gives quite accurate porosity measurement since vacuum saturation enables the samples to be fully saturated. Thereafter weight of the plugs was measured. To get a precise estimate of the bulk volume a digital vernier caliper was used to measure the diameter and length of the each core. The weight analysis (described in theory part) is used to determine the initial porosity. Typical properties of the outcrop chalks and their testing temperature are given in table 3.1-3.2.

Sample ID	M 4	M 2	M 3	M 6
Core length, (mm)	72,47	73,04	72,2	72,02
Core diameter, (mm)	38,1	38,1	38,1	38,1
Dry weight, (g)	128,13	129,2	127,23	127,54
Saturated weight, (g)	163,2	164,18	162,21	162,19
Porosity, %	42,34	42,11	42,50	42,20
Test temperature, C	60	92	92	130

Table 3.1 Physical data for Mons cores

Sample ID	K 3	K 1	K 2
Core length, (mm)	71,32	71,12	72,11
Core diameter, (mm)	38,1	38,1	38,1
Dry weight, (g)	139,49	139,06	140,59
Saturated weight, (g)	169,04	168,61	170,58
Porosity, %	36,34	36,44	36,48
Test temperature, C	60	92	130

Table 3.2 Physical data for Kansas core

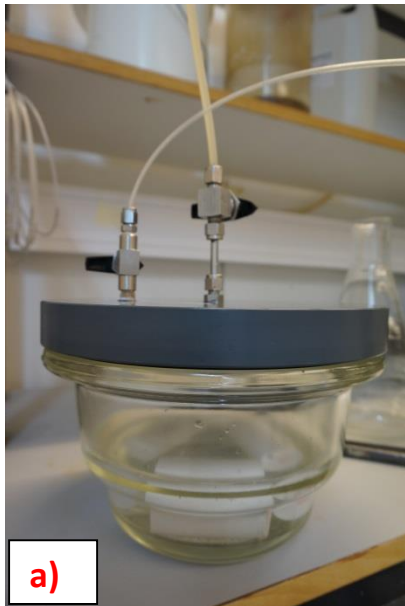


Figure 3.1 a) Saturating the plug in the vacuum chamber with distilled water



Figure 3.1 b) the conical flask is placed on a magnetic stirrer.



Figure 3.1 c) Filtrate-apparatus from Millipore used to filtrate the brine. A 0.65 µm filter used consistently for all the brine prepared.

3.1.2 Saturating and flooding fluids

Distilled water (DW) is used as a saturating fluid, while as a flooding fluid, we used MgCl₂ brine. To prepare the brine, conical flask filled with nanopure distilled water and mixed with 44, 5 g/l MgCl₂ ·6H₂O. Then this conical flask is put on a magnetic stirrer and left for about 2 hours to mix before filtration (Fig. 3.1 b). The filtrating apparatus was used with 0.65 μm filter from millipore to remove any impurities that contain solution (Fig. 3.1 c). Afterwards, the brine was measured for pH using pH meter.

The ionic strength of the brine is calculated as:

$$I = \frac{1}{2} \sum_{i=1}^n C_i Z_i^2$$

Where C_i is the molar concentration (mol/l) of an ion i and Z_i is valence number of the ion. It is important to be aware of that the calculated ionic strength of MgCl₂ brine has to be similar to those of synthetic sea water that is injected to North Sea chalk reservoirs.

Ion	Concentration, mol/l
<i>Mg</i> ²⁺	0,219
<i>Cl</i> ⁻	0,438
Ionic strength	0,657

Table 3.3 Ionic composition of test brine

3.2 Test equipment

3.2.1 The triaxial cell

The cell consists of three main building blocks: the loading piston, confining chamber and a loading frame. By simply pumping oil into and out of the upper and lower chambers respectively, the piston can be the moved. The axial movement of the piston is recorded into the logging software by using LVDT (Linear Variable Differential Transformers), placed on top of the piston outside the cell. The confining chamber is filled with synthetic

oil after the core mounted within the cell. Oil is systematically pumped throughout the test into the chamber to build and maintain confining pressure. The illustration of the triaxial cell is given in figures 3.2-3.3. The triaxial cell is designed such that the application of confining pressure is also compensated in the axial direction. Because of friction between cell and top piston, an additional axial load is required for the piston to follow the core deformation. Based on the friction area for the individual cell, the friction is calculated. With the extra load applied on the piston, the additional axial pressure compared to the confining pressure during isotropic compression test is very small, less than 0.3 MPa. All the tests in the present work were performed under drained condition, where fluid is allowed to exit out of the core, regulated by back pressure valve. Prior to starting any mechanical test, all the tests were preset to the reference condition. These are: confining pressure of 1,2 MPa, pore pressure of 0,7 MPa, and additional axial pressure of 0,4-0,7 MPa (depending on the particular cell used), and also temperature are set to 60, 92 and 130 °C. To ensure homogeneity in the test condition, the same triaxial cell is used for similar series of tests.

3.2.2 Additional belongings of the test apparatus

Pump and flooding cell

In total three Gilson 307 pumps were used to control: confining, piston and flooding pressures in each experimental setup. The confining and piston pressures were operated by pumping directly oil into the system, while the flooding pump was operated through flooding cell. Distilled water is pumped into the upper chamber of the cell that enables brine in the lower chamber to be displaced to the flooding system. Since the injecting brine contains salt, this might cause clogging of the tubing lines, and consequently salt precipitation and corrosion inside the tubing might take place. This is the primary reason of utilizing flooding cells.

Gauges

Digital pressure gauges manufactured by Emerson Rosemount were employed for measuring confining, piston, pore pressures and differential pressure resulted from the flooding of the fluid through the core. These gauges send signal to the logging software that displays it on the computer connected to the test cell.

Heating system

It is necessary to have a heating system in order to perform the experiments at elevated temperatures. This is done by using heating jacket which is mounted outside the confining chamber and regulated by an Omron control box and PID-routine. Since room temperature is not always stable, small fluctuations in the temperature might also observed (± 0.02 °C).

Software

The conducted experiments were controlled through LabView (Laboratory Virtual Instrument Engineering Workbench) programming. It is ideal tool for monitoring, remotely controlling, graphing in real time the triaxial test performance, and data acquisition, through data-loggers. Data logged by the program is written to a file that can be opened by *Microsoft Excel*. The pressures, axial strain dynamics, and also stress state are logged into the LabView such that the mechanical behavior of the core can be monitored as an effect of temperature, injected brine and applied stress throughout testing.

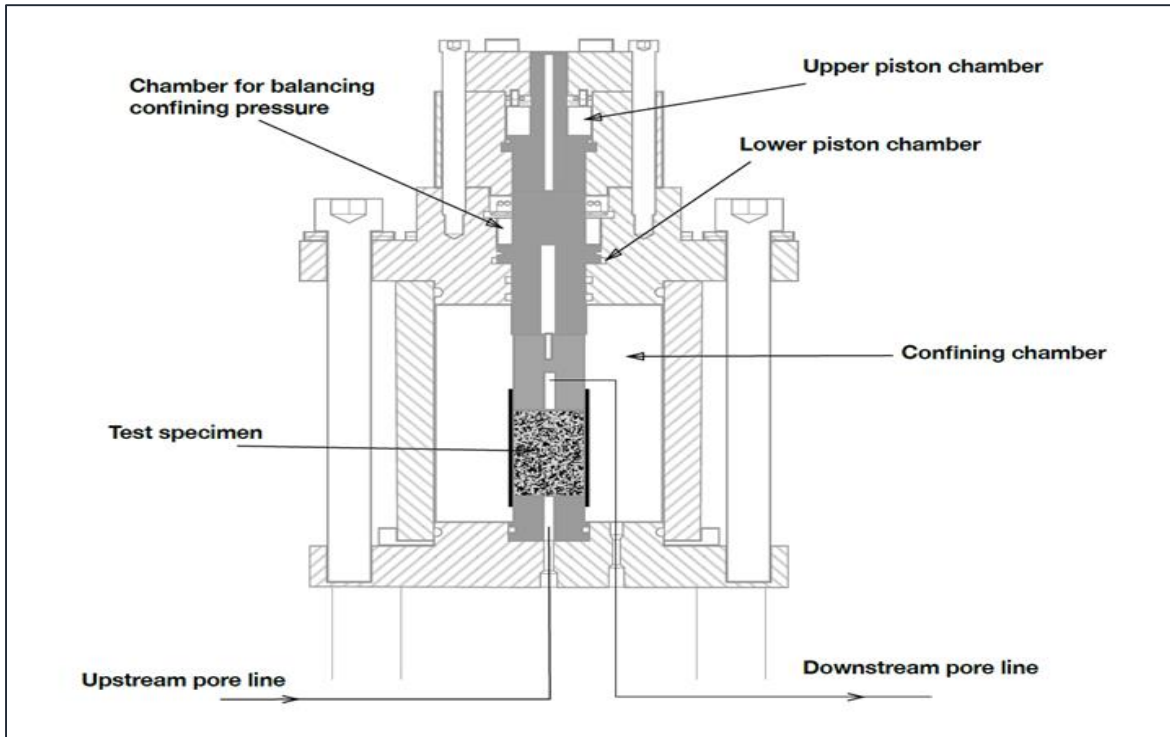


Figure 3.2 Principle sketch of the interior of a triaxial cell (Kjørsløvik and Østensen, 2014).

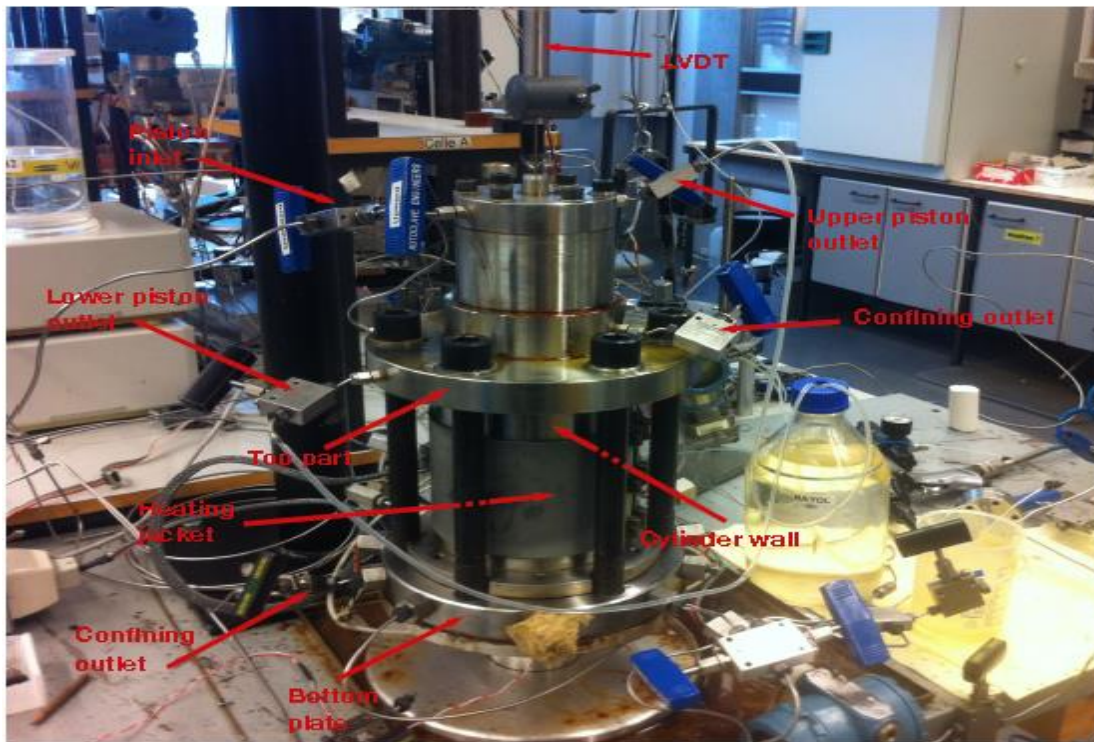


Figure 3.3 Illustration of the exterior of a triaxial cell (Kjørsløvik and Østensen, 2014)

3.3 Testing procedure

3.3.1 Mounting the cell

Before mounting the core within the cell, first the system must be flooded with distilled water to ensure that there is no air present in valves and tubes. Afterwards, a drainage disk, that enables the fluid to be evenly distributed around the circumference of the core, is placed on the lower flooding piston (Fig. 3.4 a). From one of the experiment that failed, we came to conclusion that it's better to have holes in the drainage disk far away from the edge of the core to avoid excessive gathering of fluid near the edge of the core during flooding experiment. This causes erosion of core material and leads to expansion of holes resulting in failure.

The saturated core is placed on top of the disk, and then followed the second drainage disk (Fig. 3.4 b, c). Silicone grease is applied around these upper and lower pistons and fastened by rubber seals. The purpose of applying silicone grease is to prevent leakage between rubber seal and piston. Now the upper flooding piston is placed to complement the lower one and then shrinking sleeve put on top of all, which has to be long enough to cover the rubber seals and the core (Fig. 3.4 d). A heat is gently applied around the core to jacket the sleeve around the core to prohibit leaking of confining oil into the core (Fig. 3.4 e). The final step in mounting the core is to connect upper flooding piston to the bottom plate which in later stage will be used to build up pore pressure by opening bypass valve (Fig. 3.4 f). When the core is mounted, the cylindrical steal wall is placed that makes up the confining chamber (Fig. 3.4 g). Before that, heat resistant o-rings are used to ensure that the system remains closed during the high pressure and high temperature test. A heating jacket must be put around the cylindrical wall to carry out the experiment at elevated temperatures before attaching the top part of the cell (piston assembly) (Fig. 3.4 h). While doing so, the upper confining outlet has to be opened to release the abundant oil inside the confining chamber. Six steal bolts are used to tighten the top part of the cell to the lower plate. Eventually, the LVDT is placed on top of the cell (Fig. 3.4 i). The LVDT has an uncertainty in

the measurements of ± 0.05 mm. Step by step illustration of the procedure is given in figure 3.4.

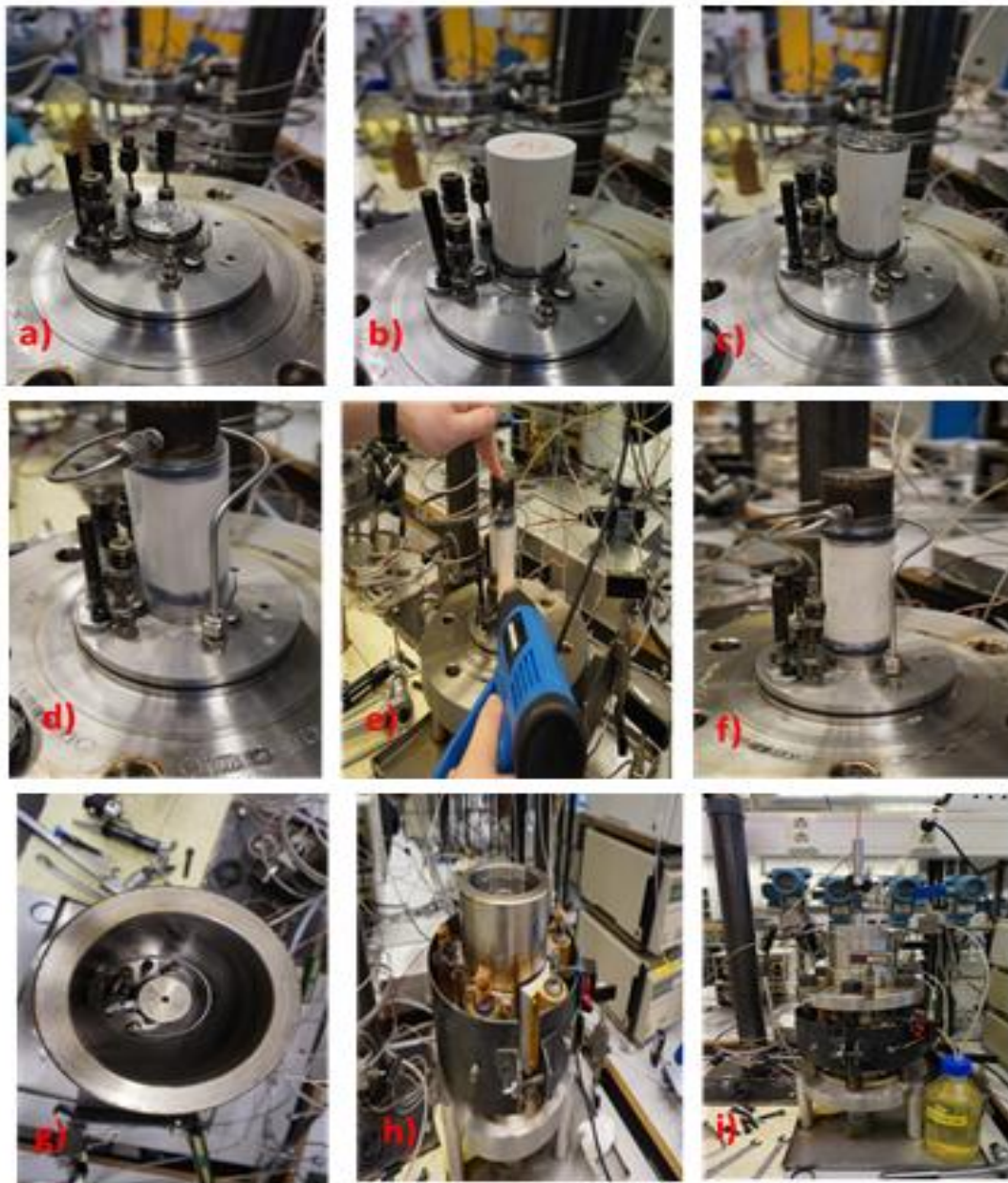


Figure 3.4 Step-wise mounting process of the core in the triaxial cell.

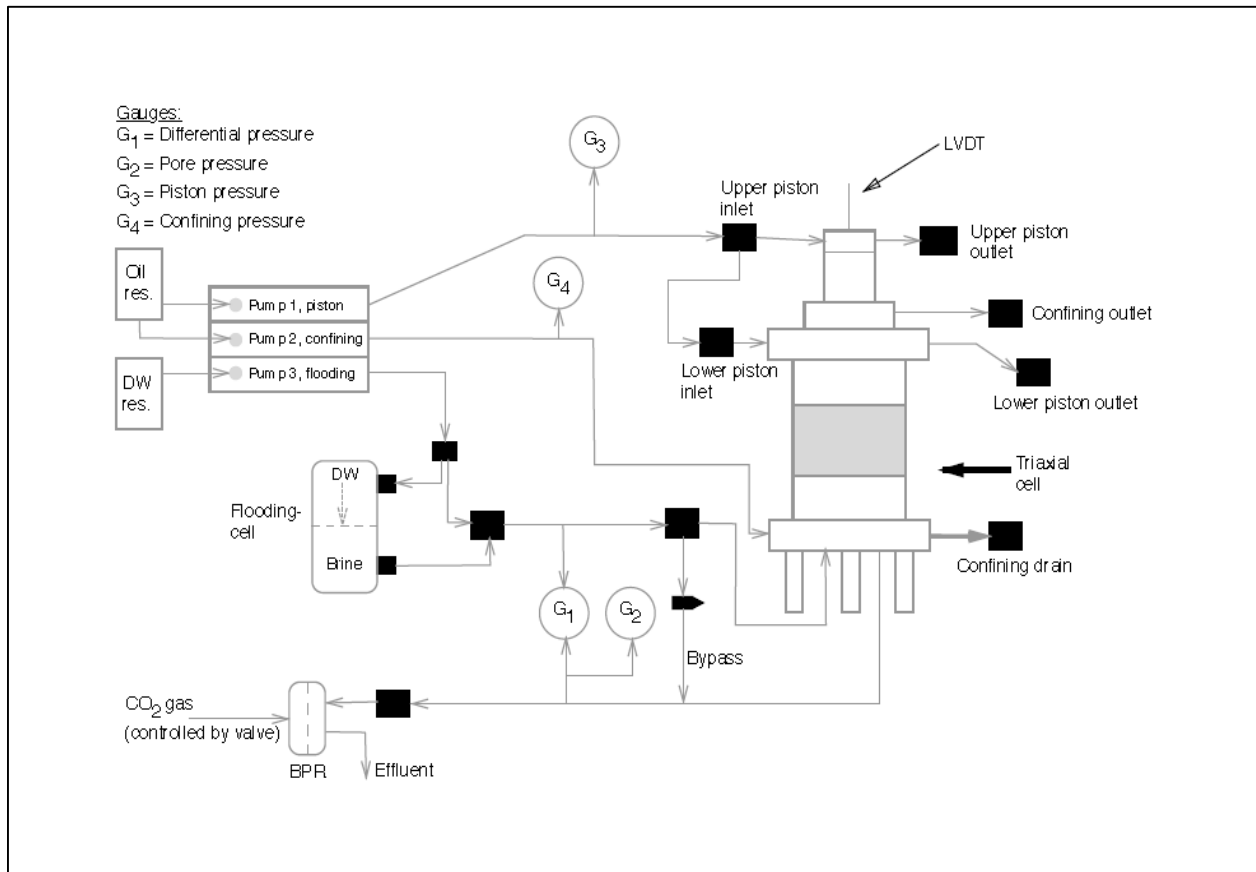


Figure 3.5 Illustration of the experimental setup (Kjørsløvik and Østensen, 2014).

3.3.2 Starting the test

Prior to increasing the confining pressure, the air inside the cell is let to go out of the system by opening upper confining valve so that pressure can build up faster. When continuous flow of oil is observed without bubbles inside the tubing the valve can be closed. Setting flow rate maximum 2 ml/min the confining pressure is increased to 0.5 MPa. After reaching the desired pressure, the core must be cleaned by flooding distilled water (minimum two pore volumes) with a flooding rate of maximum 0.2 ml/min by starting the permeability pump. Puntervold et al. (2007) claim that this way ensures a clean pore system, due to the fact that different ions might be present as natural pollutions originating from the location of outcrop (Madland et al., 2011). Later, injection of magnesium brine

was started with a rate of maximum 0.2 ml/min to saturate the core. At least two pore volumes are flooded.

3.3.3 Increasing pore pressure

After flooding minimum two pore volumes of the test brine, the pore pressure was increased to 0.7 MPa by running the permeability pump. Prior to that, the bypass valve has to be opened so that brine will not flow through the core, but deflected in the outlet thereby flooding simultaneously both sides of the core and rapidly increasing the pressure. As mentioned earlier, the flooding brine comes from the flooding cell. The permeability pump started pumping distilled water with 3ml/min flow rate into upper chamber of the flooding cell and this in turn pushed down the piston inside the cell and letting to test brine to be flooded through the flooding line with the same rate as distilled water was pumped into the flooding cell. During pressure build-up, the confining pressure and pore pressure were simultaneously increased to a differential stress equal to 0.5 MPa, having $\sigma_{iso}=1.2$ MPa and $P_p=0.7$ MPa respectively. The pore pressure is controlled using back-pressure regulator ensuring constant pore pressure of 0.7 MPa. This back-pressure valve operates using CO₂ gas. To be able to increase the pore pressure, the gas pressure has to be increased, that pushes a circular plastic disk inside the valve to the direction opposite to the flow of brine, and thus retarding the effluent to exit from the core until the pore pressure reaches 0.7 MPa. When the pore pressure reaches 0.7 MPa it has capacity to overcome the opposite force coming from the disk so the effluent starts flowing. As long as the pore pressure has reached the desired value, the bypass can be closed and the permeability pump rate is reduced so that one pore volume per day is injected. This rate is determined from the ratio of pore volume to the time; usually it has approximate value as 0.024 ml/min.

3.3.4 Increasing temperature

The next step after the pore and confining pressure was increased to differential pressure 0.5 MPa, the heating jacket was connected to the control box. To have a control over the

temperature increase (60°C, 92°C and 130°C), the PID values for each set of experiment were identified.

When the temperature of the system is increased, the oil inside the confining chamber expands, thereby leading to increase in confining pressure. Thus a spring valve connected to the bleed of valve (confining outlet) is used to regulate the confining pressure throughout this temperature increase stage. The outlets of piston chambers have to be open during the temperature increase; otherwise the oil in the piston chambers will expand resulting in very high pressure values.

3.3.5 Pushing down the piston

After the set temperature was reached, the piston has to be lowered until it hits the core. To lower the piston, the oil is pumped with a flow rate of 0.3 ml/min using piston pump through the upper piston inlet; upper piston outlet and lower piston inlet has to be closed. However, lower piston was kept open to allow the oil to come out when piston displaces down. When piston hits the core, an overpressure of around 0.3 MPa is necessary to make certain that piston is in contact with the core.

3.3.6 Hydrostatic compression test

Hydrostatic compression tests (isotropic test) were performed during all cases of study. As mentioned earlier, the extra axial pressure relatively to the confining pressure under hydrostatic compression test is small, less than 0.3 MPa. Thus, the test is not purely isotropic, but rather quasi-isotropic. Before starting the hydrostatic loading phase, the confining outlet valve has to be closed and the spring valve utilized during the temperature increase stage has to be removed. The hydrostatic test was performed by increasing the confining pressure to a desired value with a pumping rate of 0.05-0.1 ml/min corresponding to approximate 0.02 bars per minute. In test series performed on Mons chalk, the desired value was around 13 MPa, while for Kansas chalk about 23 MPa. The pore pressure kept constant equal to 0.7 MPa. When the confining pressure is increasing,

the friction on the piston will also increase. This might lead to stop the piston, thus during hydrostatic loading phase the axial movement has to be monitored, so if the piston stops its movement down, then to overcome the friction the piston pressure must be increased. When desired value of confining pressure is reached, the hydrostatic phase is ended. Then the test will be running in the creep phase for a desired amount of time frame. From the stress versus strain plot, yield point and bulk modulus are calculated.

3.3.7 Creep phase

The creep is followed after the hydrostatic compression phase, where the core left to deform under constant stress. Flooding of $MgCl_2$ brine is kept at constant rate throughout the creep period. Deformation is measured continuously with a minimum of 3 minute resolution time. Creep strain is calculated with reference to the displacement after the compression test. Creep stress level is kept same within the same chalk type, 14 MPa and 23 MPa for Mons and Kansas chalks respectively.

3.3.8 Sampling fractioned effluent

The fractioned effluent samples were collected with two purposes: firstly, to analyse the samples for ionic composition; secondly, to analyse how the pH of the injected fluid will behave throughout the experiment. The collection of fractioned effluent samples for ionic composition analysis started from hydrostatic loading phase, where initially samples were been collected in the first 3-4 days, later three times in a week. The reason for sampling effluent so often in the beginning is to obtain sufficient data about how rock-fluid interacts when reactive test brine is injected into the core, since the injected fluid to obtain equilibrium with the core takes time and chemical reactions might take place. For the composition analysis the sampling glasses weighted before and after the flooding, so the flooding rate of the test brine can also monitored. Then samples were labelled with name, time, weight, and stored in the refrigerator to avoid evaporation. For the pH analysis, the effluent was sampled twice in a week and the values of each measurements and sampling date were recorded.

3.3.9 Dismantling the test

When time to stop the test had come, the cores were washed with distilled water by switching the flooding from test brine to distilled water. At least two pore volumes of water were used for flooding.

After cleaning, the upper piston inlet valve is closed and lower one is opened so the piston can be lifted up. The upper piston outlet valve is opened; the lower piston valve is closed. Then, the temperature has to be turned off by disconnecting the heating jacket from the control box. As temperature decreases, the volume of the oil inside the chamber will reduce, causing decline in the confining pressure. To overcome this, constant rate of 1.0 ml/min oil flooded into the chamber to keep confining pressure at 11 MPa.

When the temperature is low enough, the pore pressure is reduced by setting the back pressure regulator to 0 bars. Afterwards, permeability and confining pump is stopped and confining pressure is also reduced to 0 bars by opening the lower confining outlet valve. Compressed air is used to completely squeeze out the oil from the system. Now the cell can be dismantled. After dismantling, the saturated weight of the core was immediately measured and then dried at 110°C in the heating chamber until the weight is stabilized to measure the dry weight.

3.4 Chemical analysis of fractioned effluent

Gilson GX-271 liquid handler was used to dilute the effluent samples. The reason for diluting the sampled effluents is to stay in the linear region of the calibration curve while testing on the ionic concentrations with Dionex ICS-300 182 ion-exchange chromatograph. The effluent has been tested for Mg^{2+} , Ca^{2+} , Na^+ and Cl^- ions.

The first step in performing dilution is to prime the machine, then dilute effluent samples and also reference standards 500 times with distilled water. The standards include:

1. Original injected $MgCl_2$ brine. Concentrations of ions in the standard: 0.219 mmol/g Mg^{2+} , 0.438 Cl^- mmol/g.
2. Synthetic sea water (SSW)
3. Magnesium-calcium chloride $MgCaCl_2$ standard. Concentrations of ions in the standard: 0.219 mmol/g Mg^{2+} , 0.438 mmol/g Cl^- , 0.013 mmol/g Ca^{2+} .

Then the diluted samples have to be prepared for Ion Chromatograph (IC) test. For that, the syringe is cleaned with distilled water and wet with diluted sample. Then the remaining diluted fluid is filled up with syringe, flushed through filter until 3 ml is left inside the syringe and transferred into two special glasses designed for IC test with the filter on.

Prior to the ion analysis test, the anion and cation pumps, and also syringe were primed. The following settings were used for the test:

1. Anion: 12 min, 18 mM effluent concentration, 45 mA suppressor current
2. Cation: 30 min, 15 mM effluent concentration, 44 mA suppressor current

After the IC test finished, the peak values were adjusted to obtain better comparability of the data, then the obtained area values for each sample were transferred into spreadsheet to calculate the concentrations. Molar concentration of standards was used as a reference such that relative areas of each sample can be converted into molar concentrations.

3.5 Measurement of chalk mineral density

The solid volume of samples was obtained with *AccuPyc II 1340 gas pycnometer*. This technique is non-destructive and accurate since gas displacement method used to measure the volume. The dry sample of chalk was placed into the volume chamber and helium gas filled the pores of the sample. Depending on the size of the particles, 35 cm^3 and 15 cm^3 chambers were used. Based on the measured solid volume and dry weight of the sample, average mineral density was estimated.

3.6 Scanning Electron Microscopy (SEM)

Surfaces of freshly broken core chips can be imaged using a Zeiss Supra 35VP field emission scanning electron microscopy (SEM) in high vacuum mode with an accelerating voltage of 12 kV, aperture size of 30 μm , and working distance of 10–12 mm (0.39–0.47 in.). EDAX Genesis energy-dispersive x-ray spectroscopy (EDS) applied for determining the semiquantitative elemental and mineralogical composition of the samples. The EDS measurements usually acquired together with the corresponding SEM microscopic images. (Zimmermann et al., 2015). Both flooded and unflooded samples are analysed, where unflooded ones are the end pieces from the same sample of chalk.

3.7 Post processing of data

3.7.1 Triaxial test

Effective confining stress of the system is calculated by subtracting pore pressure (P_p) from confining/radial (σ_{iso}) pressure:

$$\sigma_{conf} = \sigma_{iso} - P_p \quad (3.1)$$

The effective axial stress (σ_{ax}) is calculated from the piston pressure, effective confining pressure, and frictional pressure ($P_{fric}=0.3$ MPa) that occurs from the movement of the piston in the triaxial cell. Also a conversion factor for the area factor is used that takes into account the cross area of the plug and piston pressure chamber ($f_{area}=1.265$):

$$\sigma_{ax} = \sigma_{conf} + f_{area} (P_{pist} - P_{fric}) = (\sigma_{iso} - P_p) + f_{area} (P_{pist} - P_{fric}) \quad (3.2)$$

3.7.2 Chemical test

From IC test, the concentrations of both anion and cation in the fractioned fluid can be detected. Knowing elemental concentrations of fractioned effluent and injected brine, it is possible to quantify to what extend the chemical reactions (dissolution/precipitation) taking place inside the core.

To quantify the molar concentrations of the samples, as a reference molar concentrations of Mg^{2+} , Ca^{2+} and Cl^{-} in standards were used.

General formula for concentration calculation is:

$$\text{Molarity of ion 1} = \frac{\text{Area of peak of ion 1}}{\text{Av.area of peak of ion in standard}} \text{Molarity of ion 1 in standard} \quad (3.3)$$

For particular refill, Mg^{2+} and Cl^{-} concentrations are calculated using the average area of $MgCl_2$ brine from that refill. While Ca^{2+} concentration calculated using two different methods. The first method calculated in similar manner to Mg^{2+} and Cl^{-} , but SSW standard was used instead of $MgCl_2$. The second method accounts for Ca^{2+} concentration present in the $MgCaCl_2$ standard.

Production or precipitation of divalent ions such as Mg^{2+} and Ca^{2+} calculated as:

$$\text{Amount of substance } i \text{ [mol]} = \text{Flooding rate of brine} \left[\frac{l}{d} \right] \cdot \sum_1^k \text{concentration of substance } i \left[\frac{mol}{l} \right] \quad (3.4)$$

Whereas mass of the substance can be found as:

$$\text{Mass of substance } i \text{ [g]} = \text{Amount of substance } i \text{ [mol]} \cdot \text{Molecular mass of substance } i \left[\frac{g}{mol} \right] \quad (3.5)$$

CHAPTER 4

EXPERIMENTAL RESULTS AND COMMENTS

This section presents results obtained from mechanical tests, chemical analysis of the effluents and core analysis after testing, in addition to estimation of evolution of permeability and porosity. All the cores were hydrostatically loaded beyond the yield and thereafter left to creep at a constant stress level of 13.2 MPa and 23.3 MPa for the Mons and Kansas cores, respectively. Throughout the mechanical testing, the testing brine was continuously injected and sampling of the effluent was conducted to quantify any chemical changes of the core material.

The initial objective was to perform rock-mechanical tests (both hydrostatic and creep tests) on Mons and Kansas cores at three different testing temperatures, lasting 60 days. The first set/round of experiment started by performing mechanical tests on Mons cores at 60°C and 130°C, while Kansas core tested at 92°C. In the second set, Mons core at 92°C, and Kansas cores at 60°C and 130°C were tested. After about 30 days of creep, the Mons core tested at 92°C failed, following this, a new experiment was started, thus in total 7 chalk cores were mechanically tested. Another important point to note is that the tests done in the second set are still running under creep phase instead of planned 60 days of creep test. The reason for pursuing long-term experimental investigation is that it enables an in depth investigation of chemo-mechanical compaction and give better understanding of rock-mechanical behaviour of chalk.

4.1 Mechanical tests- Mons cores

4.1.1 Hydrostatic loading phase

From the hydrostatic tests, to characterize the mechanical strength of chalks, the yield point and bulk modulus was determined. The yield point is defined when the stress vs. strain curve starts to deviate from a linear trend as shown in fig. 4.1. The bulk modulus was

calculated from the linear slope of stress vs. strain curve within the elastic region. Table 4.1 lists the cores that have been tested at different testing temperatures and porosities along with yield point, bulk modulus and axial strain. The initial porosities lie in the range of 42.2-42.5 %. As seen from table 4.1, the values of hydrostatic yield strength are ranging from 8.64 to 8.87 MPa. The core tested at 92°C gives the lowest yield point value, $\sigma_h = 8.64$ MPa, while the core tested at 60°C shows the highest yield strength, $\sigma_h = 8.87$ MPa. In regards to bulk modulus, it ranges from 0.89 GPa to 1.27 MPa. When it comes to strain, as loading to the pre-set creep stress, the cores tested at 92°C deform more than the other cores. Also, it is clearly seen that the core tested at 130°C deforms relatively less compared to others. In overall, all the cores reveal similar trend to the applied stress and strain response.

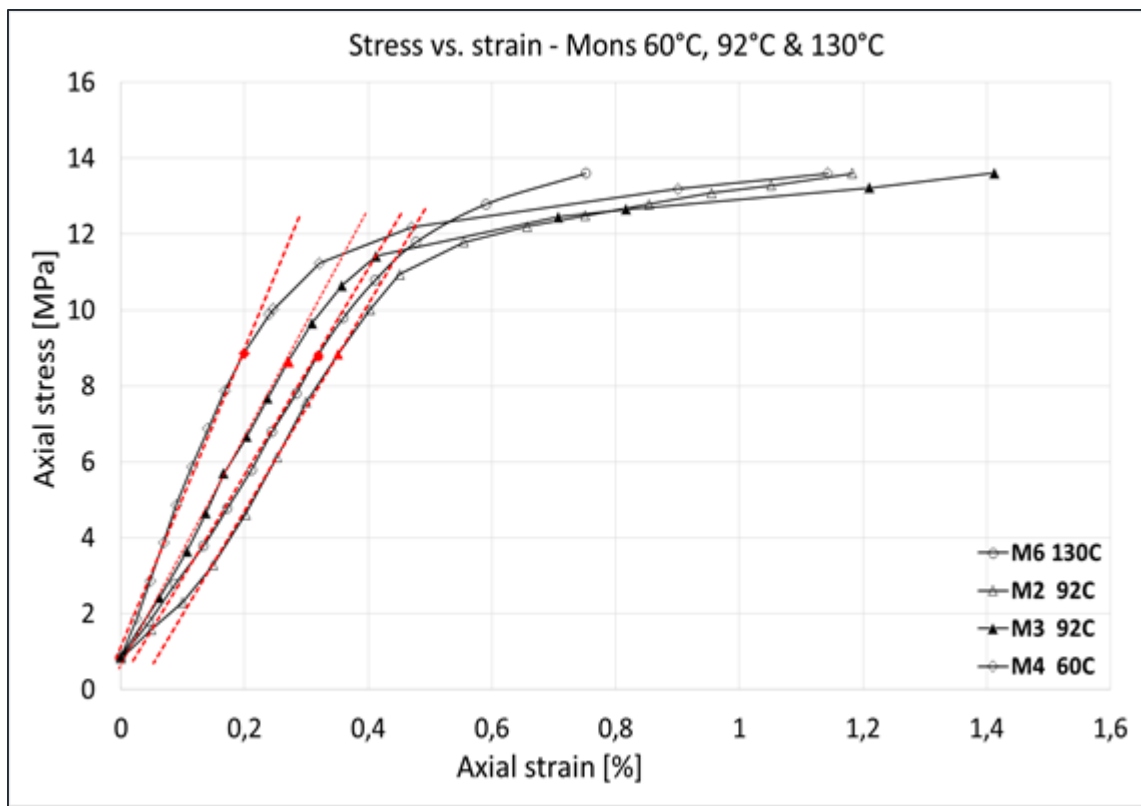


Figure 4.1 Axial stress versus axial strain for Mons cores tested at three different temperatures.

Sample ID	Test temperature [°C]	Porosity [%]	Yield point [MPa]	Bulk modulus [GPa]	Strain [%]
M4	60	42,47	8,87	1,27	1,14
M3	92	42,52	8,64	1,01	1,41
M2	92	42,28	8,83	1,01	1,18
M6	130	42,22	8,79	0,89	0,75

Table 4.1 Defined hydrostatic yield strength and calculated bulk modulus values for Mons cores tested at 3 different temperatures.

4.1.2 Creep phase

Following the hydrostatic loading, when the constant stress level of 13.2 MPa is reached, a creep period starts. Fig. 4.2 depicts the axial deformation as a function of time during the creep period. Even though the stress-strain relationship from hydrostatic phase did not give obvious differences, the creep developments show clear distinction in their behavior. As can be seen from fig. 4.2, the cores tested at 60°C and 92°C present similar creep development throughout the test, with an initial period where the rate of time dependent deformation decreases with time followed by steady-state creep phase. The Mons cores tested at 92°C is extrapolated to predict beyond the observed range (the red lines defines extrapolation) and seems that both cores deforms slightly higher than at 60°C. On the other hand, the core tested at 130°C reveals third stage of creep behavior – accelerating creep (extrapolation showing how steady-state creep would develop). In this case, the core deforms with an enhanced rate compared to others, which further caused the strain rate to increase by a factor more than two throughout the testing time. The experimental results obtained during creep phases are summarized in the table 4.2.

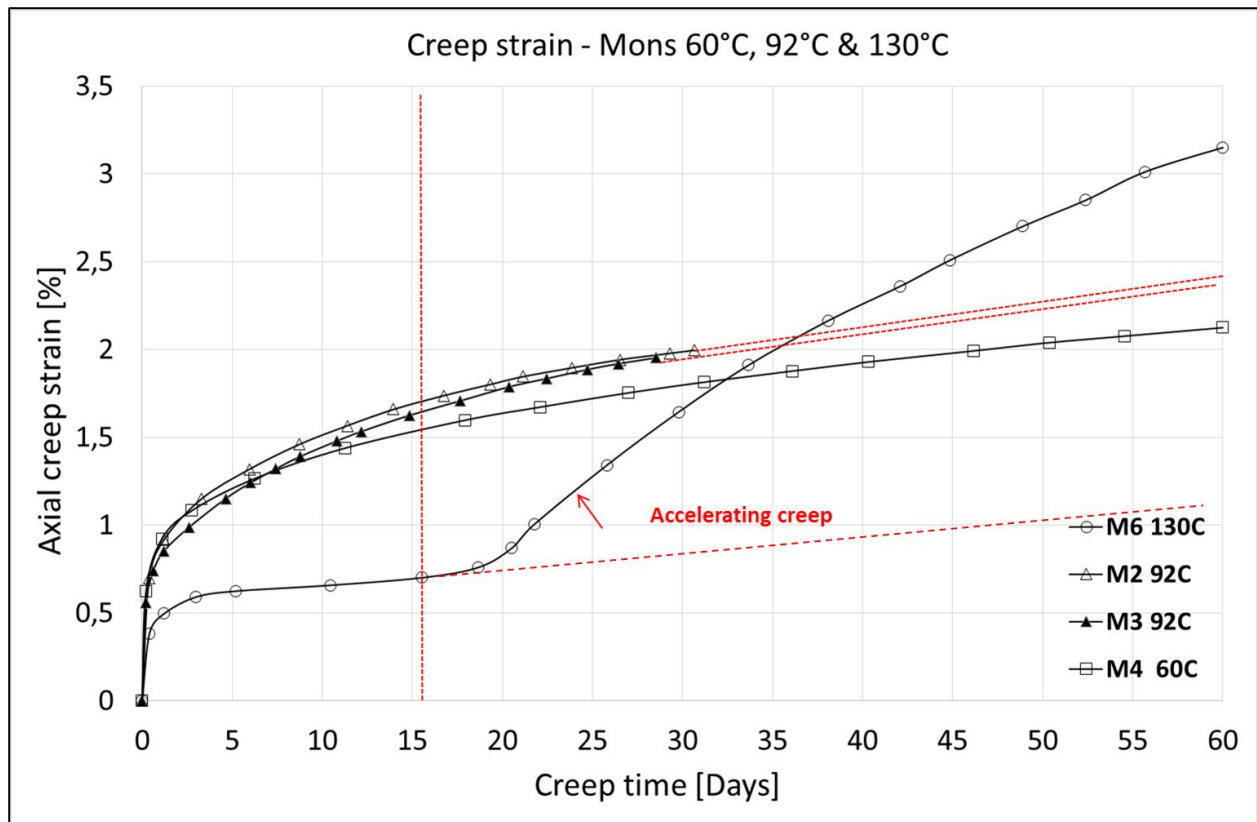


Figure 4.2 Axial creep strain versus creep time for Mons cores tested at three different temperatures.

Note that unlike others, the core tested at 130°C shows enhanced creep development started after about 15 days of creep phase (the red lines define the starting point of the accelerating creep and also extrapolated line for tests conducted at 92°C).

Sample ID	Test temperature [°C]	Total axial creep strain [%]
M4	60	2,13
M3	92	2,4
M2	92	2,3
M6	130	3,15

Table 4.2 Accumulated axial creep deformation from creep phase for Mons cores.

4.1.3 Relationship between permeability and strain

It is widely known that porosity and permeability is interlinked. When the core is hydrostatically loaded, the pore volume reduces as the core is compressed; this has effect on the permeability evolution. To further investigate this, the estimated permeability values (eq. 2.19) are plotted against the axial strain during hydrostatic loading (see fig. 4.3). As seen, the general trend is – permeability decreases with increasing deformation. Initially, the cores tested at 60°C and 92°C had more or less similar permeability, and as the core is continuously deformed under isotropic loading, the Mons cores tested at 60°C and 92°C (M2) show similar reduction in their permeability values, both has reduced to about 50%. In addition, these cores exhibit same deformation to the applied stress. Unlike others, the core tested at 92°C (M3) starts to accelerate after some period of deformation. This happened due to incorrect flooding rate during testing. By extrapolation, we could observe that it follows similar trend as other cores. The core tested at 130°C exhibits lower percentage of permeability reduction, approximately 35%.

In regards to permeability evolution during creep phase, clearly same tendency here, under constant loading the cores tend to show reduced permeability (fig. 4.4). Apparently the core tested at 130 °C, during initial 20 days of creep exhibits smooth permeability reduction with time and as accelerating creep starts, sudden drop in permeability is observed. The mentioned time period coincides with the time lag accelerating creep. From creep phase, the cores tested at 130°C and 92°C (M2) and 60°C shows cumulative permeability reduction of about 60 %, while the core tested at 92°C (M3) gives around 70% reduction compared to initial values. Some fluctuations seen for core M3 related to flooding rate changes.

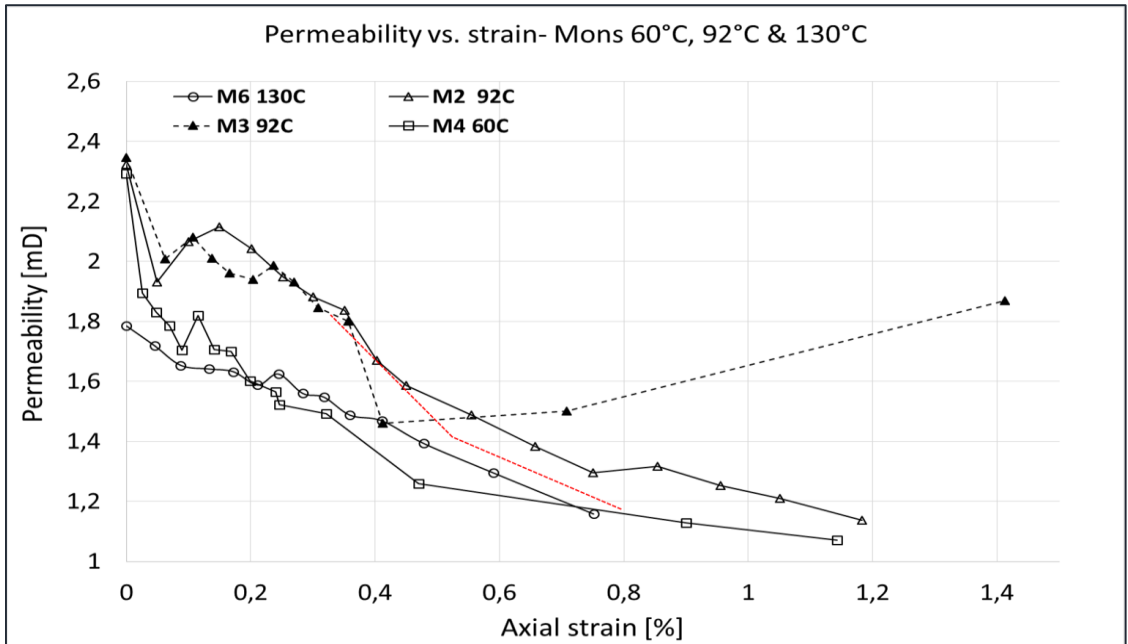


Figure 4.3 Permeability and axial strain relationship for Mons cores tested under hydrostatic loading at three different temperatures.

In extrapolation shown by red line, we could observe that M3 core follows similar trend as others.

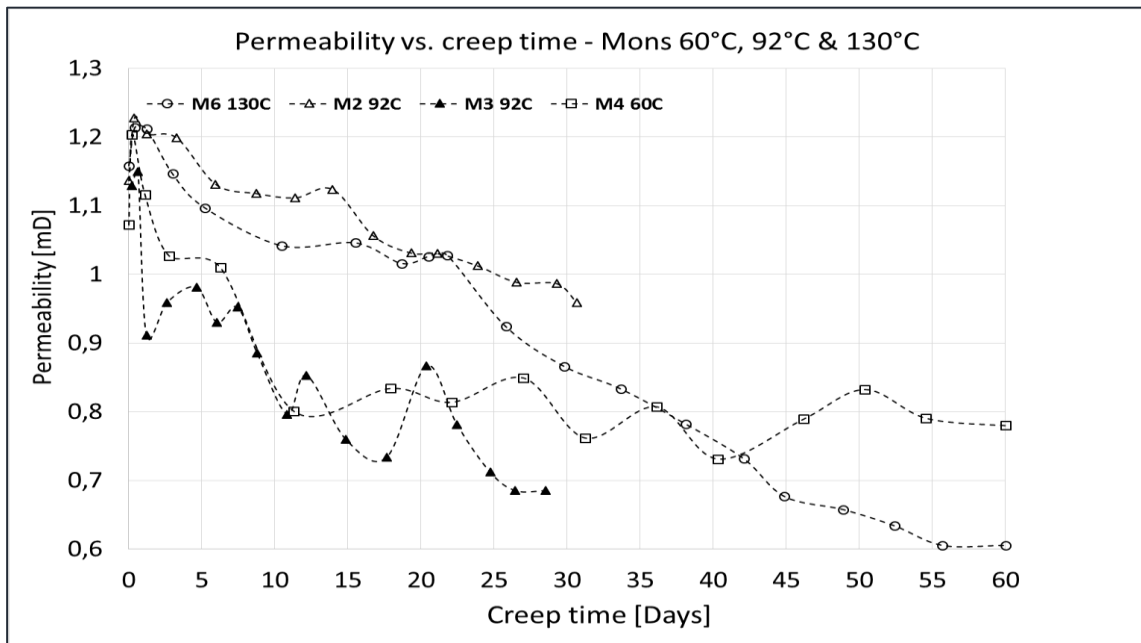


Figure 4.4 Permeability and creep time relationship for Mons cores tested under creep phase at three different temperatures.

4.2 Mechanical tests - Kansas cores

4.2.1 Hydrostatic loading phase

Similar to Mons, from the stress vs. strain relation the yield point was determined for Kansas cores. In addition, the bulk modulus was estimated from the linear slope of stress vs. strain curve within the elastic region. The initial porosities of Kansas chalks lie in the range of 36.3-36.5 % that is lower compared to the Mons chalks. As seen from fig.4.5 and table 4.3, Kansas cores comparatively to Mons exhibits higher values of hydrostatic yield strength, which are ranging from 12.75 to 13.06 MPa. Similar to the Mons chalks, the core tested at 92°C gives the lowest yield strength, $\sigma_h = 12.75$ MPa; but in contradiction to Mons, the core tested at 130°C not 60°C, reveals highest yield point value, $\sigma_h = 13.06$ MPa. While the bulk modulus shows values between 1.34 GPa and 1.54 GPa. As loading to the pre-set creep stress, all the cores strain nearly the same and the entire cores exhibit similar trend in their stress-strain relationship. Moreover, the Kansas cores compared with the Mons cores deformed relatively less, with an exception that both the cores deformed similarly at 130°C.

Sample ID	Temperature [°C]	Porosity [%]	Yield point [MPa]	Bulk modulus [GPa]	Strain [%]
K3	60	36,36	12,75	1,36	0,73
K1	92	36,46	12,88	1,54	0,80
K2	130	36,50	13,06	1,34	0,74

Table 4.3 Defined hydrostatic yield strength and calculated bulk modulus values for Kansas cores tested at 3 different temperatures.

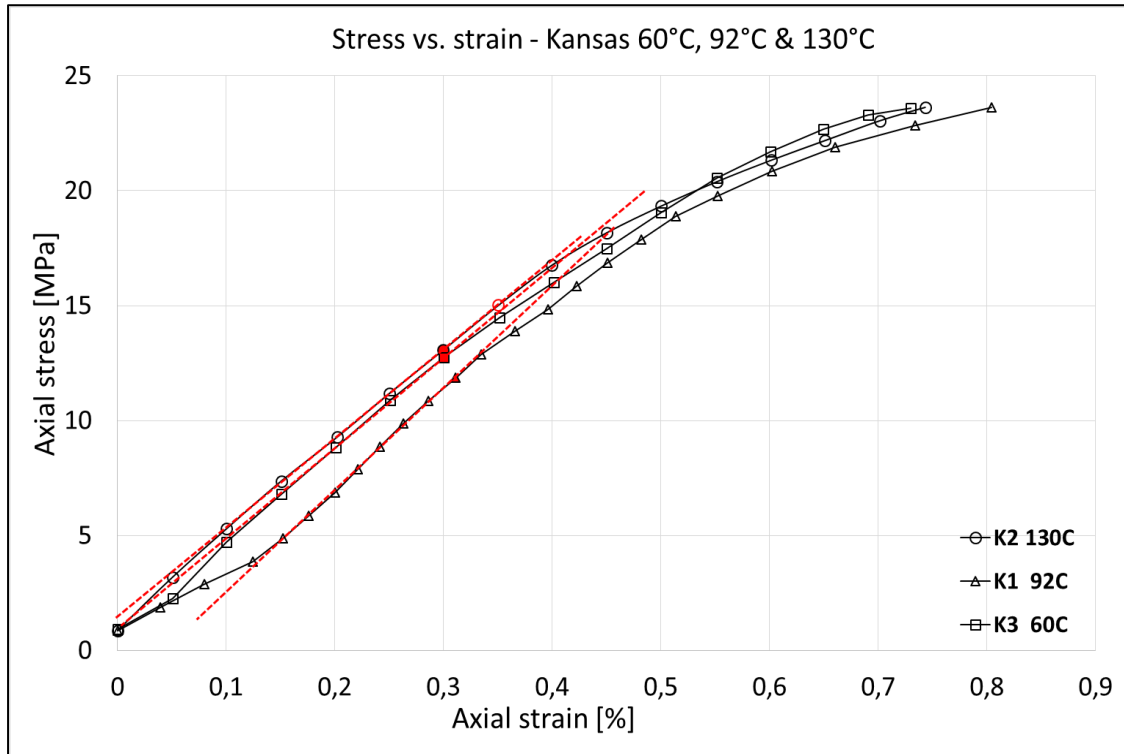


Figure 4.5 Axial stress versus axial strain for Kansas cores tested at three different temperatures.

4.2.2 Creep phase

When the constant stress level of 23.3 MPa was reached, a creep period starts for each core. Fig. 4.6 depicts the axial deformation as a function of time during the creep period. With respect to creep phase, in overall, the cores tested at 60°C and 92°C show similar behaviour in their time-dependent deformation to Mons cores; although the core tested at 130°C also reveal accelerating creep deformation (extrapolation line shows how would steady-state creep develop), but acceleration develops quite earlier compared to Mons chalk and its deformation magnitude is more than twice compared to other Kansas cores all along creep time. In all respects, less porous Kansas cores deform relatively less as compared with higher porous Mons chalks, which is in line with the intuitive conviction. The experimental results obtained during creep phases are summarized in the table 4.4.

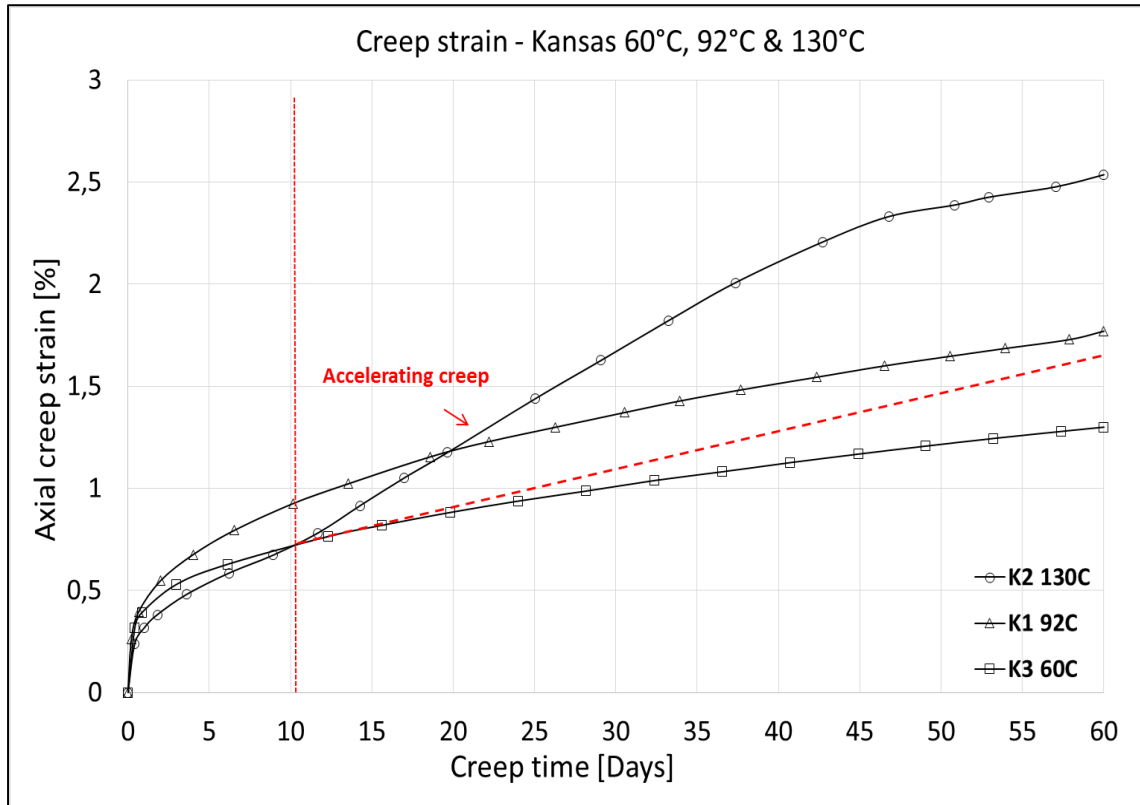


Figure 4.6 Axial creep strain versus creep time for Kansas cores tested at three different temperatures.

Note that unlike others, the core tested at 130°C shows enhanced creep development and in this case it starts at earlier time frame (the red line defines the starting point of the accelerating creep and also extrapolation showing how steady-state creep would develop).

Sample ID	Temperature [°C]	Total axial creep strain [%]
K3	60	1,30
K1	92	1,77
K2	130	2,54

Table 4.4 Axial creep strain versus creep time for Kansas cores tested at three different temperatures.

4.2.3 Relationship between permeability and strain

In consideration of permeability development during hydrostatic phase, (fig. 4.7) verifies the earlier established results from Mons cores that there is a certain inverse relationship between deformation and permeability. From the plot it is seen that initial permeability is ranged from 2,4-2,8 mD, and in the end of isotropic loading the core tested at 130°C lost permeability by 45%, while the one tested at 92°C shows reduction in permeability almost by 69%, even though they experienced similar deformation. On the other hand, the core tested at 60°C lost 60% of its initial permeability.

In regards to permeability evolution during creep phase, in overall all cores show reducing permeability trend (fig. 4.8). However, within 25 days of creep the core tested at 130°C reduces with maintained rate until reaches the plateau then tends to stabilize for the rest of the creep period. During this test, the core tested at 130°C shows reduction in permeability almost by a factor of 10 compared to its initial value, while the one tested at 92°C shows reduction in permeability by about 85%, and that of at 60°C gives around 75% reduction.

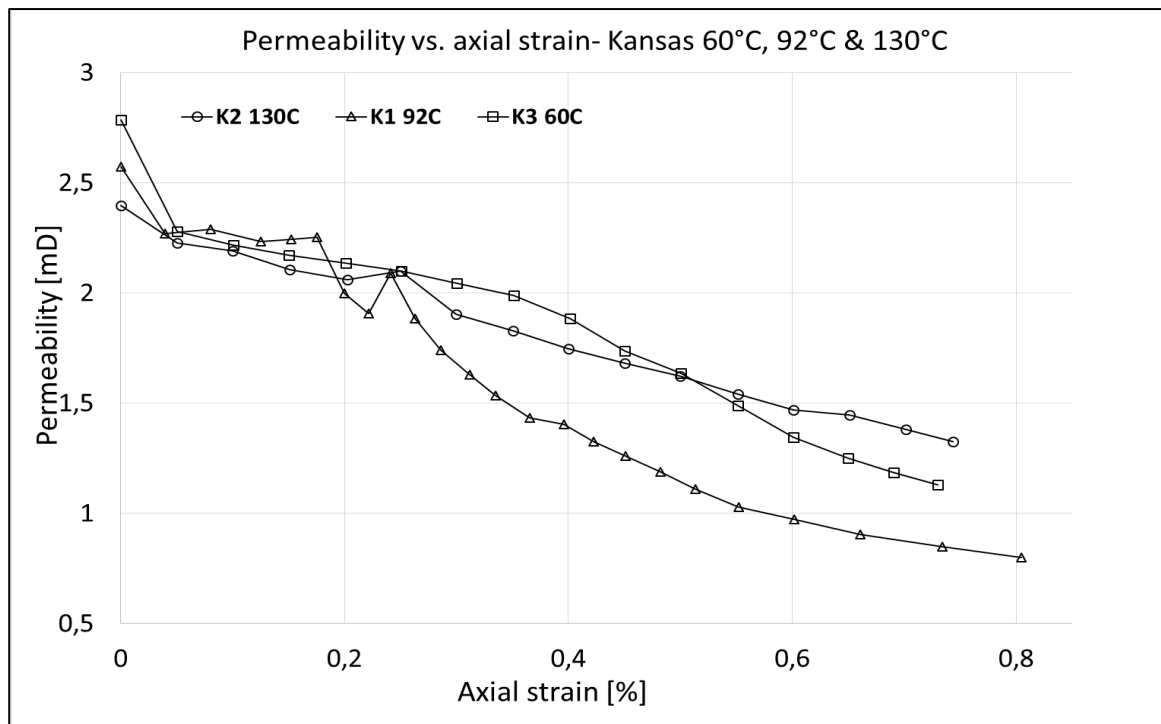


Figure 4.7 Permeability and axial strain relationship for Kansas cores tested under hydrostatic loading at three different temperatures.

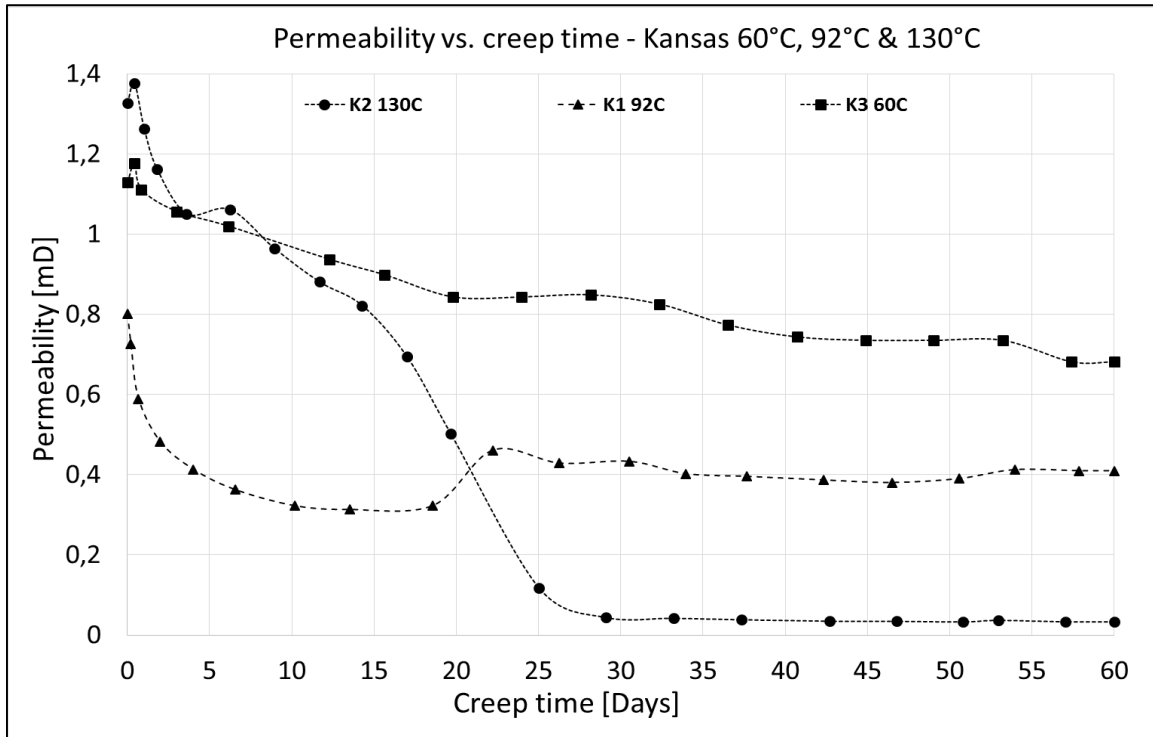


Figure 4.8 Permeability and creep time relationship for Kansas cores tested under creep phase at three different temperatures.

4.3 Chemical analysis of fractioned effluent

The flooding effluent from each mechanical test was sampled during the entire test period. Each effluent sample was analysed in IC on the ion concentration (two cations Mg^{2+} and Ca^{2+} , and also one anion Cl^- , in addition to pH measurement. The following subsections first present results from IC analysis followed by pH analysis.

4.3.1 IC analysis – Mons cores

The time evolutions of the ion concentrations for three tests are given in fig. 4.9 - 4.11 and cumulative values of Ca^{2+} and Mg^{2+} ions are presented in table 4.5. The chemical analysis of fractioned effluent tested at $60^{\circ}C$ present an insignificant production of Ca^{2+} ion and retention of Mg^{2+} ion, i.e. 0.008 mole/l and 0.003 mole/l respectively. This amount seems to be reasonable since the chemical reactions involving dissolution-precipitation is not affected much at this temperature range. When the core tested at $92^{\circ}C$, throughout the experiment shows accumulated 0.011 mole/l Ca^{2+} ion production, and 0.009 mole/l Mg^{2+}

ion depletion. When it comes to the core tested at 130°C, significant gain of Ca²⁺ ion and retention of Mg²⁺ ion inside the core was observed; 0.04 mole/l and 0.045 mole/l accordingly. Unlike other analysed samples, here from the beginning of sampling time to about 20 days the Mg²⁺ ion is increased with maintained rate until it reached plateau and then remains constant, but never reaches original injected concentration. Within this time span, Ca²⁺ production initially decreased then maintains constant production rate. This manner is reflected in the creep deformation behaviour, where initially time-lag creep is seen before accelerating creep started to develop.

When comparing the mass loss during testing, the loss is correlated to increase in temperature. The core tested at 130°C shows the highest amount of mass loss, 0.182 g. The mass loss is calculated from the difference between amount of Ca²⁺ produced and retained Mg²⁺. Moreover, when adding the concentrations of magnesium and calcium in the effluent, the sum approximates the original injected concentration of test brine for all cores, indicating stoichiometry is important (fig. 4.9-4.11). Although there is apparent inequality between one to one produced Ca²⁺ and retained Mg²⁺ ions stoichiometry, revealing that more complex geo-chemical processes taking place inside the core rather than simply Ca²⁺-Mg²⁺ ion exchange.

Analysis from all cores indicates that Cl⁻ remains close to its original concentration. Even though the cores tested at 92°C and 130°C gives some fluctuations in the effluent concentration, but it spans around the original injected one. The chemical analyses of the effluent fluid samples show that during the entire injection period, the Cl⁻ concentration remains close to its original concentration.

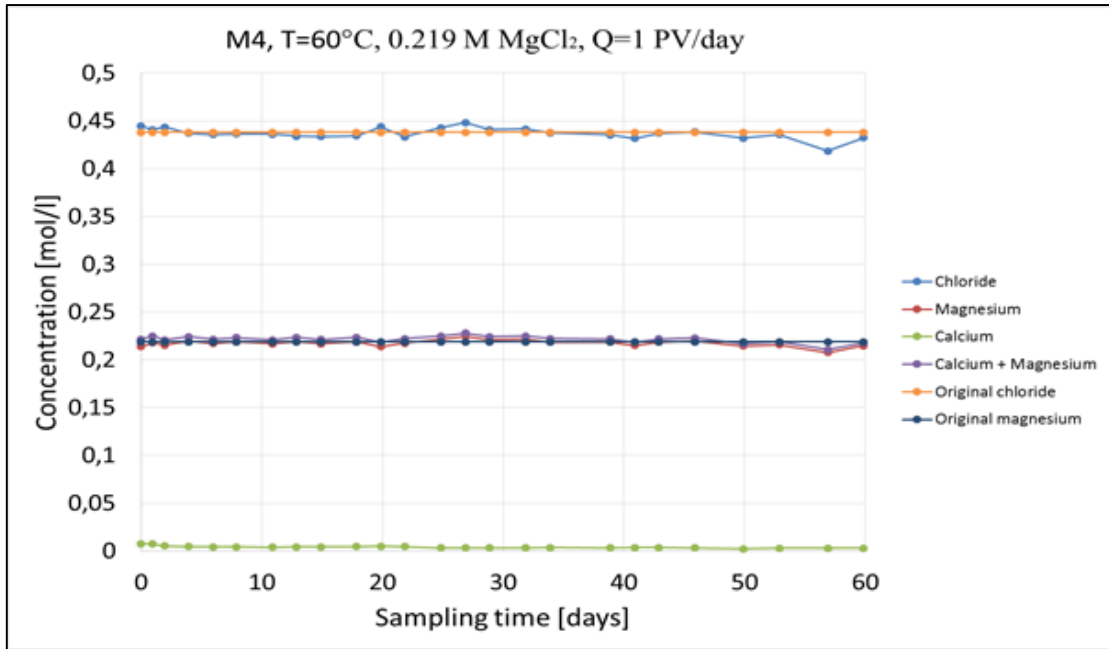


Figure 4.9 Mg²⁺, Ca²⁺ and Cl⁻ concentrations in sampled effluents from core tested at 60°C flooded with 0.219 M MgCl₂.

As seen, the added calcium and magnesium concentrations give similar to those of injected, meaning stoichiometry is preserved.

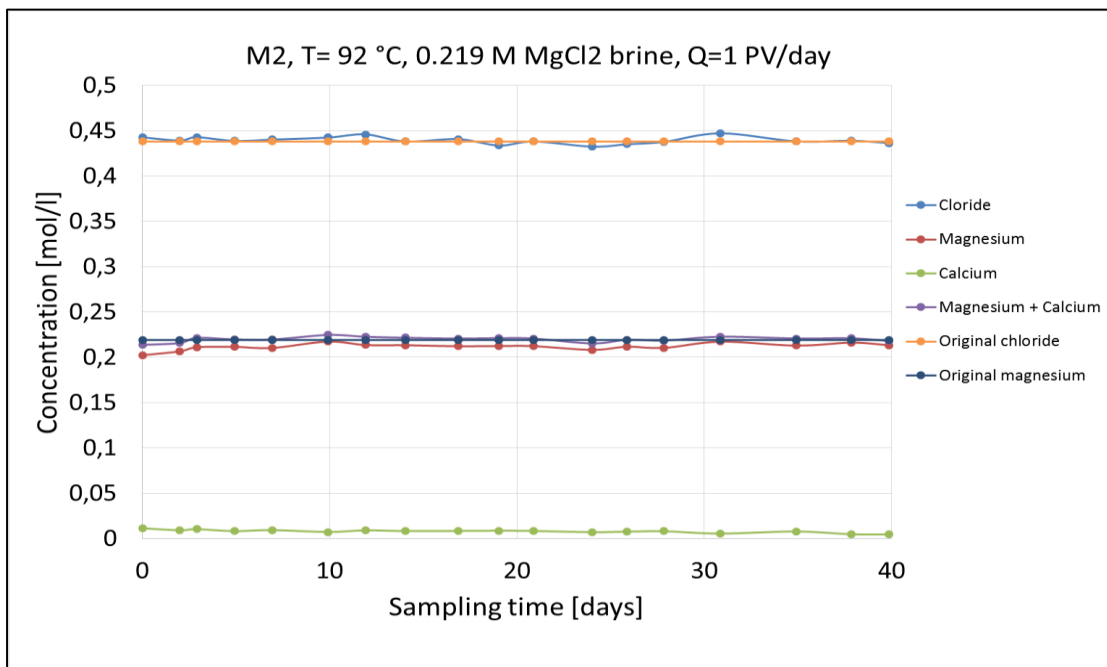


Figure 4.10 Mg²⁺, Ca²⁺ and Cl⁻ concentrations in sampled effluents from core tested at 92°C flooded with 0.219 M MgCl₂.

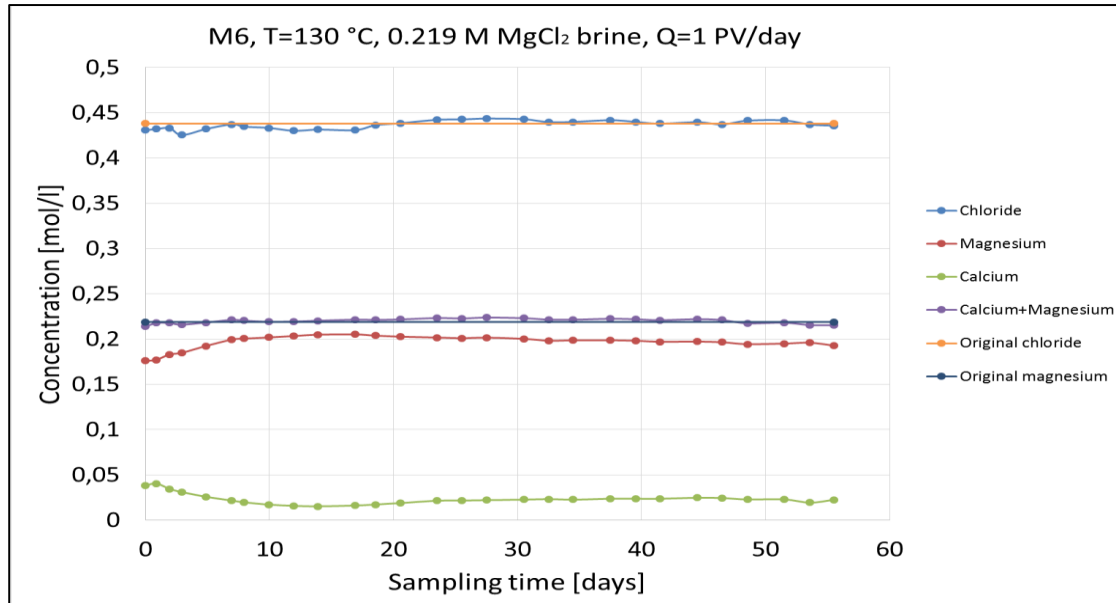


Figure 4.11 Mg²⁺, Ca²⁺ and Cl⁻ concentrations in sampled effluents from core tested at 130°C flooded with 0.219 M MgCl₂.

Core ID	Ca ²⁺ production [Mol]	Ca ²⁺ production [g]	Mg ²⁺ retention [Mol]	Mg ²⁺ retention [g]	Total mass loss [g]	Testing temperature [°C]
M4	0,008	0,315	0,003	0,077	0,238	60
M2	0,011	0,435	0,009	0,223	0,212	92
M6	0,045	1,799	0,041	0,988	0,812	130

Table 4.5 Produced Ca²⁺ and retained Mg²⁺ concentrations in sampled effluents from Mons cores tested at three different testing temperatures.

As it can be noted, the dissolution-precipitation and mass loss is temperature dependent.

4.3.2 IC analysis - Kansas cores

Chemical analysis of the fractionated effluent was also performed for the Kansas, in the same way as it was done for the Mons cores. The time evolutions of the ion concentrations for three tests are given in fig. 4.12 - 4.14 and accumulated values of Ca²⁺ ion produced and Mg²⁺ ion retained are presented in table 4.6. Similar with the Mons chalk, at 60°C testing temperature, very low Ca²⁺ ion concentration detected and Mg²⁺ ion retained, 0.008 mole/l

and 0.002 mole/l respectively. As testing temperature was increased (92°C), slightly more Ca^{2+} ion produced from the core, whereas Mg^{2+} ion to some extent retained more compared with the Mons core, i.e 0.012 mole/l and 0.013 mole/l accordingly. The same tendency is observed here when the cores tested at 130°C, large concentration of Ca^{2+} ion is present in the effluent and Mg^{2+} ion is kept in the core. Ca^{2+} concentration close to those of Mons core, 0.05 mole/l; however retained Mg^{2+} ion as compared with Mons is almost doubled, 0.08 mole/l.

Similar to the Mons tested at 130°C, in the beginning of sampling time Mg^{2+} ion is increased with maintained rate until it reached plateau and then remains constant, but here this time span is short, lasting only about 10 days comparatively to Mons core that lasted about 20 days. Within this time frame, Ca^{2+} production initially decreased then maintains constant production rate. This manner is reflected in the creep deformation behavior, where initially transient creep is seen before accelerating creep started to develop about 10 days of creep time. When adding the concentrations of magnesium and calcium in the effluent, obtained values were close to the original injected concentration for all cores. Here is also seen distinction between one to one Ca^{2+} - Mg^{2+} stoichiometry, where produced amount of calcium ion does not equal to the retained magnesium.

Analysis from all cores here also indicates that chloride seems to be inert to the chalk surface and no significant difference observed between original and effluent concentrations. Although some fluctuations exist in the effluent concentrations and this could relate with uncertainties in the measurement.

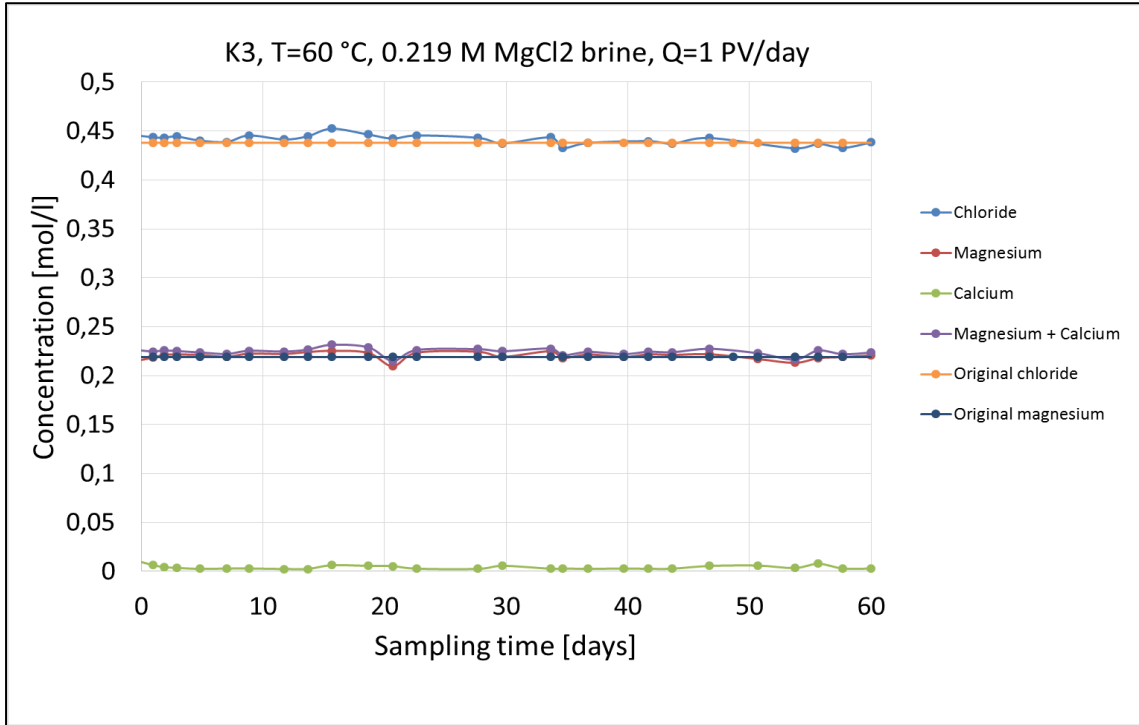


Figure 4.12 Mg²⁺, Ca²⁺ and Cl⁻ concentrations in sampled effluents from Kansas core tested at 60°C flooded with 0.219 M MgCl₂.

As seen, the added calcium and magnesium concentrations give similar to those of injected, meaning stoichiometry is preserved.

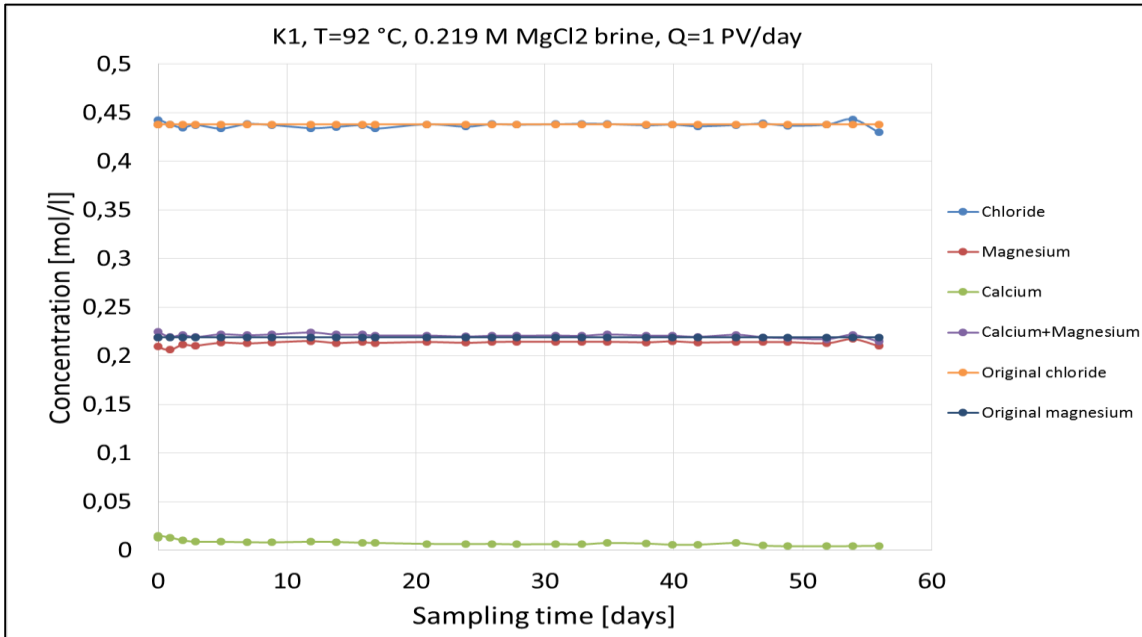


Figure 4.13 Mg²⁺, Ca²⁺ and Cl⁻ concentrations in sampled effluents from Kansas core tested at 92°C flooded with 0.219 M MgCl₂.

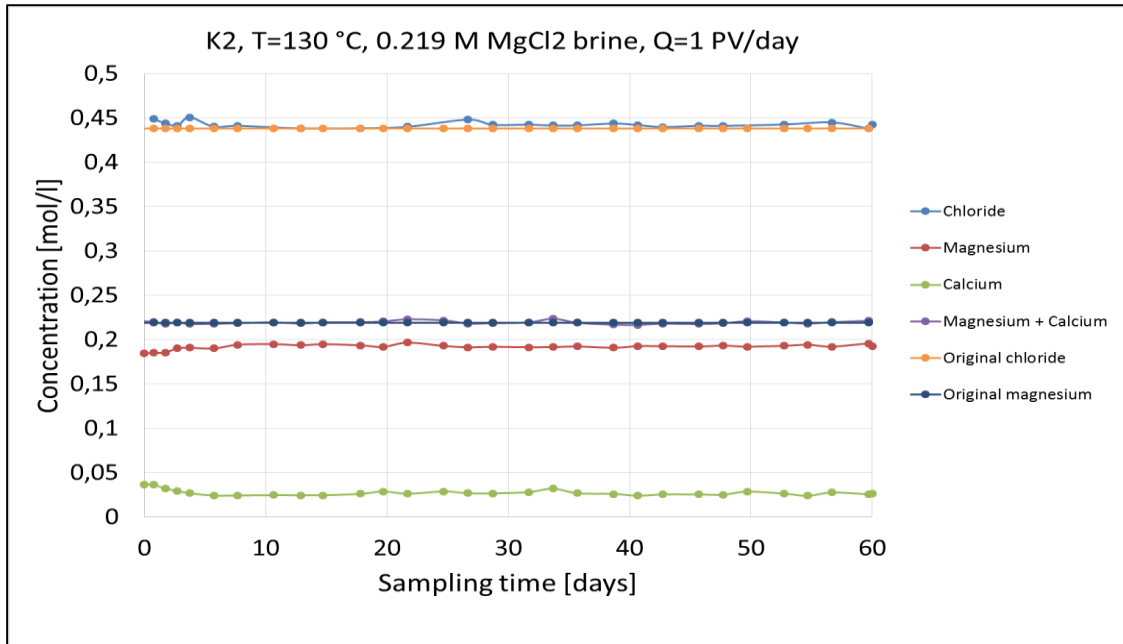


Figure 4.14 Mg²⁺, Ca²⁺ and Cl⁻ concentrations in sampled effluents from Kansas core tested at 130°C flooded with 0.219 M MgCl₂.

As seen, the added calcium and magnesium concentrations give similar to those of injected, meaning stoichiometry is preserved.

Core ID	Ca ²⁺ production [Mol]	Ca ²⁺ production [g]	Mg ²⁺ retention [Mol]	Mg ²⁺ retention [g]	Total mass loss [g]	Testing temperature [°C]
K3	0,008	0,321	0,002	0,059	0,379	60
K1	0,012	0,479	0,013	0,326	0,153	92
K2	0,049	1,989	0,081	1,962	0,028	130

Table 4.6 Produced Ca²⁺ and retained Mg²⁺ concentrations in sampled effluents from Kansas cores tested at three different testing temperatures.

4.4 pH analysis – Mons and Kansas cores

The trend of pH vs temperature in general is pH decreases with increased temperature. It is supported by the Le-Chatelier's Principle, where he states that when chemical system at equilibrium experiences a change in concentration, temperature, pressure, etc. then the equilibrium shifts to counteract the imposed change and a new equilibrium is established.

As seen from the figure 4.15-4.16, time evolutions of the effluent pH values for the Mons and Kansas cores present similar behaviour with that of stated above. Initial values of pH of injected fluid was usually around 5.5, however in the last conducted experiment new pack of $\text{MgCl}_2 \cdot 6\text{H}_2\text{O}$ salt was used, therefore for that test pH shows slightly higher value than 6.

In overall, the effluent samples from the Mons core tested at 130°C shows the lowest values of pH with time which is in line with theory, although the core effluent from 60°C test supposed to show the highest pH evolution through time, but it did not (fig. 4.15). The effluent samples from the both cores tested at 92°C shows the highest values, which might relate to the initial value of pH of the injected brine. The core tested at 60°C shows average 6.07 pH value, whereas at 92°C about 6.35 and the core tested at 130°C gives 5.76. Fluctuations in the graph most probably related with brine change during testing.

On the other hand, the fractioned effluent pH values from the Kansas core presents consistent tendency with the theory. The core tested at 60°C depicts in average pH of 6.27, while at 92°C reveals average pH value of 6.12, and at 60°C shows pH of 5.84 (fig. 4.16).

Another important point to highlight is that the sampled pH values after first measurement were re-measured several times within 3 weeks until they displayed constant values. The pH value for the core tested at 60°C stabilized around pH 7.97 within three weeks, while the core tested at 130°C remained balance around pH 7.8. Whereas the Kansas core tested at 92°C stabilized around pH value of 7.92. To support this observation the behaviour of pH with temperature was simulated for chalk cores considering the mineralogical content and testing brine composition using PHREEQC simulator (detailed information will be on section 4.4. PHREEQC analysis). As seen from figure 4.17, as calcite equilibrated with injected MgCl_2 brine, the pH has to be around 7.2 at 130°C , whereas at 60°C above pH of 8. Thus, from this we can deduct that when pH first measured, the fractioned effluent was not in equilibrium, meaning it takes time for all ions inside the effluent to reach equilibrium.

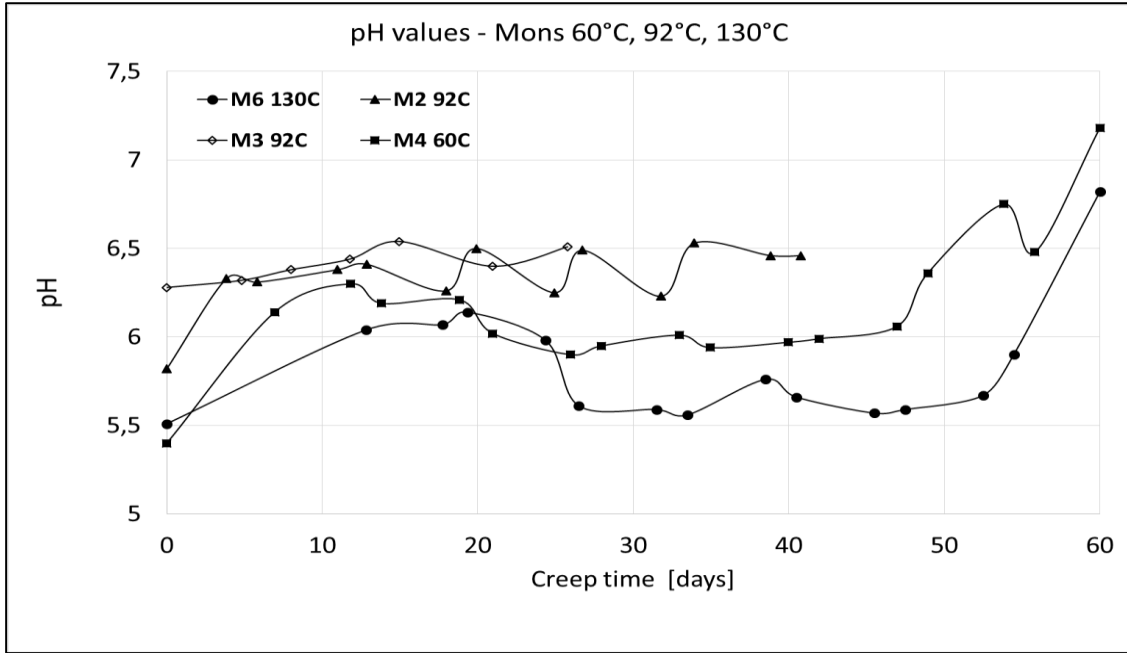


Figure 4.15 Evolution of pH with time for Mons cores tested at three different temperatures.

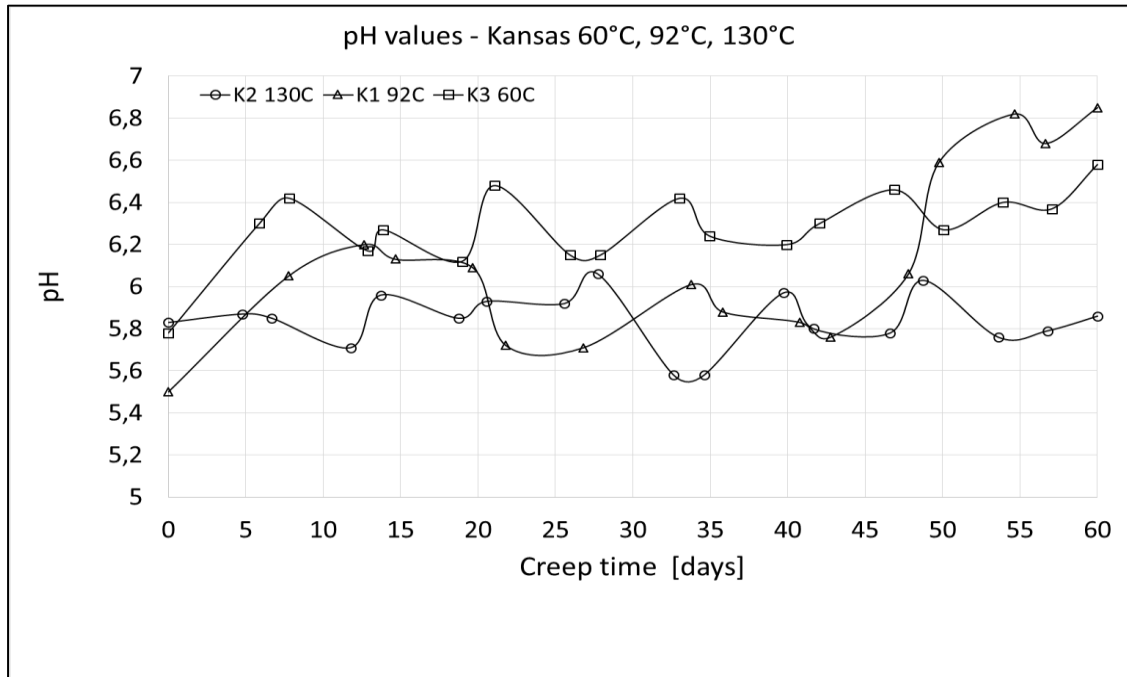


Figure 4.16 Evolution of pH with time cores tested at three different temperatures.

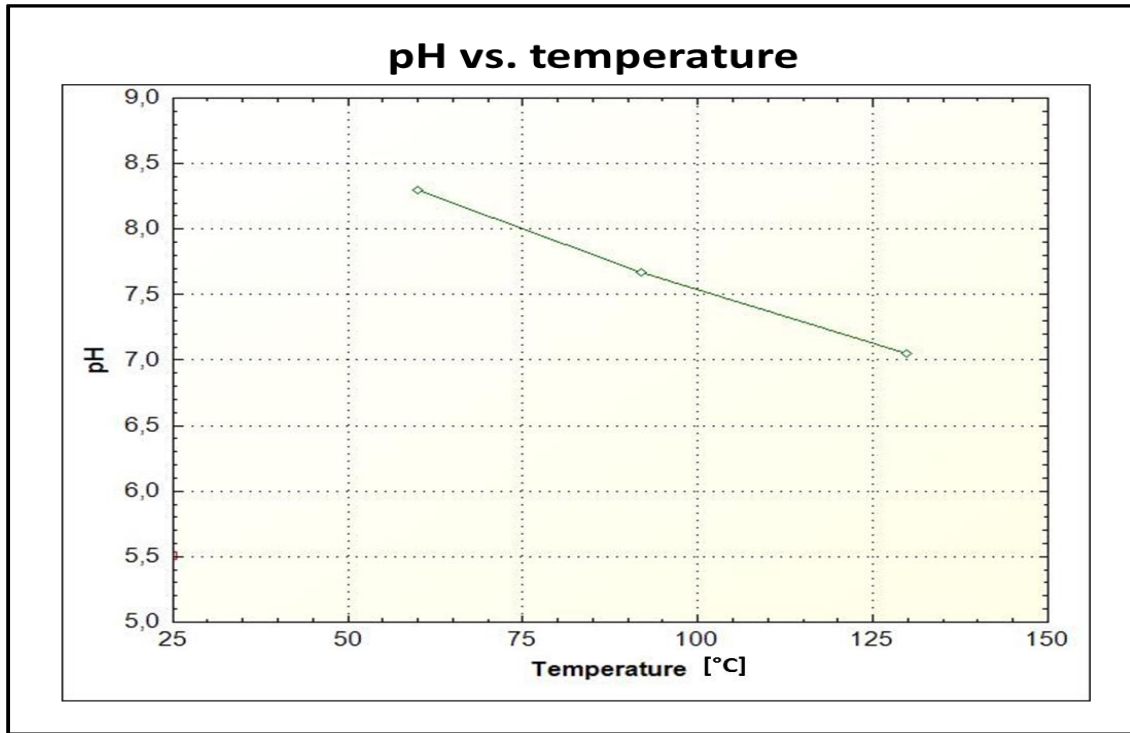


Figure 4.17 Evolution of pH with temperature. Simulated using PHREEQC considering mineralogical content of chalk and injected tested brine composition.

4.5 Analysing the core after test

4.5.1 Bulk volume measurement

After finishing each test, the triaxial cell was dismantled, and then the tested core subsequently carried out on core analysis. Test samples after removing from the cell were marked with a 1 mm distance in order to estimate the distribution of axial and radial deformations. The evolved length and diameter along the core measured in three different directions. The accuracy in this measurement is usually 0.1 mm. Then, using average values of measured length and diameter, total bulk volume is calculated by the equation of truncated wedge. As pointed out by Madland et al. (2006), the strain measured during the test cannot be directly compared to the measurements of the plug after the test, since the effect of decompression has to be taken into account. Thus, there always exist some inaccuracy when estimating bulk volume after test.

As seen from the external geometry of the Mons core tested at 60°C (table 4.7) the core did deform axially and radially. The core deformed from initial bulk volume 82.58 cm³ to 78.17 cm³. Moreover, the core shortened to 1.96 cm and contracted radially to 0.36 mm. In the inlet part of the core we observed small void so approximate range that cover this voids was estimated to be 0.6 cm³. Then, this value was subtracted from the calculated bulk volume. Thus, 77.57 cm³ value was used for porosity estimations instead of 78.17 cm³.

Length [cm]		Diameter measurements [mm]			Average diameter [mm]
Outlet	0	38,02	38	-	38,01
	1	38,06	37,58	37,71	37,78
	2	37,99	37,51	37,51	37,67
	3	37,95	37,33	37,42	37,57
	4	37,99	37,31	-	37,65
	5	37,94	37,41	37,51	37,62
	6	37,99	37,62	37,66	37,76
Inlet	7,05	38,06	37,84	37,81	37,90
Total volume [cm ³]					78,17

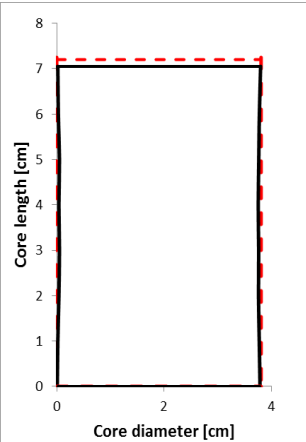


Table 4.7 Diameter measurements from inlet to outlet for Mons core tested at 60°C and calculated bulk volume using truncated wedge equation.

While the Kansas core tested at 92°C (table 4.8) shows also moderate change, both radially and axially. The bulk volume is reduced from 81.04 cm³ to 77.65 cm³. However, same as above 0.4 cm³ was subtracted to compensate the void. It was also evaluated that length is shortened to 1.22 mm and diameter is reduced to 0.5 mm. Same as above, to compensate the voidage 0.4 cm³ subtracted from the bulk volume estimation after testing.

Moreover, as seen from the table 4.9, Mons core tested at 130°C experienced significant external geometry alteration. Difference of external geometry between the initial and tested core can be observed, where significant changes starts from the inlet side of the core. The bulk volume is reduced from 82.07 cm³ to 76.69 cm³. Moreover, the core shortened to 2.37 mm and diameter was reduced to 0.78 mm.

Length [cm]		Diameter measurements [mm]			Average diameter [mm]
Outlet	0	37,95	37,77	37,81	37,84
	1	37,49	37,58	37,66	37,58
	2	37,4	37,38	37,45	37,41
	3	37,38	37,53	37,45	37,45
	4	37,33	37,49	37,38	37,40
	5	37,5	37,68	37,56	37,58
	6	37,83	37,96	37,95	37,91
Inlet	6,99	38,01	38,03	38,06	38,03
Total volume [cm ³]					77,65

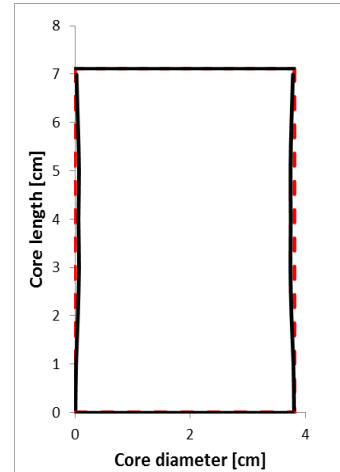


Table 4.8 Diameter measurements from inlet to outlet for Kansas core tested at 92°C and calculated bulk volume using truncated wedge equation.

Length [cm]		Diameter measurements [mm]			Average diameter [mm]
Outlet	0	38,07	38,07	38,05	38,06
	1	38,04	38,02	38,03	38,03
	2	37,87	38,02	38,01	37,97
	3	37,51	37,92	37,91	37,78
	4	37,14	37,65	37,54	37,44
	5	-	37,06	36,73	36,90
	5,5	36,11	36,69	36,35	36,38
	6	36,12	36,63	36,47	36,41
6,5	36,52	36,85	36,79	36,72	
Inlet	6,965	37,43	37,65	37,51	37,53
Total volume [cm ³]					76,69

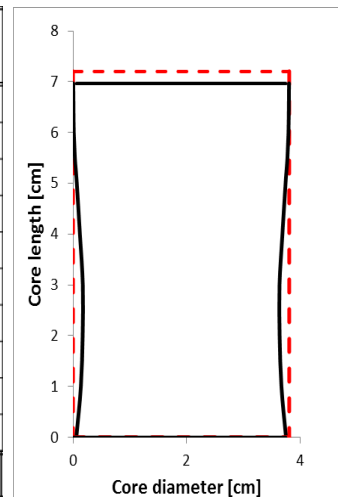


Table 4.9 Diameter measurements from inlet to outlet for Mons core tested at 130°C and calculated bulk volume using truncated wedge equation.

4.5.2 Solid volume measurement by pycnometer

The cores were initially cut into two pieces, and then measured for solid/mineral density using pycnometer. In order to more accurately estimate the average solid density, these two big pieces were measured again by dividing them into seven smaller pieces, where latter was used in SEM-EDS analysis. Before estimating solid volume in pycnometer, the weight of each slice was measured, thereafter by employing these values, the density values were estimated. Once the densities of all pieces were calculated, using weighted

average method the average solid density was obtained (eq. 2.17). Along with flooded cores, the inlet and outlet parts of unflooded core were also measured to compare the density obtained from the bulk volume method.

The table 4.10 presents the measured values of solid volume and estimated values of density for three cores: Mons tested at 60°C and 130°C in addition to Kansas core tested at 92°C. The unflooded core pieces from each sample were also measured to compare with the values of density obtained from the difference between saturated and dry core weight before testing. Both measurements show consistency in the density values. As seen, the cores tested at 60°C and 92°C show no significant change in density values. Whereas, the core tested at 130°C reveals density increase from 2.69 g/cm³ to 2.72 g/cm³.

Mons core, T=60°C			Kansas core, T=92°C			Mons core, T=130°C		
Unflooded sample			Unflooded sample			Unflooded sample		
Inlet	Weight [g]	16,39	Inlet	Weight [g]	17,98	Inlet	Weight [g]	16,39
	Density [g/cm ³]	2,69		Density [g/cm ³]	2,70		Density [g/cm ³]	2,69
Outlet	Weight [g]	16,28	Outlet	Weight [g]	15,23	Outlet	Weight [g]	16,28
	Density [g/cm ³]	2,70		Density [g/cm ³]	2,71		Density [g/cm ³]	2,70
Weighted average density [g/cm ³]		2,69	Weighted average density [g/cm ³]		2,70	Weighted average density [g/cm ³]		2,69
Flooded sample			Flooded sample			Flooded sample		
Inlet	Weight [g]	51,61	Inlet	Weight [g]	55,04	Inlet	Weight [g]	59,82
	Density [g/cm ³]	2,70		Density [g/cm ³]	2,71		Density [g/cm ³]	2,72
Outlet	Weight [g]	70,78	Outlet	Weight [g]	80,00	Outlet	Weight [g]	63,79
	Density [g/cm ³]	2,70		Density [g/cm ³]	2,71		Density [g/cm ³]	2,72
Weighted average density [g/cm ³]		2,70	Weighted average density [g/cm ³]		2,71	Weighted average density [g/cm ³]		2,72

Table 4.10 Measurements of the average solid densities for Mons cores tested at 60°C and 130°C, and also Kansas core tested at 92°C.

4.5.3 Textural analysis

Microscopic analysis by SEM-EDS is also included to identify any textural changes on the chalk microstructure. The flooded core material was cut into seven slices of thicknesses of about 1 cm and each slice was analysed in SEM-EDS. No alteration was observed using

SEM-EDS in the Mons core tested at 60°C and Kansas core tested at 92°C. Although EDS measurements indicate that some compositional changes occurred induced by brine injection, few magnesium ion retention can be seen across the core, dominating in the first couple of centimetres (fig. 4.18-4.19). In contrast, after testing at 130°C, mineralogical morphology of the core mineralogy severely altered. It was extraordinary to see that the M6 core was strongly enriched in Mg-bearing in the first couple of slice and EDS measurements supports compositional changes (fig. 4.20-4.21). Relative to initial composition, the first couple of centimetre of the flooded chalk sample shows an increase in Mg^{2+} by a weight percent up to 1.8 %.

SEM imaging indicates that retention of Mg^{2+} from the testing brine is present as newly precipitated magnesite carbonate mineral. This mineralogical evolution is most commonly observed close to the inlet and decreases towards the outlet. Moreover, due to rock-fluid interaction, in the inlet part of the sample void half-spheres were created, where most likely accumulation of the magnesite minerals concentrated in abundance. The diagenetic degree cannot be determined so far, but in the nearest future in depth geo-chemical analysis will be performed.

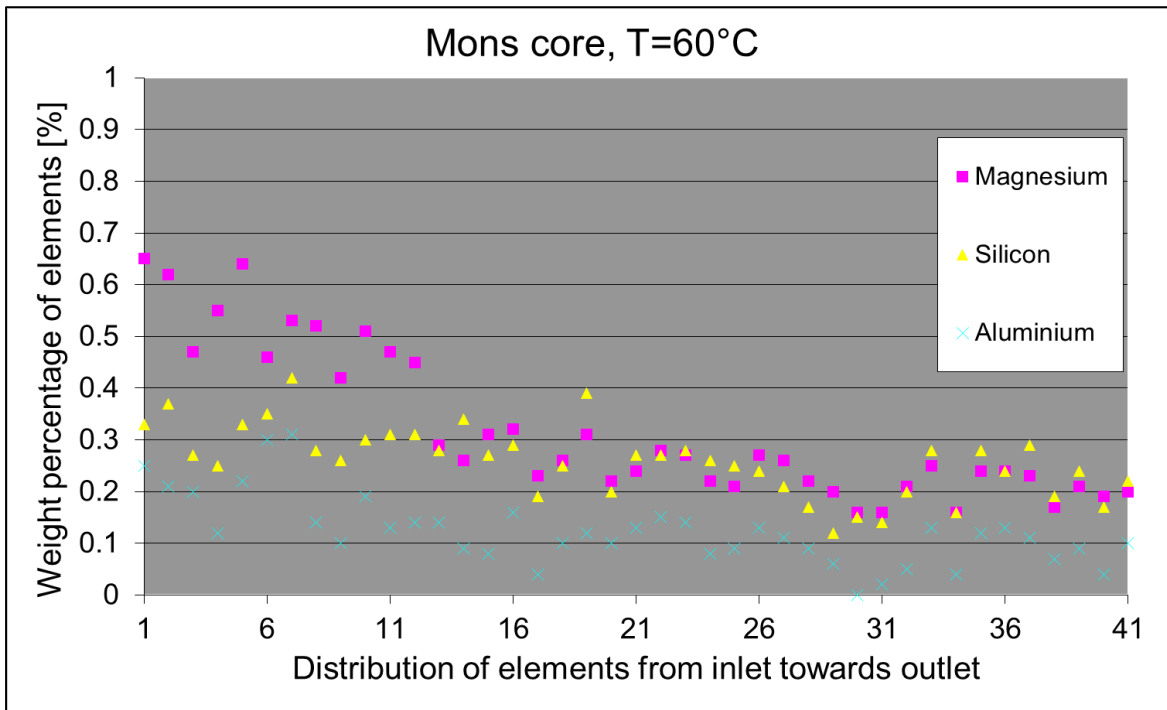


Figure 4.18 EDS analysis showing distribution of Mg^{2+} , Si^{2+} , Al^{3+} elements from the inlet towards outlet part of the Mons core tested at 60°C

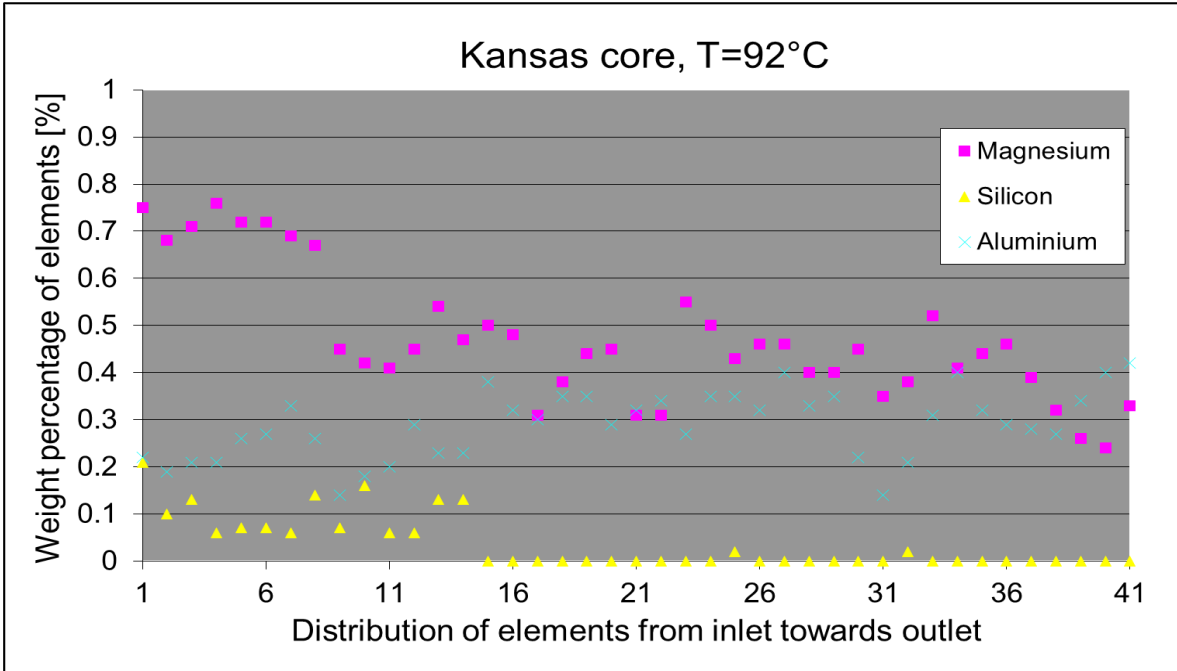


Figure 4.19 EDS analysis showing distribution of Mg²⁺, Si²⁺, Al³⁺ elements from the inlet towards outlet part of the Kansas core tested at 92°C.

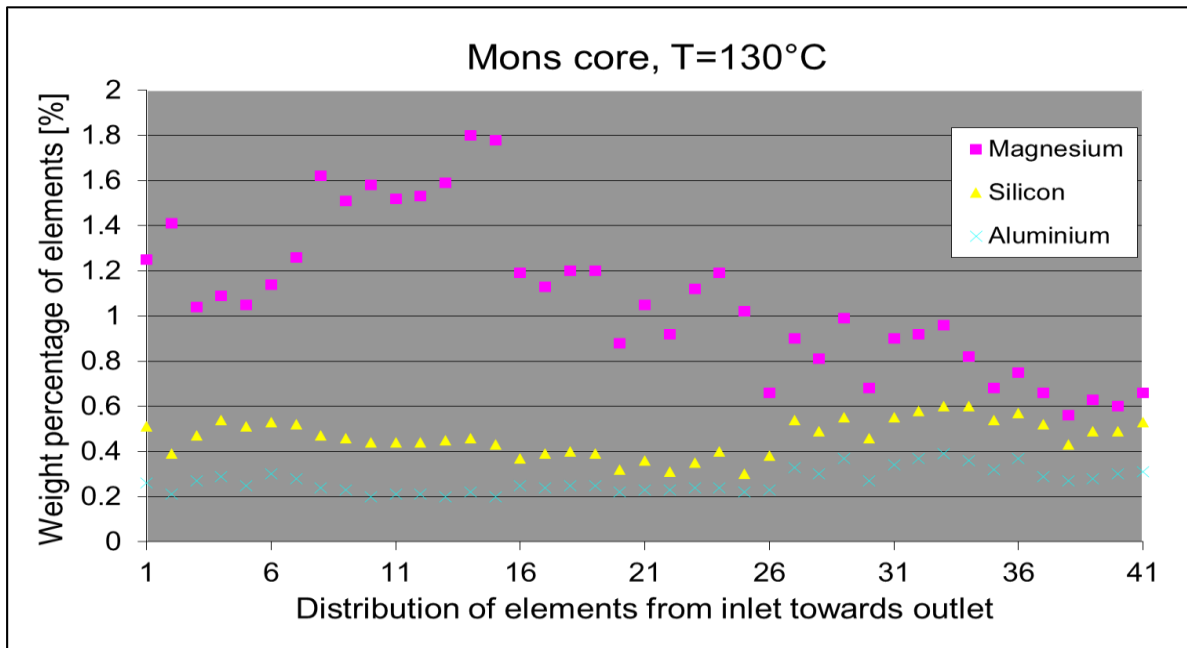


Figure 4.20 EDS analysis showing distribution of Mg²⁺, Si²⁺, Al³⁺ elements from the inlet towards outlet part of the Mons core tested at 130°C.

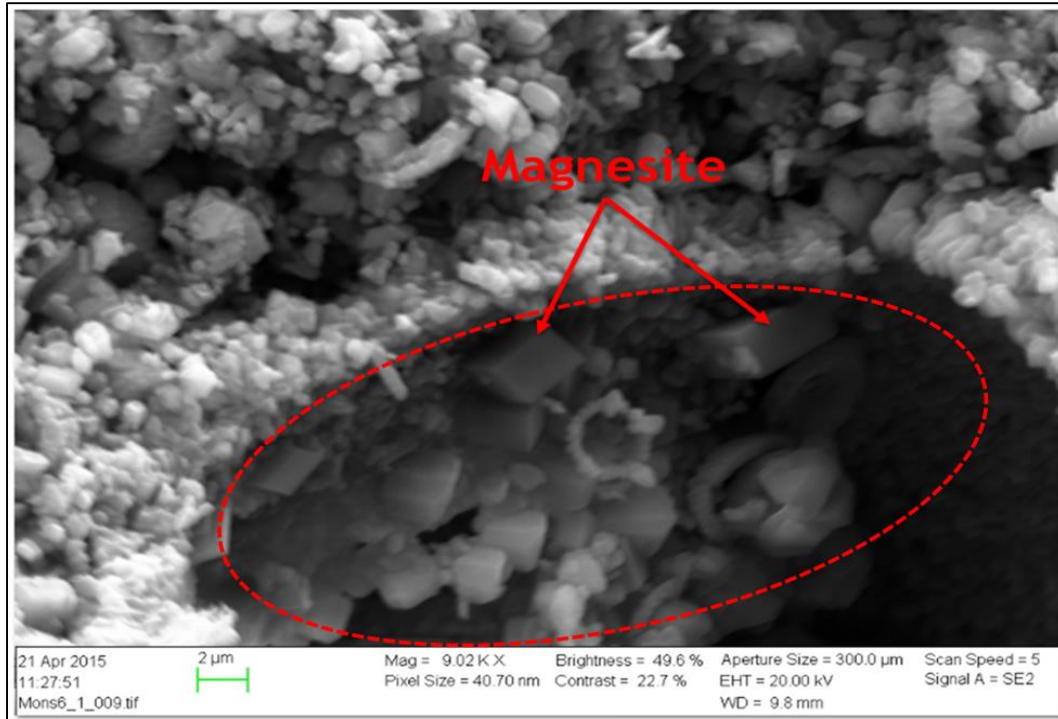


Figure 4.21 SEM micrograph shows common occurrence of magnesite crystals with rhombic habit (arrows) in the Mons core tested at 130 °C.

Most likely accumulation of the magnesite minerals concentrated in the inlet side where void half-spheres were created.

4.5.4 PHREEQC simulation

PHREEQC is a geochemical reaction model that enables to simulate a variety of geochemical processes such as equilibrium between water and minerals, ion exchangers, surface complexes, etc. (Charlton and Parkhurst, 2011). As there is no pressure dependent database in PHREEQC, comparison between flooded cores was simulated based on three different testing temperatures. In the present work, we used PHREEQC Pitzer database, since Pitzer provides more accurate results at high ionic strengths (Charlton and Parkhurst, 2011).

The simulation example is simply a baker with the initial solution. In the solution phase, we introduced 219 mmole/l Mg^{2+} and 438 mmole/l Cl^- ions. Calcite was added as a main

mineral while dolomite was incorporated as a non-carbonate phase; thereafter the system was simulated at atmospheric condition. The input values are mentioned in table 4.11.

Table 4.13-4.15 lists main aqueous species in the solution and complex phases that might precipitate at the temperature range of 60°C-130°C. If to refer to the saturation index values, calcite is in saturated state, while minerals such as magnesite, aragonite, etc. in undersaturated state. However, we can see with increasing temperature (130°C), the amount of forming magnesite minerals increases, which supports the SEM-EDS analysis. Moreover, with increasing temperature the pH of the system reduces, which also confirms laboratory analysis described in section 4.4.

Mons cores, T= 60°C and 130°C		Kansas core, T= 92°C	
Solution		Solution	
Mg ²⁺ concentration, mmol/l	219	Mg ²⁺ concentration, mmol/l	219
Cl ²⁺ concentration, mmol/l	438	Cl ²⁺ concentration, mmol/l	438
pH	5,5	pH	5,5
Equilibrium phases		Equilibrium phases	
Calcite, mole	9,95	Calcite, mole	9,75
Dolomite, mole	0,05	Dolomite, mole	0,25

Table 4.11 Input values for the simulation

Solution species	Molality	Solution phases	Saturation Index
Ca ²⁺	1,663e-01	Aragonite	-0,16
Mg ²⁺	5,744e-02	Bischofite	-7,37
HCO ₃ ⁻	2.763e-05	Brucite	-2,20
Cl ⁻	4,473e-01	Calcite	0,00
ph	7,61	CO ₂ (g)	-4,25
		Dolomite	0,00
		H ₂ O(g)	-0,71
		Magnesite	-1,18
		Nesquehonite	-3,97
		Portlandite	-7,07

Table 4.12 Output values from simulation for Mons core tested at 60°C.

Solution species	Molality	Solution phases	Saturation Index
Ca2+	5.498e-02	Aragonite	-0,13
Mg2+	1.687e-01	Bischofite	-7,03
HCO3-	1,695e-04	Brucite	-1,80
Cl-	4,473e-01	Calcite	0,00
ph	6.785	CO2(g)	-2,19
		Dolomite	0,00
		H2O(g)	0,41
		Magnesite	-1,07
		Nesquehonite	-4,03
		Portlandite	-7,07

Table 4.13 Output values from simulation for Mons core tested at 130°C.

Solution species	Molality	Solution phases	Saturation Index
Ca2+	1,396e-02	Aragonite	-0,15
Mg2+	8,410e-01	Bischofite	-7,24
HCO3-	5,432e-04	Brucite	-2,08
Cl-	4,473e-01	Calcite	0,00
ph	7,128	CO2(g)	-3,25
		Dolomite	0,00
		H2O(g)	-0,14
		Magnesite	-1,24
		Nesquehonite	-4,12
		Portlandite	-6,92

Table 4.14 Output values from simulation for Kansas core tested at 92°C

4.6 Estimation of porosity evolution

4.6.1 Mons core tested at 60°C

The porosity of the tested chalk before the experiment was estimated to be 42.47 % based on differences between saturated and dry weight of the sample (eq. 2.9). The change in bulk volume before and after testing used to estimate the volumetric strain (eq. 2.10) and

in overall the bulk volume is reduced by 5.34 %. The porosity estimation based on mechanical porosity evolution (eq. 2.14) assumes that deformation is accumulated by reduction in pore volume due to compaction, and no mineralogical changes occur when injecting reactive brine. Thus, if this assumption is valid, then the mechanical porosity resulted from the volumetric deformation reveals porosity alteration from 42.47% to 39.22%. Similarly, the porosity estimation based on chemical methods give also reduced values of porosity than initial, but in comparison to mechanical method, shows a slightly lower porosity reduction. As seen from the table 4.15 the dry mass of the core does change after the test. The second chemical method of estimating porosity (eq. 2.15) based on the mass change, subsequently leading to porosity reduction from initial to 39.73%. The third method is based on solid volume change (eq. 2.18). Having accurate estimates of the average solid density from pycnometer, and using dry mass and bulk volume after the experiment the porosity evolution is estimated to be 39.66%. As noticed, there is no large difference between the estimated porosities from all three methods, indicating the chemo-mechanical alterations taking place inside the core at this temperature range is insignificant.

Original core data		Core data after testing	
Dry weight, [g]	128,13	Dry weight, [g]	127,46
Saturated weight, [g]	163,20	Saturated weight, [g]	158,52
Length, [cm]	7,25	Mass loss during testing, [g]	0,67
Diameter, [cm]	3,81	Length, [cm]	7,05
Bulk volume, [cm ³]	82,58	Diameter, [cm]	3,78
Pore volume, [cm ³]	35,07	Bulk volume, [cm ³]	78,17
Porosity, [%]	42,47	Pore volume, [cm ³]	31,06
Density, [g/cm ³]	2,70	Volumetric strain, [%]	5,34
		Density, [g/cm ³]	2,71
		Method 1: Mechanical porosity, [%]	39,22
		Method 2: Chemical porosity, [%]	39,73
		Method 3: Chemical porosity, [%]	39,66

Table 4.15 Collected data before and after experiment for Mons core tested at 60°C.

4.6.2 Mons core tested at 130°C

The initial porosity of the core before testing was 42.2%. After mechanical test with continuous injection of non-equilibrium test brine, the bulk volume (eq. 2.10) is reduced by 6.55%, which is relatively high compared to the Mons core tested at 60°C. The porosity estimation based on mechanical method (eq. 2.14) shows that porosity is reduced from 42.2% to 38.17%. This reduction is based only on applied stress and resulted compaction, where grain reorganize with minimum solid volume change. In regards to porosity evolution that takes into account the chemical effects, in this case also porosity estimations give slightly higher values compared to mechanical method. As seen from table 4.16 significant changes compared to initial core parameters are observed after the test. The second chemical method (eq. 2.15) based on alteration of mass reveals porosity evolution from initial to 39.62%. The third method of estimating porosity (eq. 2.18) that takes into account solid volume change shows reduction in porosity to 39.54%. In overall, both chemical methods indicate estimation of porosity taking into account new density, new mass and new solid volume gives higher values of porosity compared with mechanical porosity, where minimum mineralogical changes considered.

Original core data		Core data after testing	
Dry weight, [g]	128	Dry weight, [g]	126,13
Saturated weight, [g]	162	Saturated weight, [g]	156,51
Length, [cm]	7,2	Mass loss during testing, [g]	1,41
Diameter, [cm]	3,81	Length, [cm]	6,97
Bulk volume, [cm ³]	82,1	Diameter, [cm]	3,73
Pore volume, [cm ³]	34,7	Bulk volume, [cm ³]	76,69
Porosity, [%]	42,2	Pore volume, [cm ³]	30,39
Density, [g/cm ³]	2,69	Volumetric strain, [%]	6,55
		Density, [g/cm ³]	2,72
		Method 1: Mechanical porosity, [%]	38,17
		Method 2: Chemical porosity, [%]	39,62
		Method 3: Chemical porosity, [%]	39,54

Table 4.16 Collected data before and after experiment for Mons core tested at 130°C.

4.6.3 Kansas core tested at 92°C

The Kansas core has initial porosity that is lower compared to those of Mons, it is 36.46%. After mechanical test, the bulk volumetric (eq. 2.10) strain reached 4.68%. Under mechanical compaction, estimated by mechanical method (eq. 2.14), shows porosity reduction from initial 33.46% to 33.35%. Porosity estimation taking into account chemical effects (eq. 2.15 and 2.18) indicates that 2 and 3 methods give more or less similar results, i.e 33.96% and 34.04% respectively. As seen from table 4.17 no substantial changes took place when the core tested at 92°C. In general, no significant distinction between three estimated methods observed at this testing temperature range.

Original core data		Core data after testing	
Dry weight, [g]	139,06	Dry weight, [g]	138,10
Saturated weight, [g]	168,61	Saturated weight, [g]	164,34
Length, [cm]	7,11	Mass loss during testing, [g]	0,96
Diameter, [cm]	3,81	Length, [cm]	6,99
Bulk volume, [cm ³]	81,04	Diameter, [cm]	3,77
Pore volume, [cm ³]	29,55	Bulk volume, [cm ³]	77,25
Porosity, [%]	36,46	Pore volume, [cm ³]	26,24
Density, [g/cm ³]	2,70	Volumetric strain, [%]	4,68
		Density, [g/cm ³]	2,71
		Method 1: Mechanical porosity, [%]	33,35
		Method 2: Chemical porosity, [%]	33,96
		Method 3: Chemical porosity, [%]	34,04

Table 4.17 Collected data before and after experiment for Kansas core tested at 92°C.

CHAPTER 5

DISCUSSIONS

5.1 The link between mechanical behaviour, porosity and temperature

All the mechanical tests in the present work were performed under hydrostatic loading. Such loading condition and the open structure of chalk framework promote a failure mechanism known as pore collapse. According to Risnes (2001), even though no macroscopic shear stress present under hydrostatic loading, however, on the grain scale, shear stress still exist leading to local shear-failures in between the grains. Therefore, 'pore collapse can be regarded as distributed shear failures within the material where gradual change from the linear trend is observed from the stress-strain relationship and the yield point is consequently rather uncertain to determine' (Megawati, 2015).

Experimental results from hydrostatic test (fig. 5.1) show that the slope of the stress-strain plot starts to curve from the linear trend during the stress increment, indicating some plastic deformation might occur on the grain scale. Such behaviour is more pronounced for Kansas chalk which has relatively high yield point, around 12.8 MPa; while for Mons chalk the yield was more obvious to determine, around 7.8 MPa. Thus, this behaviour confirms that shear failures in the grain scale have strong influence on the stress-strain behaviour of chalk even in the elastic region as claimed by Megawati (2015).

In overall there is a significant discrepancy between the yielding strength and accumulated axial strain from hydrostatic test between two types of cores. As seen from figure 5.1, the yield strength is not dependent on the temperature, two distinct trend rather point towards the initial properties of the core. As DaSilva et al. (1985) claimed that mechanical strength of chalk is dependent on porosity and silica content. Considering all above and also the fact that Kansas core has lower porosity, in average 36.4%, whereas the Mons chalks have 42.33%, these might be the reason for Kansas cores in general showing higher mechanical strength.

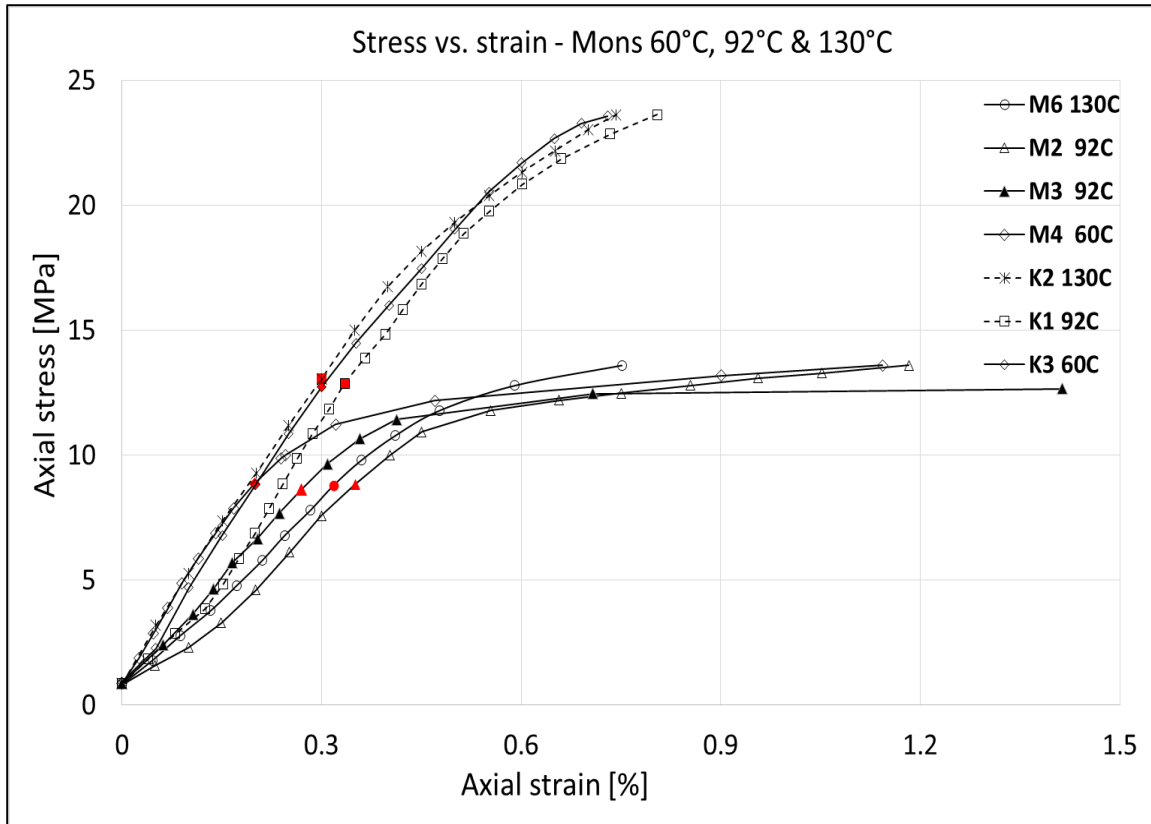


Figure 5.1 Axial stress versus axial strain for the Mons and Kansas cores tested at three different temperatures.

5.2 The link between creep behaviour and dissolution/precipitation

Irrespective of chalk type and initial porosities, the cores tested at 60°C and 92°C show conformity in their creep development behavior over time: secondary creep is developed after primary stage. Whereas, the cores tested at 130°C show additional tertiary-like accelerating creep development. From this observation we can interpret that testing temperature has an effect on the chemical interaction between rock and brine. The consequence of accelerating creep mechanism on creep behavior is remarkable; however this mechanism is not fully understood yet.

Series of experimental data by (Madland et al. 2011; Megawati et al. 2011, 2013, 2015; Nermoen et al., 2015 a, b) on pure and impure chalks have provided some clue on the

physico-chemical mechanisms of creep. Their extensive performed chemo-mechanical compaction tests have shown complete creep phases including the accelerated creep when the experiment were carried out at 130°C; however in other cases when experiments were conducted at temperatures other than 130°C and with chemical solutions containing Ca^{2+} , SO_4^{2-} or Na-rich were used, accelerating creep was not reported. Furthermore, such observation of accelerating creep along with Mons and Kansas chalks is documented on other chalk types as Stevns Klint, Liege and Obourg Saint Vaast chalks. From these experiments, it was also observed that creep deformation in pure chalks (Stevns Klint) is characterized by an initial stage of creep diminution before accelerating creep develops. Whereas for impure chalks (Liege, Obourg Saint Vaast) tertiary like creep immediately develops with an accelerated rate. Moreover, all experimental results consistently show increased Ca^{2+} production during accelerating creep (Megawati, 2015).

Figure 5.2 depicts creep development and dissolution relation for both type of cores tested at 130°C. As seen, for the pure Mons chalk the effect of dissolution is reflected in the time-dependent deformation, where creep response is characterized by time-lag until 20 days of creep period. Within this time, creep first diminishes and then a tertiary-like creep subsequently develops at an accelerated rate. Furthermore, in the acceleration stage a significant increase in Ca^{2+} production and Mg^{2+} retention is observed, confirming chemical reactions involving dissolution-precipitation taking place. In regards to the Kansas core, the effect of dissolution on accelerating creep show rather different behavior. The creep strain is immediately enhanced after 10 days of creep period and it develops with maintained rate over time. Similarly to the Mons core, increased production of Ca^{2+} and retention of Mg^{2+} ions is observed. When it comes to strain, even though the accelerating deformation for Kansas core started earlier, having lower porosity than the Mons core; Kansas shows higher strength even when the creep loading is 23.3 MPa, compared to the Mons where is it 13.2 MPa.

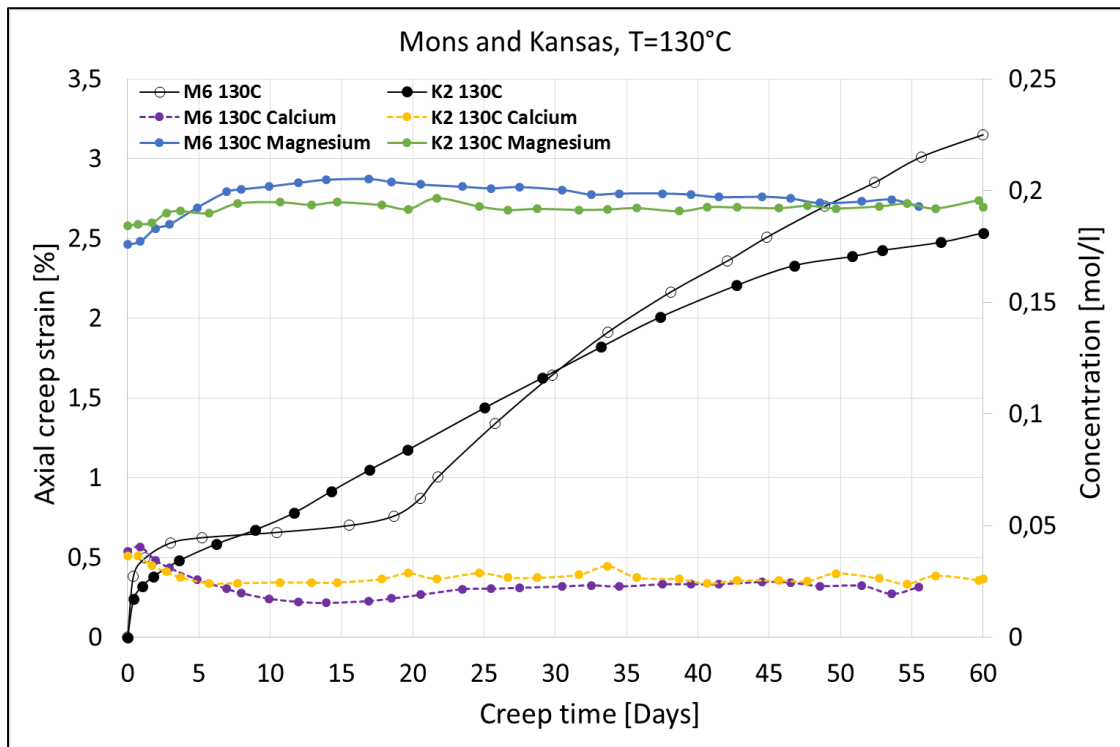


Figure 5.2 Creep development and fractionated effluent concentrations for Mons and Kansas cores tested at 130°C.

It has been generally described that creep in chalk is a cascade of failure redistribution process. As stated by Andersen et al. (1992), the main mechanism underlying the rate-type creep model is commonly assumed as off-sliding asperities under friction in between the granular contacts. When non-equilibrium brine is injected into the core, under high temperature more energy is created in the system, resulting in increased chemical reactions. When the chalk is dissolved, then the morphology of calcite surface is modified in terms of grain rounding and negative crystal creation in a form of prism or/and rhombohedral faceted faces (Gautier et al., 2001).

Based on experimental data in Madland et al. (2011), Megawati et al. (2011, 2015) a link between dissolution and the additional creep strain is reasonably established. They suggest that effect of dissolution is coupled with precipitation, which surely, depending on where these processes are taking place within the core might cause an enhanced weakening of the chalk framework itself. In other words, there might be zones of different strength, where stronger zones can bear the load while weaker zones might collapse first. With time these

stronger zones cannot handle the load, subsequently the collapse is distributed within the whole system leading to accelerated creep. Considering moving asperities as primary mechanism in chalk compaction any morphological changes in the calcite grains will affect the mechanical friction, thus favouring the creep mechanism. Depending on the degree of diagenesis, Fabricius (2012) states that high-porosity chalk may be partly or fully cemented if non-carbonate phase is present in the chalk; thus, non-carbonate minerals that fills the intergranular voids can act as contact cement holding the calcite grains together. Furthermore, Madland et al. (2011), Megawati et al. (2011, 2015) point out if non-carbonate phase is dissolved first that carries granular contact, then this might trigger enhanced deformation. In studies by Madland et al. (2011), Megawati et al. (2011, 2015) non-carbonate dissolution has been indicated by silicon ions measured in the effluent from the ICP-OES analysis.

5.3 The link between flow properties and chemical alterations

The implication of chemical effect is not only observed on the mechanical deformation but also might affect the flow properties, although to a great extent for the cores tested at 130°C. Irrespective of chalk type and testing temperatures, all cores under hydrostatic loading phase tend to show decreasing trend in permeability evolution. Neramoen et al. (2015b) propose the idea that initially the flow in the core might be focused within the areas with highest porosity, following this within these regions the compaction occurs. The compaction by grain re-organization leads to local permeability loss which is in line with the observed results from the present study.

On the other hand, the permeability evolution during creep phase shows rather different trend that seems to depend on temperature (fig. 5.3). Mons cores at temperatures below 130°C shows maintained declining trend with creep time, whereas at 130°C the permeability is stabilized during steady-state phase and reduces with maintained rate as accelerating creep starts. This might imply that during steady-state phase the permeability might dominate by compaction while later by dissolution. Similarly, all the Kansas cores

show reduced trend with time (fig. 5.4). However, at 130°C, initially permeability reduces gradually which is reflected during steady-state creep stage, then suddenly reduces with following accelerating creep, then after 25 days remains constant over time. This behaviour is similar to what is observed in the case of Mons core tested at 130°C, might relate initially to mechanical compaction thereafter to dissolution.

Such observed permeability behavior during creep phase might be related as suggested by Nermoen et al. (2015b) to local porosity alterations through deformation by grain reorganization and pore collapse. They suggest that most probably material parameters are heterogeneous therefore deformation is non-uniform through the core, such that permeability field is also expected to change with time and space, thus changing flow pattern. Knowing that, dissolution/precipitation is limited by the flow and the amount of fluids passing through a volume of a core within time interval determined not by chemical kinetics, rather by degree of chemical alteration. As dissolution/precipitation reactions reduce the solid volume, a positive effect of this to the flow might be expected. When the flow is focused within a particular region this leads to enhanced chemical reactions which in turn leads to solid volume reduction and consequent porosity increase which again focuses the flow through this regions. This cycling positive effect is termed as worm-holing and is used to understand the destruction of dams (Nermoen et al., 2015b).

Furthermore, when compaction is also taken into account, it is usually localized to regions of the core with higher porosities. As grain volume reduces with time, local porosity increases enabling compaction to activate within the next time-interval. Such a negative effect would distribute the flow over larger regions and inhibit worm-holing. However, this mechanism according to Nermoen et al. (2015b) is likely to occur at high stress level experiments, where injected brine comes in contact with all the reactive surfaces in the core that triggers chemical reactions. In contrast, at low stress experiments, as conducted in the present study, worm-holing seems to localize chemical alterations. From our experiment, worm-holing can be seen on the inlet side of the all cores tested where voids with half-spheres formed (verified in SEM-EDS analysis), but more pronounced in the test at 130°C. Since the flow first passes through drainage plate at the inlet side of the core and

injected test brine is not in equilibrium with the rock, the dissolution might localize mainly in the inlet part of the core where first reactive brine and core chemically equilibrate (Nermoen et al., 2015b).

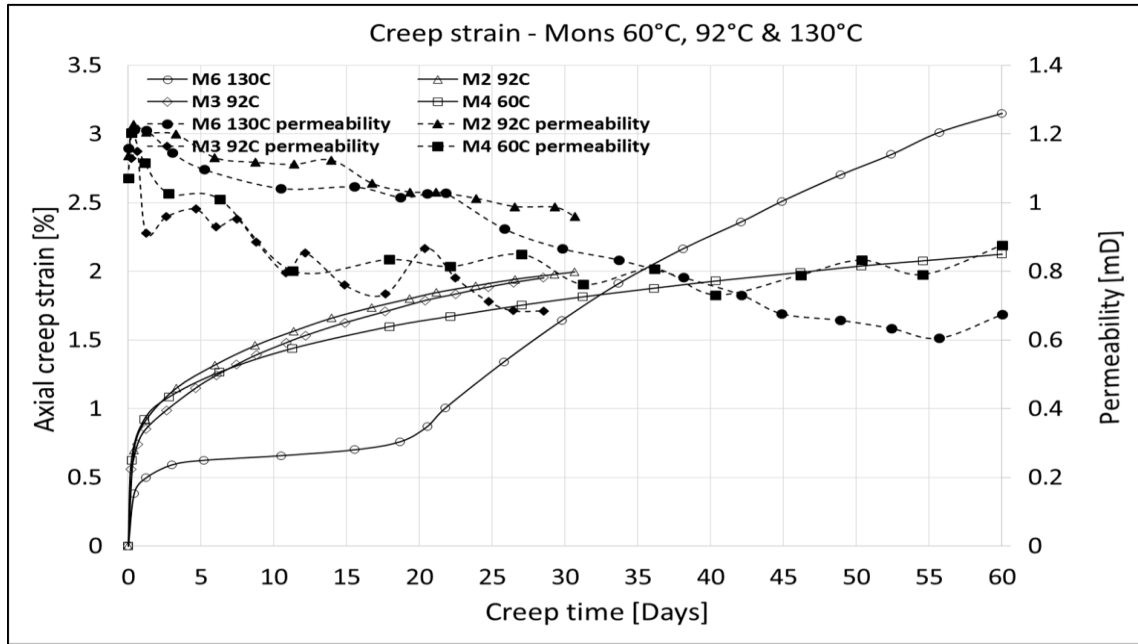


Figure 5.3 Permeability evolution during creep phase for the Mons cores tested at three different temperatures.

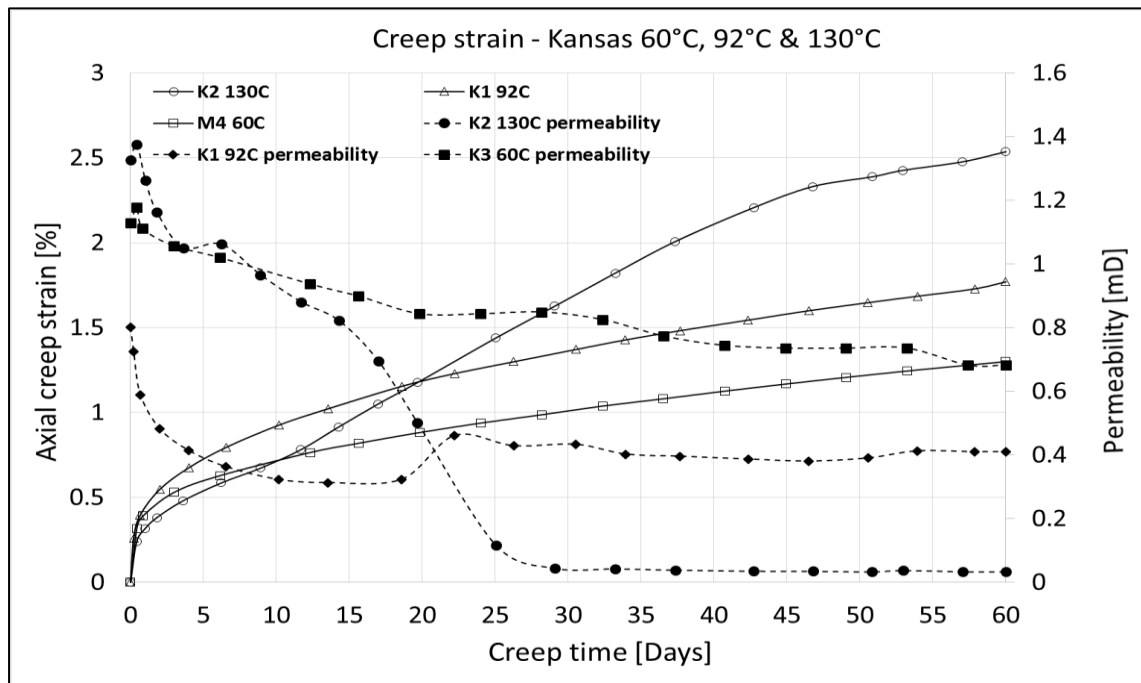


Figure 5.4 Permeability evolution during creep phase for the Kansas cores tested at three different temperatures.

5.4 Effect of chemical alterations on solid volume change

In more recent study by Nermoen et al. (2015a) and Wang et al. (2015) on the Liege outcrop chalks, the change of solid volume was shown to be considerable especially for long-term creep test with continuous flooding of MgCl_2 brines at elevated temperatures. As a result of dissolution of calcite and retention of Mg^{2+} new magnesium-bearing minerals are precipitated. Moreover, as per Madland et al. (2009) research on the same outcrop chalk Liege with injection of MgCl_2 brine at 130°C , significant loss of magnesium and production of calcium from the effluent is detected that could be accounted for as magnesium bearing mineral precipitated and calcite dissolved in the core. Furthermore, by modelling the experiment using EqALT program, Huntite ($\text{CaMg}(\text{CO}_3)_2$) was the most supersaturated mineral (Madland et al.,2009). These above mentioned minerals have a density larger than the calcium carbonate, thus any morphological changes alter the solid volume.

In the present study largest mineralogical alteration was observed for the Mons core tested at 130°C , which was verified by mass and density measurements, where density is increased from 2.69 g/cm^3 to 2.72 g/cm^3 . In addition, analysis in SEM-EDS indicates that retained Mg^{2+} ion present as magnesite mineral.

Since Mg^{2+} ion has the molecular weight of 24.31 g/mole and Ca^{2+} ion of 40.08 g/mole , any exchange during production of Ca^{2+} and retention of Mg^{2+} reduces the mass of the core. For constant mass, increase in solid density induces solid volume reduction; however when simultaneously both mass and density is changing, this further induces reduction of above.

Mass loss from IC analysis estimated as cumulative production of Ca^{2+} ion and retention of Mg^{2+} ion is not in accordance with weight measurements. Table 5.1 shows significant discrepancy between these two methods. This might relate to the uncertainties in IC measurement. Regardless of that, this difference might imply that not only dissolution of calcium carbonate and precipitation of magnesium carbonate might occur which was also observed by Nermoen et al. (2015). As per Nermoen et al. (2015a) equilibrium calculation

indicates that silicate minerals that initially present in the chalk are under saturated, thus further geochemical analysis of the rock chemistry is required to further investigate this issue.

Core ID	Core mass loss from IC [g]	Core mass loss from weight measurement [g]
M4 (60°)	0,238	0,67
M6 (130°)	0,904	1,41
K1 (92°)	0,153	0,96

Table 5.1 Mass losses for Mons and Kansas cores at three different temperatures from both IC analysis and dry weight measurements after testing.

5.5 Effect of mineralogy and temperature on porosity evolution

During the conducted chemo-mechanical experiments different response is observed depending on tested chalk type and temperature. As outlined earlier, mechanical method (eq. 2.14) of estimating porosity is only based on bulk volumetric deformation. Mons cores tested at 60 °C and 130°C exhibited bulk volumetric strain of 5.34% and 6.55% and consequently the core lost porosity by 7.7% and 9.6% respectively. Whereas Kansas core tested at 92°C shows less bulk volume deformation, 4.68%, with corresponding 8.5% reduction in porosity. As noticed, initial porosity of the chalk controls to which extend the core deforms.

When it comes to chemical porosities, where rock and non-equilibrium brine interaction is taken into account, continuous calcium dissolution and magnesium precipitation causes mass loss and change of the solid volume which in turn reflected in solid volume change. As discussed in above section, with increasing temperature the chemical reactions trigger ion exchange (Ca^{2+} production and retention of Mg^{2+} , but not one to one) inside the core thereby the cores tend to lose mass with temperature in addition with bulk volumetric change. Porosity estimation based on 1 chemical method (eq. 2.15) show porosity decrease by 6.45% and 6.15% for Mons cores tested at 60°C and 130°C correspondingly. While

Kansas core tested at 92°C gives 6.86% reduction. In regards to 2 chemical method (eq. 2.18), it has been also discussed in above section that geochemical alterations do not conserve the volume of the solids when higher dense magnesite mineral replaced with less dense calcite. Results of 2 chemical method of estimating porosity produces 6.62% (60°C) and 6.35% (130°C) porosity reduction for Mons cores; whereas 6.64% reduction (92°C) for Kansas core. As seen, with increasing temperature, the 1 and 2 chemical methods of estimating and porosity produce almost close values. If for comparison, irrespective of chalk type to calculate the difference between the average chemical and mechanical methods, with progressing temperature, the mechanical and chemical methods have distinct difference (1.12% - 60°C, 1.78% - 92°C, 3.40% - 130°C).

Extensive experimental data by (Wang et al., 2015, Nermoen et al., 2015a,b; Zimmermann et al., 2015) have shown that porosity is a dynamically evolving parameter and this dynamics is controlled by the rate of compaction, rate of dissolution-precipitation, and temperature. In studies by Nermoen et al. (2015a) presented lasting 1072 days of chemo-mechanical compaction experiment on Liege chalk (91-95% calcite) revealed porosity change from 41.31% to 40.02% and density altered from 2.68 g/cm³ to 2.89 g/cm³, despite the fact the plug had accommodated more than 25% bulk volumetric strain. This means that that long-term investigation provides a valuable approach for the analysis of compaction and fluid-rock core scale experiments that paves the way for further insight into the experimental diagenesis.

CHAPTER 6

CONCLUSIONS

We presented analysis of compaction and fluid-rock core scale experiments that have been carried out in hydraulically operated triaxial cells. Two mineralogically distinct Mons and Kansas chalks have been tested at three temperatures: 60°C, 92°C and 130°C, where the last two analogues to Valhall and Ekofisk field temperatures. Hydrostatic loading followed by creep test, where cores left to load under constant stress of 13.2 MPa and 23.3 MPa for the Mons and Kansas cores respectively. Throughout the experiment continuously MgCl₂ test brine injected into the core and the fractioned effluent has been collected to further study on chemical analysis, in order to quantify any chemical alteration of the core material. Furthermore, after dismantling the test, the flooded cores subsequently carried out on core analysis (weight measurements, density, textural analysis, etc).

Experimental results demonstrate that geo-chemical alterations occur when injecting non-equilibrium brine into the chalk cores. Effects of original porosity, non-carbonate content and temperature on the final porosity, dynamic compaction, as well as on permeability evolution have been highlighted in the thesis. In addition, implication of dissolution/precipitation mechanism on the chalk mechanical behavior, rock properties and also flow properties are investigated. Furthermore, present study makes comparison between the conventional porosity estimation method, based on mechanical compaction with minimal mineralogical changes, with the new chemical approaches where mineralogical alterations taken into account.

6.1 Concluding remarks:

1. We discussed the effect of test temperature and mineralogical content on the mechanical strength of chalk. It might be argued that under hydrostatic loading phase temperature has little effect if any on the mechanical strength; rather initial porosity has profound effect on the stress and observed strain relationship.
2. Microstructural changes in the grain roundness as a result of dissolution may reduce the intergranular friction, and thus favoring the creep mechanisms. This effect has been observed on both cores tested at 130°C where tertiary-like accelerating creep is developed. For the pure Mons chalk the creep response is characterized by a time lag, where creep initially diminishes and then tertiary-like creep subsequently develops at an accelerated rate. Whereas, for impure chalk the effect of dissolution is immediately reflected in the time-dependent deformation. We observed the immediate enhance of creep deformation that develops with maintained rate over time. Irrespective of chalk type, during acceleration stage increased production of Ca^{2+} ion and retention of Mg^{2+} ion observed in the effluent. Unfortunately, the mechanism of accelerating creep is not fully understood, but we relate the creep acceleration with the dissolution of non-carbonate phases which triggers the frictional sliding. The fact that the sum of Mg^{2+} and Ca^{2+} ions concentration deviates from the injected Mg^{2+} concentration suggests possibility of production of other cations from the core.
3. We discussed that implication of dissolution/precipitation also affects flow properties and to a great extent depend on temperature and non-carbonate minerals. Irrespective of chalk type and testing temperature, all cores show similar trend in permeability evolution under hydrostatic loading. This might relate to the idea that initially the flow in the core might focused within the areas with highest porosity, followed by compaction occurs within these regions. Compaction by grain re-organization leads to local permeability loss. Whereas, under creep test the cores show rather complex behavior. In this case we relate permeability evolution to dissolution/precipitation mechanism apart from mechanical compaction.

4. We also presented that chemical alterations produce mineralogical changes, this is profound with increasing temperature. In our study we could compare three cores tested at different temperatures and observations point towards increasing mineral density with temperature and time also plays a role.
5. Textural analysis also verifies that chemical alterations occur inside the core. No alteration observed for Mons and Kansas cores tested at 60°C and 92°C. However, SEM-EDS analysis in Mons chalk indicates notable mineralogical alteration occurred in the first centimeters of inlet part. Here retained Mg²⁺ ion present as a magnesite mineral.
6. In regards to porosity evolution methods, the first mechanical method based on compaction with minimum solid volume alteration reveals higher porosity reduction. On the other hand, both chemical methods consider density, mass and solid volume alteration during injection of non-equilibrium brine which reveals more or less close values. The difference between these chemical methods comes from the fact that in the first chemical method only bulk volume change is considered with little attention on solid density, while in the second chemical method of estimating porosity, more accurate density values used obtained by pycnometer. Therefore, with increasing temperature the solid density change is significant, therefore we can see slight difference between these chemical methods. In overall, the chemical methods of estimating porosity produce much less porosity reduction compared with mechanical method, where no chemical effects are considered. Thus when non-equilibrium brine is injected into the core, porosity estimation has to take into consideration not only compaction mechanism but also chemical alterations inside the core.

6.2 Future work

1. It is essential to study the dissolution-precipitation influence on time dependent deformation, and improve an understanding of why pure chalks exhibits time-lag acceleration creep behaviour, whereas impure chalks shows immediate response on dissolution.
2. Investigate long term effects of precipitation of secondary minerals on the mechanical strength of chalk. Considering chalk as frictional material, in a long term perspective, precipitation of new mineral phases may induce increased resistance against mechanical deformation due to increased intergranular friction. Such a mechanism is however, still an open discussion. In-depth investigation on the nano-scale can be a tool to investigate this further.
3. Weight measurement mass loss is not in accordance with IC measurements. Specific chemical analysis designed to detect non-carbonate minerals from the effluent should be investigated further.
4. Depending on where dissolution-precipitation processes are taking place within the core might cause an enhanced weakening of the chalk framework. Therefore it is necessary to localize the mineralogical alterations and where chemical processes preferentially take place.
5. At the moment translating the effect of water chemistry on oil recovery from core to field scale is highly non-trivial. Therefore, upscaling of laboratory results for field implementation would further insight into deep understanding of water-weakening phenomenon.

REFERENCES

- Andersen, M., Foged, N., Pedersen, H. 1992. The rate-type compaction of a weak North Sea chalk.
- Andersen, M. 1995. Petroleum research in North Sea chalk. RF Rogaland Research, Stavanger.
- Andreassen, K. A. 2011. Temperature Influence on Rock Mechanical Properties High-Porosity, Low-Cemented Chalk. PhD thesis, DTU.
- Austad, T., Strand, S., Madland, M., Puntervold, T., Korsnes, R. 2008. Seawater in Chalk: An EOR and Compaction Fluid. Paper SPE 118431 presented at International Petroleum Technology Conference, Dubai, 4-6 December.
- Austad, T., Strand, S., Høgnesen, E.J., and Zhang, P. 2005: Seawater as IOR in Fractured Chalk. SPE 93000 presented at the 2005 SPE International Symposium on Oilfield Chemistry, The Woodlands, Texas, 2-4 February.
- Barkved, O., Heavey, P., Kjelstadli, R. 2003. Valhall Field - Still on Plateau after 20 Years of Production. Paper SPE 83957 presented at Offshore Europe, Aberdeen, UK, 2-5 September.
- Barkved, O., Kristiansen, T. 2005. Seismic time-lapse effects and stress changes: Examples from a compacting reservoir. The Leading Edge, December, 1244-1248.
- Bjørlykke, K. Petroleum Geoscience: From Sedimentary Environments to Rock Physics. 2010. Springer Science & Business Media, 2010921863.
- Charlton, S., Parkhurst, D. 2011. Modules based on the geochemical model PHREEQC for use in scripting and programming languages. Computers & Geosciences, Vol.37, issue 10, October, Pages 1653–1663
- DaSilva, F., Sanda, J. P., Schroeder, C. (1985). Mechanical behavior of chalks. Second North Sea Chalk Symposium.
- Doornhof, D., Kristiansen, T., Nagel, N., Pattillo, P., Sayers, C. 2006. Compaction and Subsidence. *Oilfield Review Autumn*, Schlumberger, 28, 50-68.
- Delage, P., Suraj De Silva, G. P. R. & Vicol, T. 1992. Suction controlled testing of non saturated soils with an osmotic consolidometer. Proc. 7th Int. Conf. on Expansive Soils, Dallas, 206–211.
- Fabricius, I. 2012. Chalk as a reservoir. 74th EAGE Conference and Exhibition –Workshops.

Fjær, E., Holt, R., Horsrud, P., Raen, A., Risnes, R. 2004. Petroleum Related Rock mechanics. Elsevier, 2nd edition.

Gautier, J., Oelkers, E., Schott, J. 2001. Are quartz dissolution rates proportional to bet surface areas? *Geochimica Et Cosmochimica Acta* 65, 1059-1070.

Gautier, D., Klett, T. 2005. Reserve growth in chalk fields of the North Sea. *Petroleum Geology Conference series v.6*, 169-175.

Gledhill, D., Morse, J. 2004. Dissolution kinetics of calcite in NaCl-CaCl₂- MgCl₂ brines at 25 °C and 1 bar pCO₂. *Aquatic Geochemistry* 10, 171-190.

Gutierrez, M., Øino, L., Høeg, K. 2000. The effect of fluid content on the mechanical behaviour of fractures in chalk. *Rock Mechanics and Rock Engineering*, 33(2):93-117.

Hardman, R. 1982. Chalk Reservoirs of the North Sea. *Bull. geol. Soc. Denmark*, vol. 30, pp. 119-137, Copenhagen, 1st September.

Heggheim, T., Madland, M., Risnes, R., Austad, T. 2005. A chemical induced enhanced weakening of chalk by seawater. *J Petrol Sci Eng* 46(3):171-184.

Hellmann, R., Renders, P., Gratier, J., Guiguet, R. 2002a. Experimental pressure solution compaction of chalk in aqueous solutions Part 1. Deformation behavior and chemistry. *Geochem Society*, pp. 129-152.

Hellmann, R., Gaviglio, P., Renders, P., Gratier, J., Békri, S., Adler, P. 2002b. Experimental pressure solution compaction of chalk in aqueous solutions Part 1. Deformation examined by SEM, porosimetry, synthetic permeability and X-ray computerized tomography. *Geochem Society*, pp. 153-178.

Hermansen, H., Thomas, L., Sylte, J., Aasbøe, B. 1997. Twenty Five Years of Ekofisk Reservoir Management. *Proceedings of SPE Annual Tech Conf & Exhib, San Antonio, SPE 38927-MS*.

Hiorth, A., Cathles, L., Madland, M. 2010. The impact of pore water chemistry on carbonate surface charge and oil wettability. *Transport in porous media*, 10.1007/s11242-010-9543-6.

Hiorth, A., Jettestuen, E., Cathles, L., Madland, M. 2013. Precipitation, dissolution, and ion-exchange processes coupled with a lattice Boltzmann advection diffusion solver. *Geochimica et Cosmochimica Acta* 104, 99-110.

Hjuler, M. 2006. Silica and clay mineralogy and distribution in reservoir chalk (Valhall) and outcrop chalks (Aalborg, Liege and Stevns). Technical report, BP.

Hjuler, M. 2007. Diagenesis of Upper Cretaceous onshore and offshore chalk from the North Sea area. PhD thesis, DTU.

Hjuler, M., Fabricius, I. 2009. Engineering properties of chalk related to diagenetic variations of upper cretaceous onshore and offshore chalk in the north sea area. Journal of Petroleum Science and Engineering.

Korsnes RI, Madland MV, Austad T, Haver S, Røslund G (2006a) The effects of temperature on the water weakening of chalk by seawater. J Petrol Sci Eng 60(3-4):183-193.

Korsnes, R., Wersland, E., Austad, T., Madland, M. 2006b. Anisotropy in chalk studied by rock mechanics. Journal of Petroleum Science and Engineering, Volume 62, Issues 1–2, 15 September, Pages 28–35.

Kjørsløvik, T., Østensen, G. 2014. The effect of stress level and temperature on water weakening of chalk. BSc thesis, UiS.

Madland, M., Midtgarden, K., Manafov, R., Korsnes, R., Kristiansen, T., Hiorth, A. 2008. The effect of temperature and brine composition on the mechanical strength of Kansas chalk. Proceedings Int Sym SCA, Abu Dhabi.

Madland, M., Hiorth, A., Korsnes, R., Evje, S., Cathles, L. 2009. Rock Fluid Interaction in Chalk exposed Injection of Seawater, MgCl₂, and NaCl Brines with equal Ionic Strength. EAGE, Paris.

Madland, M., Hiorth, A., Omdal, E., Megawati, M., ... Cathles, L. 2011. Chemical alterations induced by rock-fluid interactions when injecting brines in high porosity chalks. Transport in porous media, 10.1007/s11242-010-9708-3.

Megawati, M., Hiorth, A., Madland, M. 2013. The impact of surface charge on the mechanical behavior of high-porosity chalk. Transport in porous media, 10.1007/s00603-012-0317-z.

Megawati, M., Hiorth, A., Madland, M. 2015. Mechanical and physical behavior of high-porosity chalks exposed to chemical perturbation. Journal of Petroleum Science and Engineering, January.

Megawati, M., Andersen, P., Korsnes, R., Evje, A., Hiorth, A., Madland, M. 2011. The effect of aqueous chemistry pH on the time-dependent deformation behavior of chalk-experimental and modelling studies. Paper presented in Pore2fluid International Conference, IFP Energies Nouvelles, Paris, 16-18 November.

Megawati, M. 2015. Geochemical aspects of water-induced compaction in high-porosity chalks. PhD thesis. Faculty of Science and Technology, UiS no.247.

- Megson, J., Tygesen, T. 2005. The North Sea chalk: an underexplored and underdeveloped play. Petroleum Geology Conference series v.6, 159-168.
- Nermoen, A., Kornses, R., Hiorth, A., Madland, M. 2015. Porosity and permeability development in compacting chalks during flooding of non-equilibrium brines – insights from long term experiment.
- Nermoen, A., Kornses, R., Aursjø, O., Madland, M., Kjørslevik, T., Østensen, G. 2015. How stress and temperature conditions affect rock-fluid chemistry and mechanical deformation.
- Punternvold, T., Strand, S., Austad, T. 2007. New method to prepare outcrop chalk cores for wettability and oil recovery studies at low initial water saturation. Energy Fuels 21(6), 3425-3430.
- Richard, J., Sizun, J. 2011. Pressure solution-fracturing interactions in weakly cohesive carbonate sediments and rocks: Example of the synsedimentary deformation of the Campanian chalk from the Mons Basin (Belgium). Journal of Structural Geology Volume 33, Issue 2, February, Pages 154–168.
- Risnes, R. (2001). Deformation and yield in high porosity outcrop chalk. Phys Chem Earth, 26(1-2).
- Risnes, R., Madland, M., Hole, M., Kwabiah, N. (2005) Water weakening of chalk – Mechanical effects of water-glycol mixtures. J Petrol Sci Eng 48(1-2):21-36.
- Scholle, P. 1977. Chalk diagenesis and its relation to petroleum exploration: oil from chalks, a modern miracle. AAPG Bull 61(7):982–1009.
- Scholle, P. 1978. Potential offshore hydrocarbon reservoirs in chalk. Paper OTC 3121 presented at the 10th Annual OTC in Houston, Tex., 8-11May.
- Strand, S., Punternvold, T., Austad, T. 2008. Effect of temperature on enhanced oil recovery from mixed-wet chalk cores by spontaneous imbibition and forced displacement using seawater. Energy & Fuels, 22:3222-3225.
- Tang, G., Firoozabadi A. 2001. Effect of pressure gradient and initial water saturation on water injection in water-wet and mixed-wet fractured porous media. SPE Reservoir Evaluation & Engineering 4(6): 516-524.
- Watkins, G. 2011. Characteristics of North Sea oil reserve appreciation. The Quarterly Review of Economics and Finance, Vol. 42, 335-372.
- Wang, W., Korsnes, R., Nermoen, A., Madland, M., Zimmermann, U., Hildebrand-Habel, T. 2015. Porosity development during chemo-mechanical compaction in chalk. Reservoir

quality of clastic and carbonate rocks: analysis, modelling and prediction - The Geological Society, London, Special Publication ('Reservoir Quality of Clastic and Carbonate Rocks: Analysis, Modelling and Prediction'; accepted).

Wang, W., Madland, M., Zimmermann, U., Bertolino, S., Hildebrand-Habel, T., Korsnes, R. 2013. Geochemistry and isotope geochemistry of Upper Cretaceous chalk as equivalent for reservoir chalk of the North sea Basin for EOR. *Mineralogical Magazine*, 77(5) 2456.

Zangiabadi, B., Korsnes, R., Hildebrand-Habel, T., Hiorth, A., Sutarjana, I., Lian, A., and Madland, M. V. 2009. Chemical water weakening of various outcrop chalks at elevated temperature. In *Poromechanics IV*, Lancaster.

Zimmermann, U., Madland, M., Hildebrand-Habel, N., Bertolino, S., Hiorth, A., Korsnes, R., Audino, J., Grysan, P. 2015. Evaluation of the compositional changes during flooding of reactive fluids using scanning electron microscopy, nano-secondary ion mass spectrometry, x-ray diffraction, and whole rock geochemistry. *AAPG Bulletin*, Vols. 99, No. 5, pp. 791-805.